AD-A126 366 THE APPLICATION OF LASER RESONANCE SATURATION TO THE DEVELOPMENT OF EFFIC.. (U) TORONTO UNIV DOWNSVIEW (ONTARIO) INST FOR AEROSPACE STUDIES R M MEASURES

UNCLASSIFIED SEP 82 AFOSR-TR-83-0134 AFOSR-80-0057 F/G 20/5 NL

1/2

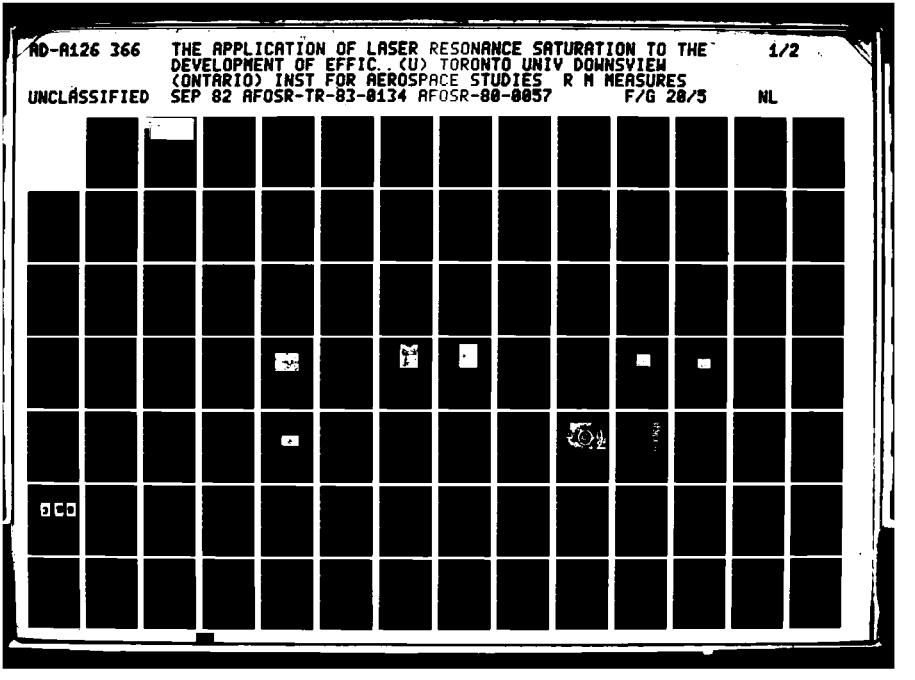

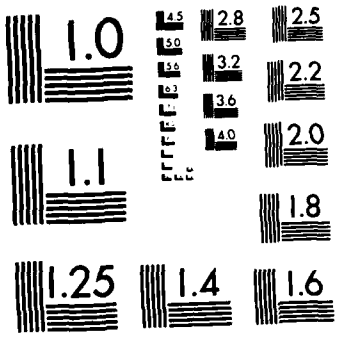

MICROCOPY RESOLUTION TEST CHART
NATIONAL BUREAU OF STANDARDS 1963-A

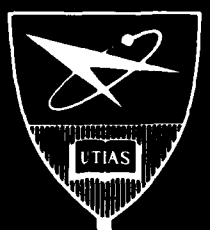

INSTITUTE
FOR
AEROSPACE STUDIES

UNIVERSITY OF TORONTO

THE APPLICATION OF LASER RESONANCE SATURATION TO THE DEVELOPMENT OF EFFICIENT SHORT WAVELENGTH LASERS

Annual Technical Report
(for period ending September 30, 1982)
US AFOSR 80-0057B

Prepared by

Dr. R. M. Measures
Professor of Applied Science and Engineering

University of Toronto
Institute for Aerospace Studies
4925 Dufferin Street
Downsview, Ontario, Canada
M3H 5T6

THE APPLICATION OF LASER RESONANCE SATURATION TO THE DEVELOPMENT OF EFFICIENT SHORT WAVELENGTH LASERS

Annual Technical Report

(for period ending September 30, 1982)

US AFOSR 80-0057B

Prepared by

Dr. R. M. Measures
Professor of Applied Science and Engineering

University of Toronto
Institute for Aerospace Studies
4925 Dufferin Street
Downsview, Ontario, Canada
M3H 5T6

Abstract

Laser resonance saturation represents an extremely rapid and efficient new method of coupling laser energy into either a gas or plasma. We have continued to study this process both theoretically and experimentally and have shown that this interaction can lead to a very high degree of ground level burnout for the laser pumped species. During the past year we have undertaken the first time resolved Stark width measurements of the free electron density within a sodium plasma created by laser resonance saturation. Currently we are exploring the feasibility of using this ground level burnout feature as the basis of a new approach towards the development of an efficient short wavelength laser. In a preliminary experiment we have been able to show that sudden joule heating of a thin foil looks promising as a technique for creating the steep gradient of neutral atoms necessary for charge exchange formation of a ground level population inversion within the species having suffered a ground level burnout through laser resonance saturation.

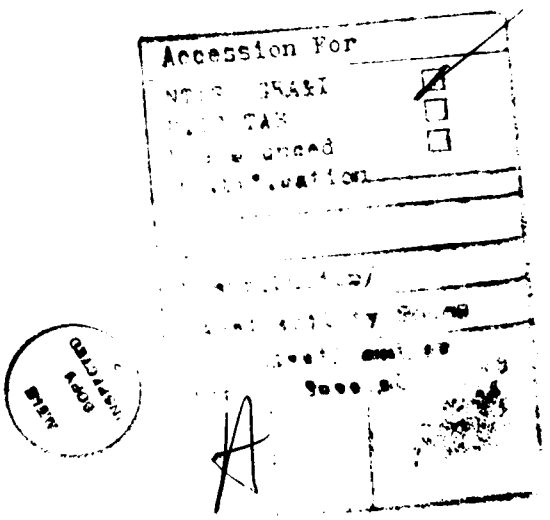

CONTENTS

RESEARCH OBJECTIVES

The main thrust of our current research program has been to study two aspects of a new approach towards the development of a relatively efficient short wavelength laser. This approach is based on the rapid *burnout* of the ground level population of a suitable species to the point where it becomes possible to think in terms of creating a *ground level population inversion* and thereby the development of a short wavelength laser of high quantum efficiency.

Laser saturation of an atomic resonance transition has, in recent years,[1-18] become recognized as a new form of laser interaction that is capable of rapidly and efficiently producing near total ionization of the laser pumped species. Our first objective is to evaluate the potential of this laser ionization based on resonance saturation LIBORS process to efficiently attain a high degree of ground level burnout and thereby provide conditions that are conducive to the formation of a ground level population inversion. Our second objective is to study how best to create such a ground level population inversion. Initially we are considering an approach based on a combination of rapid cooling and charge exchange collisions with the atoms of a dense neutral cloud.

STATUS REPORT

In order to make full use of laser resonance saturation it is important to attain a comprehensive understanding of this interaction. Of special interest is the limitation to the degree of ground level burnout that can be achieved,for the greater the degree of burnout, the easier it should be to create a ground level inverted population (GLIP).

During the past year we have made good progress in this connection. We have undertaken the *first time resolved measurements of the electron density* within a sodium plasma created by laser resonance saturation. These Stark broadening measurements have confirmed that near total ionization has been achieved and provide us with a means to determine the efficiency of the ionization process. These measurements will shortly be augmented by a *new technique* called SHADO (for Spectral Hole Atom Density Observation). This technique has been specifically devised to measure the residual ground level density in the burnout phase of the LIBORS interaction as Stark measurements alone are inappropriate for determining the degree of ionization once it exceeds about 95%.

During the past year we have also studied the possibility of utilizing *charge exchange collisions* for the purpose of creating a GLIP within the laser burned out species and have developed a criterion for estimating the steepness of the density gradient required to achieve this goal. We have also initiated an experimental program aimed at producing a dense atomic cloud with the required steep density gradient.

Since the degree of ground level burnout attained through LIBORS is an important parameter in determining the steepness of the density gradient for the neutral cloud, we have extended our steady state analysis to doubly ionized boron – a prime candidate for the charge exchange interation. Lastly, we have been able to show in a rather elegant manner that laser stimulated inverse radiative autoionization cannot be used to create a GLIP, see Appendix A.

1. LASER ABSORPTION WITH SPECTRAL HOLE BURNING

In our earlier work[19] on the attenuation of laser energy tuned to overlap the 589 nm resonance transition of sodium atoms we developed a spectrally integrated radiation transport analysis to account for the observed dependence of the laser energy absorption upon the sodium vapour density and the incident laser energy. Although this analysis describes the behaviour at low values of laser energy it appeared inadequate at higher energies. During the past year we have extended this theory to include both the transition absorption profile and the finite bandwidth of the laser pulse. Our analysis reveals that although spectral hole burning is likely to have been substantial in our experiments,[19] nevertheless, our simple theory appears to have been adequate to describe the variation of absorbed laser energy with incident laser energy provided the incident laser energy was insufficient to create appreciable excitation and ionization.

This analysis has been prepared into the form of a paper and has been accepted for publication in the Journal of Quantitative Spectroscopy and Radiative Transfer. A copy of which is appended to this report as Appendix B and therefore will not be discussed further in this section.

2. METHOD OF MEASURING THE GROUND LEVEL BURNOUT FACTOR

Our work on spectral hole burning discussed above (and presented in full in Appendix B) led us to consider this effect as a means of measuring the degree of ground level burnout achieved through laser resonance saturation. We propose to use a nitrogen pumped ring dye laser to provide us with a short ($\lesssim$ 5 nsec) broad band pulse of radiation tuned to overlap one of the resonance transitions.

If the laser spectral irradiance of this probe pulse is below the value necessary for saturating the transition then Beer-Lambert's law applies and we can write for a beam traversing a diameter of our disc shaped vapour zone,

$$I(\nu,R) = I(\nu,-R)\exp\left[-\int_{-R}^{R} N_1(r)\sigma_o(r)L(\nu,r)dr\right] \qquad (1)$$

where $I(\nu,R)$ is the spectral irradiance leaving the vapour region at radius R,

$I(\nu,-R)$ is the spectral irradiance incident upon the vapour region at radius -R,

$N_1(r)$ is the ground state population density at radius r within the vapour zone,

$L(\nu,r)$ is the normalized atomic line profile function [i.e., $\mathcal{L}(\nu,r)/\mathcal{L}(\nu_o,r)$] at radius r within the vapour zone, and

$\sigma_o(r)$ is the absorption cross section at the line centre frequency at radius r within the vapour zone, i.e., $\sigma_o(r) = \frac{h\nu}{4\pi} B_{12}\mathcal{L}(\nu_o,r)$.

Alternatively, if the laser spectral irradiance is close to (or greater than) the *saturated spectral irradiance* of the transition[20]

$$I_s(\nu) = \frac{8\pi h\nu^3}{c^2(1+g)} \left(\frac{\tau^{RAD}}{\tau} \right) \qquad (2)$$

where g $(=g_2/g_1)$ is the degeneracy ratio of the transition, $h\nu$ is the photon energy, c the velocity of light, τ^{RAD} the radiative lifetime for the transition and τ the actual lifetime, then an allowance has to be made for the redistribution of the two level population by the radiation field of the laser. From our more complete analysis [see equation (17) of Appendix B]

$$I(\nu,R) = I(\nu,-R)\exp\left[- \int_{-R}^{R} \frac{N_o(r)\sigma_o(r)L(\nu,r)dr}{1+\mathcal{J}(r)} \right] \qquad (3)$$

where

$$\mathcal{J}(r) = \frac{1}{I_s} \int_{-\infty}^{\infty} I(\nu,-R)L(\nu,r)\exp\left[- \int_{-R}^{R} \frac{N_o(r)\sigma_o(r)L(\nu,r)dr}{1+\mathcal{J}(r)} \right] d\nu \qquad (4)$$

Here, $I_s \equiv I_s(\nu)\delta\nu(s)$ where $\delta\nu[=\mathcal{L}^{-1}(\nu_o)]$ represents the effective absorption bandwidth of the transition. Under these circumstances $N_o(r)$ represents the sum of the population densities in the upper and lower levels of the transition, which in the absence of other processes just equals the ground level population prior to laser irradiation.

In general the width and depth of the spectral hole produced in the laser pulse will depend on the optical depth of the medium at the wavelength of concern. This in turn depends upon the density distribution along the path of the laser beam so that the greater the degree of ground level burnout,

the narrower and more shallow will be the spectral hole. A complication arises, however, due to the boundary region of the vapour. In these *end zones* the lower initial vapour density will result in a smaller degree of ground level burnout (see figure 1) and the possibility arises that the greater ground level population density existing in these end zones could limit the measurement of the degree of ground level burnout GLB attained in the central region.

As a means of evaluating this potential constraint on the limit of our GLB measurement we have undertaken some computer simulations for the low irradiance probe case. These calculations take account of the Stark shift and broadening incurred by the line as a result of the plasma created. The results are presented as figure 2. Here, the probe laser spectral irradiance was assumed to be much less than the saturated spectral irradiance $I_s(\nu)$ and independent of frequency over the spectral interval of interest. The initial sodium vapour was assumed to be uniform with density N_{max} over a radius r_o, then to fall off with radius according to the relation

$$N_o(r) = N_{max} 10^{-(r-r_o)/L} \qquad (5)$$

where L is the *end zone scale length*. Our simple LIBORS model[17] was used to estimate the degree of burnout achieved in the end zones.

In figure 1 and the broken curves of figure 2, $N_{max} = 10^{16}$ cm^{-3}, $r_o = 6$ cm and L = 1 cm, while the full curves in figure 2 correspond to the same values of N_{max} and r_o, but L = 0.2 cm. The ionization laser pulse irradiance I_ℓ was taken to be 10^6 Wcm^{-2} in figures 1 and 2. We can conclude from figure 2 that if we are satisfied with a measurement to 99.9% ionization (i.e., a GLB factor defined as the ratio of the neutral to ion ground level ratio $\alpha \geq 10^{-3}$) then the end zone uncertainties should limit the accuracy of the GLB measurement to about ±25%. However, if 99.99% ionization (i.e., $\alpha \geq 10^{-4}$) is to be measured, then this method is not likely to be adequate unless the end zone density scale length L is very short ($\lesssim$ 0.5 cm). As we shall see later there appears to be some evidence that the end zones are indeed fairly steep. However, this is a subject that will have to be further investigated.

At the time of writing we are testing the specially designed nitrogen laser pumped ring dye laser that will be used for these GLB measurements on the sodium plasma created within our LIBORS facility.

3. LIBORS EXPERIMENTAL PROGRAM

Within the past few years the literature has become rich with papers[3-15] that involve experimental studies of laser resonance saturation and its consequences. Although, this work has provided confirmation of the ionization capability of this interaction, none of the experiments undertaken to date have determined the temporal variation of the electron density or, even more pertinent, the degree of ground level burnout achievable through this form of laser interaction.

3.1 LIBORS *Facility and Emission Studies*

Over the past year we have continued the development of our facility for creating plasmas based on laser resonance saturation and undertaking these important measurements. A photograph of an early arrangement is presented as figure 3, while the current configuration of our LIBORS facility is schematically illustrated in figure 4. In essence a powerful flashlamp pumped dye laser (Phase-R Model 2100BX) is used to irradiate a disc shaped region of sodium vapour confined within a specially designed (heat pipe action) oven that provides 360° optical access.

The basic design of this oven involves a set of upper and lower heated plates to which are attached two stainless steel mesh discs that provide the capillary action for the liquid sodium that is germane to the heat pipe principle. The sodium vapour is prevented from coming into contact with the windows through the use of an argon buffer region that is kept cool by the flow of cold water through copper tubes positioned outside the heated zone. To relieve the radial stress apparent in the original design of this oven[21] we have incorporated a specially designed buckle. A close-up view of this *sandwich oven* and its concomitant water cooling pipes is presented as figure 5.

When the laser is tuned to one of the sodium resonance lines and fires through the sodium vapour a burst of plasma emission is clearly visible to the eye along the path of the laser beam. An example of this emission is seen in figure 6. The oven is mounted on a special sliding arrangement that provides us with the ability to tranlsate it in the plane of the laser beam. This will enable us to excite and view different regions of the vapour without changing the optical arrangement.

Spectral narrowing and tuning of the dye laser is accomplished through the use of three prisms and a back reflector. With this configuration and a $2x10^{-4}$ Molar solution of Rhodamine 6G in high purity methanol an output pulse of close to half a joule at 589 nm has been attained. The spectral width (FWHM) of this pulse is abou: 0.2 nm. If an intracavity etalon is used in proximity to the output reflector the pulse narrows to about 0.06 nm (FWHM) but the shot-to-shot reproducibility deteriorates and consequently the etalon was not employed. The spectral features of the laser pulse are measured by the spectrometer-reticon system shown in figure 7. Two photodiodes have been arranged to monitor the laser power before and after transmission through the sodium vapour. These photodiodes have been calibrated by comparison with an energy meter.

The emission from the laser produced plasma is monitored by three photomultipliers. Two are involved in evaluating the temporal behaviour of the free electron density by means of a Stark width measurement of a specific emission line, while the third is used in conjunction with a Heath monochromator to monitor the emission at various wavelengths. The experimental arrangement for undertaking the Stark width measurement involves imaging the exit slit of a SPEX 1700 monochromator onto the face of a two channel fiber optic array, see figures 4 and 8. Prior to reaching the entrance slits of the two monochromators the light from the plasma is rotated through 90° by means of prism arrangements (BR in figure 4). This rotation enables the vertical entrance slits of the monochromators to accept light from a horizontal slice of the plasma. The optical axis of both systems and that of the flashlamp pumped dye laser are aligned by means of a He-Ne laser to lie in the same horizontal plane. The length and width of the observed slice of plasma is then determined by the respective height and width of each entrance slit.

The 568.8 nm line of the sodium 4^2D-3^2P multiplet was selected as the most suitable for undertaking the Stark measurements. This choice was based on the following information: it was observed to be a strong line, our photomultipliers were fairly sensitive at its wavelength, and most important, its Stark broadening was sufficient to ensure a reasonably reliable measurement of the peak electron density at the vapour pressures of interest. The third photomultiplier (an RCA 1P21) observed several spectral lines in addition to a (3 nm) band of recombination radiation at

400 nm. Figure 9 displays a representative example of both this recombination radiation signal (the inverted upper trace) and a signal from the photodiode positioned so as to monitor the corresponding incident laser pulse (lower trace). It is quite evident from these signals that the plasma radiates for a time that is considerably longer than the duration of the laser pulse. An even more intense signal was observed at the 568.8 nm wavelength, an example of which is provided in figure 10. It is apparent that this line radiation peaks some time after the peak of the laser pulse.

The variation in the peak signal at 568.8 nm as a function of radial position across the sodium vapour disc (and along the laser beam) is shown in figure 11 for two laser wavelengths. It is apparent that when the laser is tuned to overlap the 589.0 nm sodium resonance line the signal increases at first with decreasing radial position – which reflects the increasing sodium density at the edge of the vapour disc – then proceeds to decrease fairly dramatically with further decrease of radial position. This decrease in the 568.8 nm emission signal is attributed to strong absorption of the laser pulse as it propagates through the vapour.

On detuning the laser to 590.4 nm the peak emission at 568.8 nm is again seen to increase at first (i.e., at the edge) but then remain practically constant with decreasing radial position. Although this spatial variation is reasonable on the grounds that the detuned laser pulse is expected to suffer much less absorption – what is surprising is that the magnitude of the 568.8 nm emission for the detuned case exceeds the value obtained when the laser is tuned at most radial positions! Indeed, observations fairly close to the centre of the sodium disc ($r \cong 0.75$ cm) reveal that as the laser is detuned towards longer wavelengths the peak amplitude of the 568.8 nm emission significantly increases at first, reaching a maximum that is nearly an order of magnitude greater than the 589.0 nm tuned case, then decreases with further detuning, see figure 12.

This is similar to an observation made by Muller and Hertel.[23] They showed that the infrared laser emission at 3.4 μm (corresponding to the 5^2S-4^2P multiplet of sodium) resulting from laser irradiation of sodium vapour also reached a maximum value when the exciting laser was detuned towards the red of the 589.6 nm resonance line. Indeed, their results show a minimum in the infrared emission when the irradiating laser is tuned to

either of the atomic resonance lines. This observation is consistent with strong absorption of the exciting laser beam when its wavelength coincides with the resonance lines. However, what is not so obvious is the mechanism that permits the laser to interact so strongly with the sodium vapour over such a large wavelength interval. Kumar et al[15] have also noted that strong infrared emission is observed from sodium vapour when the exciting laser is tuned over a 3.4 nm interval centred on the resonance lines. Their results do not, however, reveal a minimum in this emission when the laser is tuned onto either of the resonance lines, but this could be due to their poor spectral resolution. Kumar et al[15] attribute the large wavelength range of the interaction to laser induced power broadening of the resonance lines. We believe that this explanation is in error due to their assumption of a linear dependence of the power broadening with laser irradiance.

We suspect that the laser is capable of exciting and ionizing the vapour over such a broad range of wavelengths because it is able to couple a significant amount of power to the resonance lines even when it is appreciably detuned. In effect saturation of the resonance transitions is maintained over this wide detuning interval due to the broad wings of both the absorption and laser spectral profiles. We intend to test this explanation by measuring the spectral distribution of the laser pulse.

3.2 *Vapour Density Measurements*

The temperature within the *sandwich oven* is monitored by several thermocouples positioned between both top and bottom disc heater blocks and the oven. If the sandwich oven operated according to heat pipe principles the temperature and therefore the vapour density should be uniform over a disc shaped region, then fall rapidly with radius in the vicinity of the water cooled lip. The density in the uniform region should be determined primarily by the temperature of the vapour[24] and the radius of the vapour disc should be controlled by the argon buffer gas pressure.

Under operating conditions the temperature from the various thermocouples did not agree to better than 10%. Consequently, an independent means of assessing the sodium atom density was sought. A simple means of monitoring the sodium vapour was devised based on our spectral hole work, reported earlier. A Xenon light source and a specially designed optical

system was used to produce a narrow beam of broad band collimated radiation. This beam was directed through the sodium vapour and its transmitted spectrum was measured by means of a scanning Heath monochromator and an attendant (RCA 1P21) photomultiplier. The output of the photomultiplier was displayed on an X-Y plotter, see figure 13.

It is apparent from equation (1) that in the case of resonance broadening of an isolated line.

$$I(\lambda,R) = I(\lambda,-R) \exp\left[-\frac{\lambda^4}{8\pi c\tau_{21}}\int_{-R}^{R}\frac{\gamma N_1^2(r)dr}{(\lambda-\lambda_o)^2+\gamma^2N_1^2(r)}\right] \qquad (6)$$

where τ_{21} is the radiative lifetime and λ_o the line centre wavelength of the transition. Equation (6) also implicitly assumes that for resonance broadening the HWHM line width

$$\Delta\lambda_{1/2} = \gamma N_1(r) \qquad (7)$$

In the case of the sodium resonance doublet, the transmissivity

$$T(\lambda,R) \equiv \frac{I(\lambda,R)}{I(\lambda,-R)} = \exp\left[-\frac{\lambda^4}{8\pi c}\left\{\frac{1}{\tau_{3/2}}\int_{-R}^{R}\frac{\gamma_{3/2}N_1^2(r)dr}{(\lambda-\lambda_{3/2})^2+\gamma_{3/2}^2N_1^2(r)}\right.\right.$$

$$\left.\left.+\frac{1}{\tau_{1/2}}\int_{-R}^{R}\frac{\gamma_{1/2}N_1^2(r)dr}{(\lambda-\lambda_{1/2})^2+\gamma_{1/2}^2N_1^2(r)}\right\}\right] \qquad (8)$$

where the 3/2 and 1/2 subscripts are taken to refer to the 589.0 ($3^2P_{3/2}$-$3^2S_{1/2}$) and 589.6 nm ($3^2P_{1/2}$-$3^2S_{1/2}$) resonance transitions respectively. According to Sobelman et al[25]

$$\gamma_{3/2} = 0.93 \times \frac{1}{2} r_e f_{12} \lambda_{3/2}^3$$

and (9)

$$\gamma_{1/2} = 0.58 \times \frac{1}{2} r_e f_{12} \lambda_{1/2}^3$$

where f_{12} represents the total doublet absorption oscillator strength and r_e is the classical electron radius (2.82×10^{-13} cm).

If we further assume that for the sodium doublet

$$\frac{1}{\tau_{3/2}} = \frac{2}{3}\frac{1}{\tau_{21}} \qquad \text{and} \qquad \frac{1}{\tau_{1/2}} = \frac{1}{3}\frac{1}{\tau_{21}} \tag{10}$$

and a uniform ground state atom density N_1 across the diameter of the vapour disc, then we can write

$$T(\lambda,R,N_1) = \exp\left[-\frac{g_2}{3g_1}\cdot\frac{\lambda^9 R N_1^2}{64\pi^3 c^2 \tau_{21}^2}\,\xi(\lambda,N_1)\right] \tag{11}$$

where

$$\xi(\lambda,N_1) = \frac{1.86}{(\lambda-\lambda_{3/2})^2+\gamma_{3/2}^2 N_1^2} + \frac{0.58}{(\lambda-\lambda_{1/2})^2+\gamma_{1/2}^2 N_1^2} \tag{12}$$

For the sodium resonance doublet, $\gamma_{3/2} = 2.6\text{x}10^{-26}$ cm^4 and $\gamma_{1/2} = 1.6\text{x}10^{-26}$ cm^4.

In order to calculate the true transmissivity $T^*(\lambda,R,N_1)$ equation (11) has to be convoluted with the instrumental response function to allow for the limited resolution of the monochromator. This instrumental response function is reasonably well approximated by a Gaussian function and the resulting convolution has been performed numerically.

The diameter of the sodium disc is determined by scanning the sandwich oven past the beam in order to assess the positions at which the absorption associated with the vapour suddenly decreases. In effect, this defines R and -R, assuming circular symmetry. The transmissivity $T^*(\lambda,R,N_1)$ has been calculated for a range of densities corresponding to a given R and the resulting spectral holes compared with the experimentally observed spectral hole. Two examples are presented as figure 14. This comparison has been used to estimate the average sodium vapour density during experimental runs. These densities are, in general, lower than expected from the thermocouple temperatures. However, there is also a significant spread in the thermocouple readings which suggests that the thermocouple temperatures may not truly reflect the temperature within the oven due to temperature gradients in the oven structure.

3.3 *Stark Width Electron Density Measurements*

Stark broadening measurements represent a well known method of determining the free electron density within a plasma.[25] Grumberg et al[27] observed excellent agreement between the measured and computed[26b]

linewidths of the 568.2 and 568.8 nm lines of sodium The 568.8 nm line was chosen for our experiments for the reasons indicated earlier. Our approach involves measuring the ratio of the line emission in two adjacent spectral windows for it can be shown[22] that with the right choice of windows this ratio is directly related to the free electron density.

Basically, the voltage signal obtained across the oscilloscope input impedance and having its origin in the output current of the channel 1 photomultiplier (RCA 1P21) can be expressed in the form

$$V_1(t) = A_1 P(t) \int_{-\infty}^{\infty} \mathcal{L}(x') T_1(x'-x_1') dx' \qquad (13)$$

where A_1 represents a *system constant* that includes the photomultiplier's sensitivity and spectral response, and the oscilloscope input impedance,

$P(t)$ represents the spectrally integrated power from the 568.8 nm line falling upon the photomultiplier's photocathode,

$\mathcal{L}(x')$ represents the emission line profile function (which is assumed to be dominated by Stark broadening for the conditions of interest),

$T_1(x'-x_1')$ represents the transmission function of the receiver optics (which includes the monochromator and channel 1 of the fiber array) at the *reduced wavelength*

$$x' \equiv (\lambda-\lambda_o-d')/w' \qquad (14)$$

where λ is the observed wavelength, λ_o the unperturbed emission line centre wavelength, d' the Stark shift and w' the Stark width.[26] x_1' represents the reduced wavelength corresponding to the peak value of the transmission function for channel 1.

If we introduce the filter function for channel 1

$$K_1 \equiv \int_{-\infty}^{\infty} T_1(x'-x_1') dx' \qquad (15)$$

and assume that the transmission function can be approximated by a Gaussian profile so that we can write

$$T_1(x'-x_1') = \frac{K_1}{\delta_1\sqrt{\pi}} e^{-[(x'-x_1')/\delta_1]^2} \tag{16}$$

where δ_1 can be related to the HWHM of the transmission function, $\Delta\lambda_1$, through the relation

$$\delta_1 = \frac{\Delta\lambda_1}{w'\sqrt{\ell n 2}} \tag{17}$$

Under these conditions we can write

$$V_1(t) = \frac{A_1K_1}{\sqrt{\pi}} P(t)\eta_1(x_1', N_e) \tag{18}$$

where

$$\eta_1(x_1', N_e) = \frac{1}{\delta_1}\int_{-\infty}^{\infty} \mathcal{L}(x')e^{-[(x'-x_1')/\delta_1]^2} dx' \tag{19}$$

Similar reasoning for channel 2, which used a more sensitive RCA 8575 photomultiplier, leads us to conclude that the ratio of the voltage signals

$$V_{21} \equiv \frac{V_2(t)}{V_1(t)} = \frac{A_2K_2}{A_1K_1} R_{21}(x_1', x_2', N_e) \tag{20}$$

where the *two channel response function*

$$R_{21}(x_1', x_2', N_e) = \frac{\frac{1}{\delta_2}\int_{-\infty}^{\infty} \mathcal{L}(x')e^{-[(x'-x_2')/\delta_2]^2} dx'}{\frac{1}{\delta_1}\int_{-\infty}^{\infty} \mathcal{L}(x')e^{-[(x'-x_1')/\delta_1]^2} dx'} \tag{21}$$

has been evaluated[22] for several different wavelength settings of λ_1 and λ_2 and different transmission widths $\Delta\lambda_1$ and $\Delta\lambda_2$. Clearly the ratio of the signals from the two photomultipliers V_{21} can be directly related to the electron density by reference to the two channel response function $R_{21}(\lambda_1, \lambda_2, N_e)$ or $R_{21}(N_e)$ for short via the relation

$$V_{21} = S_{21}R_{21}(N_e) \tag{22}$$

where S_{21} is termed the sensitivity factor and is evaluated by means of a calibration experiment. The centre wavelength for channel 1 was set fairly close to the line centre wavelength of the observed line (i.e., λ_1 = 568.922 nm) while the corresponding centre wavelength for channel 2 was λ_2 = 569.128 nm.

The transmission function for each of the two optical channels was determined by sweeping the 568.8 nm line from a sodium reference lamp across the fiber optic array. Representative results with their Gaussian approximations are presented as figure 15. In this instance the channel wavelengths were λ_1 = 568.922 nm and λ_2 = 569.128 nm. It is also apparent that $\Delta\lambda_1$ = 0.10 nm and $\Delta\lambda_2$ = 0.0525 nm. The asymmetry in the experimental points for channel 1 is attributed to some damage in the fiber optic bundle. Also included in this figure (by way of illustration) are two calculated emission profiles for electron densities of 4×10^{15} and 10^{16} cm^{-3}. It is clear that while V_{21} would be expected to be of the order of unity for $N_e = 10^{16}$ cm^{-3}, this ratio would be very small for $N_e = 4\times10^{15}$. In general, the sensitivity factor S_{21} appropriate to a given configuration is obtained from such a figure by writing

$$S_{21} = \frac{p_2\Delta\lambda_2}{p_1\Delta\lambda_1} \qquad (23)$$

where p_2 and p_1 represent the peak voltage signals attained on channels 2 and 1 respectively in the calibration run.

In order to determine the sensitivity of this measurement to the electron temperature $R_{21}(N_e)$ was evaluated with λ_1 = 568.922nm, λ_2 = 569.128nm for two electron temperatures (5000 and 20,000 K). The resulting curves are presented as figure 16. The instrumental widths assumed in this calculation were $\Delta\lambda_1$ = 0.10 nm and $\Delta\lambda_2$ = 0.0525 nm. It is apparent from this figure that a reasonably accurate (to within 20%) estimate of the electron density, over the range 4×10^{15} to 1.3×10^{16} cm^{-3}, can be made even if the electron temperature is not known with any real precision.

The electron density time history for a given shot is evaluated by first digitizing the two oscilloscope traces corresponding to the signals from channels 1 and 2. A representative pair of traces is presented as figure 17, the inverted trace corresponds to the signal from channel 1. A comparison of this figure with figure 10 reveals that the signal duration of both channels 1 and 2 are considerably shorter than that of the third PMT

(the inverted trace in figure 10) which is spectrally centred on the 568.8 nm line. This is to be expected in light of the off-centred transmission functions for channels 1 and 2, see figure 15. Indeed, closer inspection of figure 17 indicates that the signal from channel 2 decays faster than that from channel 1. This can be understood in terms of a decrease in both the width and shift of the 568.8 nm line with recombination of the plasma.

A preliminary set of digitized signals, their concomitant signal ratio and the resulting electron density time history is presented as figure 18. In this shot, the average sodium atom density N_o = 1.05×10^{16} cm^{-3}; the laser energy E_ℓ = 150 (±10) mJ; and the laser wavelength λ_ℓ = 589.0 nm. These observations were undertaken 0.75 cm from the centre of the sandwich oven. Although the electron density measurements are only reliable[22] for $N_e > 5 \times 10^{15}$ cm^{-3}, it is quite apparent that full ionization is achieved, in agreement with our theoretical work. It should also be noted that if we display the signal from channel 1 with the signal from the photodiode monitoring the incident laser pulse, we could directly evaluate the time to achieve 90% ionization and compare this with the predictions of our LIBORS code.

At the time of writing we are preparing to undertake such measurements and also examine the variation in the peak electron density with detuning of the laser. We also hope to shortly undertake the first measurements of the ground level burnout factor using the spectral hole technique discussed earlier.

4. GROUND LEVEL BURNOUT IN BORON III

The degree of ground level burnout attainable through laser resonance saturation is of fundamental importance to our approach at the development of efficient short wavelength lasers. It is evident that the greater the reduction in the ground level population the easier it becomes to create a ground level population inversion. In order to estimate the limiting value of the *ground level burnout factor*,

$$\alpha \equiv N_1^q / N^{q+1} \tag{24}$$

where N_1^q represents the ground level population of the ion of charge q and

N^{q+1} represents the density of ions of charge *q+1*, we have undertaken a steady state analysis. This analysis was described in our (1981) AFOSR report where the calculations were undertaken for the case of sodium vapour. Our analysis revealed that when allowance was made for both radiation cooling and thermal conduction the ground level burnout factor α at first decreased with increasing density, then beyond some critical density increased with increasing density. In the case of sodium we found

$$\alpha_{min}^{Na} \cong 6.6 \times 10^{-5}$$

and this was predicted to occur for a sodium density $N_o \cong 2 \times 10^{17}$ cm^{-3}.

We have now extended this analysis to the case of doubly ionized boron, for, as pointed out in the 1981 AFOSR report, this looks like an attractive candidate for creating a GLIP through charge exchange (and rapid cooling) with an atomic cloud of copper. A significant difference between our present calculations and that undertaken previously for sodium relates to our inclusion of *inverse bremsstrahlung* heating. This was neglected in our earlier work on sodium. As might be expected this improves the degree of burnout predicted and in the case of boron III this improvement amounts to a factor of close to two. As with the sodium case we find that the ground level burnout factor for a doubly ionized boron plasma also rapidly decreases with density, achieving a minimum value

$$\alpha_{min}^{BIII} \cong 4.6 \times 10^{-4} \quad \text{(for BIII density of } 2 \times 10^{18} \text{ cm}^{-3}\text{)}$$

This is indicated in figure 19 for $\beta = 1.0$, where β represents the *conduction loss factor* – a parameter that we have introduced to allow for the fact that under certain conditions the conduction loss may well be somewhat less than used in this calculation. For example, if the plasma is expanding into a vacuum or across a magnetic field electron thermal conduction could be reduced. The broken curves in figure 19 correspond to $\beta = 0.1$ and under these circumstances $\alpha_{min}^{BIII} \sim 2.3 \times 10^{-4}$ (for BIII density of 7×10^{17} cm^{-3}). These values for the minimum ground level burnout factors are quite attractive in terms of being able to create a ground level inversion within a doubly ionized boron plasma.

5. GROUND LEVEL INVERSION BASED ON RESONANT CHARGE EXCHANGE

In our main approach towards the development of an efficient short wavelength laser we assume that a high degree of ground level burnout is achieved within some ionic species through laser resonance saturation. Subsequently this plasma is projected into a dense cloud of atoms leading to a rapid cooling and repopulation of the upper states of the GLB-ion through three-body recombination. Even more important, we assume that the atoms that constitute this cloud have been chosen to undergo *resonance charge exchange* with the ion and thereby selectively populate a particular upper level of the GLB-ion. Potential combinations are presented as figure 20.

A criterion for the creation of a "*ground level* inverted population" GLIP can be developed in terms of the density gradient of the atomic cloud if we assume that charge exchange collsiions are the dominant mechanism for repopulation of the upper levels of the GLB-ion. In reality rapid cooling will enhance the three-body recombination rate which also preferentially populates the upper levels. A simplified energy level diagram for the two constituents involved is presented as figure 21.

The volume rate of population of the level $|q,3\rangle$ (which in this instance represents the potential laser level — q is taken as the charge on the GLB-ion) through *resonance charge exchange* collisions with the atoms in their ground level is assumed to be S(t). In the rest frame of the (q+1)-ions we can write

$$S(t) = N_A(t) N_1^{q+1} \langle \sigma v \rangle_{cx} \tag{25}$$

where N_1^{q+1} represents the density of ground state ions of charge *q+1*, $N_A(t)$ represents the density of ground state atoms at the instant of interest — which corresponds to the density of these atoms at a distance ut within the atomic cloud, u representing the relative velocity between the cloud and the (q+1)-ions. $\langle \sigma v \rangle_{cx}$ represents the resonance charge exchange collision rate coefficient.

For a semi-infinite cloud of atoms having a zero density boundary at the z=0 plane we can write

$$N_A(t) = \int_0^t \left\{ \frac{\partial}{\partial t} N_A + u \frac{\partial}{\partial z} N_A \right\} dt \tag{26}$$

so that if we assume a steady state within the cloud,

$$N_A(t) = \int_0^{ut} \frac{dN_A}{dz}\, dz \tag{27}$$

and for a linear density profile over the range $0 < z \leq z_A$, we have

$$N_A(t) = N_A ut/z_A \tag{28}$$

where N_A is the maximum atom density within the cloud (for $z > z_A$). Furthermore, if the relative velocity of approach between the ions and the cloud is of the order of the thermal velocity of the ions, then

$$\langle \sigma v \rangle_{cx} \cong \sigma_{cx} u \tag{29}$$

and if we introduce

$$S_o \equiv N_A N_1^{q+1}\, \sigma_{cx} u^2/z_A \tag{30}$$

then we can write

$$\frac{d}{dt}\, N_3^q(t) = S_o(t) - N_3^q(t)\{A_{31}^q + N_e K_3^q\} \tag{31}$$

where $N_3^q(t)$ is the population density of the $|q,3\rangle$ level (the potential laser level), A_{31}^q represents the Einstein spontaneous transition probability for the potential laser transition, N_e is the free electron density and K_3^q represents the total rate coefficient for electron collisional depopulation of the $|q,3\rangle$ level. Clearly, to minimize the requirements for creating a GLIP, we must assume that $A_{31}^q >> N_e K_3^q$ and so we have

$$\frac{d}{dt}\, N_3^q(t) = S_o t - N_3^q(t)/\tau \tag{32}$$

and

$$\frac{d}{dt}\, N_1^q(t) = N_3^q(t)/\tau \tag{33}$$

where we have introduced the radiative lifetime of the potential laser level

$$\tau \equiv 1/A_{31}^{q} \tag{34}$$

and $N_1^q(t)$ represents the GLB-ion ground state population density (the potential terminal level for the laser transition). It should be noted that equation (33) tantamounts to stating that the only means of populating the ground level of the GLB-ion is through radiative decay of the level being selectively populated by charge exchange collisions. This assumption is based on the premise that radiative decay dominates collisional decay and that A_{31}^q is one of the largest radiative decay rates for repopulating the ground level of the ion.

If we assume that $N_3^q(o) = 0$, i.e., essentially no population existed in the $|q,3\rangle$ level prior to repopulation through charge exchange collisions, then the solution of equation (32) takes the form

$$N_3^q(t) = S_o\tau^2 \left\{\left\{ \frac{t}{\tau} - 1\right\} + e^{-t/\tau}\right\} \tag{35}$$

We introduce the *ground level population inversion density*

$$\mathcal{N}(t) \equiv N_3^q(t) - gN_1^q(t) \tag{36}$$

where $g \equiv g_3/g_1$ is defined as the ratio of the degeneracies of levels $|q,3\rangle$ and $|q,1\rangle$, respectively. Combining equations (32) and (33) yields

$$\frac{d\mathcal{N}(t)}{dt} = S_o t - (1+g)N_3^q(t)/\tau \tag{37}$$

and with the solution given by equation (35) we have

$$\frac{d\mathcal{N}(t)}{dt} = S_o[(1+g)\tau\{1-e^{-t/\tau}\} - gt] \tag{38}$$

This yields

$$\mathcal{N}(t) = \mathcal{N}(o) + S_o\left[(1+g)\tau\{t + \tau(e^{-t/\tau} - 1)\} - \frac{gt^2}{2}\right] \tag{39}$$

where

$$\mathcal{N}(o) = -gN_1^q(o) \tag{40}$$

This follows from the definition of $\mathcal{N}(t)$ and the condition $N_3^q(o) = 0$. From physical considerations we expect that $\mathcal{N}(t)$ will be a maximum when $d\mathcal{N}(t)/dt = 0$, or from (38) when

$$t = (1+g)\tau\{1-e^{-t/\tau}\}/g \tag{41}$$

Although this is a transcendental equation for t, it can nevertheless be used directly in (39) to yield

$$\mathcal{N}_{max} = S_o t^*[\tau - gt^*/2] - gN_1^q(o) \tag{42}$$

where t* is the solution of equation (41).

Clearly, a ground level inversion can only arise if $\mathcal{N}_{max} > 0$, that is to say,

$$S_o > \frac{gN_1^q(o)}{t^*[\tau - gt^*/2]} \tag{43}$$

This criterion can be restated in terms of the *density gradient* of the atomic cloud, or from equation (30),

$$\frac{dN_A}{dz} = \frac{N_A}{z_A} > \frac{gN_1^q(o)}{N_1^{q+1}\sigma_{cx}u^2 t^*[\tau - gt^*/2]} \tag{44}$$

Now if the GLB-ion has been selected to achieve a high degree of ground level burnout, then the excited states of the (q+1)-ion will be very energetic in terms of the ionization energy of the q-ion and consequently they will only be sparsely populated – this means that the bulk of the (q+1)-ions will reside in the ground level and hence $N^{q+1} \simeq N_1^{q+1}$. Furthermore, if in the times of interest (i.e., the times to create a GLIP) only a small fraction of the (q+1)-ions have recombined, then we can replace the ratio $N_1^q(o)/N_1^{q+1}$ in (44) by g, the GLB factor achieved prior to the recombination promoted by the resonant charge exchange collisions. We may thus write

$$\frac{dN_A}{dz} > \frac{g\sigma}{u^2\sigma_{cx}t^*[\tau - gt^*/2]} \tag{45}$$

For the lithium isoelectronic series of ions, B_eII, BIII, CIV, etc.,

$$g = 3 \tag{46}$$

and since the solution of the transcendental equation for t*, equation (41) yields

$$t^* \cong 0.6\tau \tag{47}$$

we can see that the criterion for creating a GLIP becomes

$$\frac{dN_A}{dz} > \frac{50\alpha}{u^2\sigma_{cx}\tau^2} \tag{48}$$

In the case of BIII, $\tau \cong 0.8$ nsec, and if we take $\sigma_{cx} \cong 10^{-15}$ cm^2 then

$$\frac{dN_A}{dz} > 7.8 \times 10^{34} \frac{\alpha}{u^2} \tag{49}$$

It is not unreasonable to expect that we could make the relative velocity between plasma and the atomic cloud of the order of 10^6 cm sec^{-1}. Under these circumstances we require

$$\frac{dN_A}{dz} > 7.8 \times 10^{22}\alpha \ (cm^{-3}/cm) \tag{50}$$

and we see that the criterion now boils down to a limit on the density gradient of the atomic cloud in terms of the GLB factor achieved through laser resonance saturation. In accordance with our above calculations for BIII, we can write $\alpha_{min}^{BIII} \sim 5 \times 10^{-4}$. This would lead to the criterion

$$\frac{dN_A}{dz} > 3.9 \times 10^{19} \ (cm^{-3}/cm) \tag{51}$$

which can be thought of as a density jump of about 4×10^{18} cm^{-3} in a 1 mm layer – a fairly strong density gradient, but one that might be attainable.

If we assume that a comparable degree of ground level burnout could be achieved in singly ionized beryllium through laser resonance saturation, then in this instance we would require

$$\frac{dN_A}{dz} > 6.9 \times 10^{17} \text{ cm}^{-3}/\text{cm} \qquad (52)$$

which translates into a density jump of 6.9×10^{16} cm^{-3} in a 1 mm layer. The more reasonable density gradient associated with B_eII follows from the 6 nsec lifetime of the 103.67 nm transition, assuming all of the other factors remain the same.

6. NEUTRAL ALUMINUM CLOUD EXPERIMENTS

As indicated above, the attainment of a ground level inversion through resonant charge exchange requires the production of a relatively dense cloud of suitable atoms having a steep density gradient. In the case of the B_eII and AlI, charge exchange pair, see figure 20, we have estimated that the gradient of ground state aluminum atoms would probably have to exceed 7×10^{17} cm^{-4}.

We believe that there are several possible methods of attaining this kind of neutral atom density gradient: Laser heating of a thin foil-glass interface, electron beam heating of a foil or joule heating of a foil in a vacuum. In keeping with our high efficiency philosophy we have chosen to study the sudden joule heating approach first. However, the diagnostic techniques we are developing should be applicable to evaluate the density gradients attained, whichever approach is used.

6.1 *Exploding Foil Facility and Preliminary Emission Measurements*

We have constructed a capacitor discharge circuit for generating a large current pulse within a strip of aluminum foil placed in a vacuum. The small capacitor bank comprises six 8.5 μF BICC capacitors that are connected in parallel and charged to 1650 volts. A small EEV GHX-T sparkgap is used to discharge this 70 J through the strip of aluminum foil called a *fuse*. Ten such foil strips are cut out of one sheet of foil and mounted on a rotateble holder within an evacuated six-port glass chamber as shown in figure 22. The complete fuse holder assembly is shown in figure 23. Each fuse is connected in turn to the capacitor bank via a banana plug. This approach has eliminated the arcing observed in our earlier arrangement.

The emission from the atomized aluminum cloud was monitored by two photomultipliers (RCA 1P28A and a RCA 931A). The 931A photomultiplier was positioned in front of the fuse in order to respond to the earliest emission and thereby provide a zero time reference signal. The 1P28A photomultiplier was used to either detect the emission from the expanding atomized cloud at some distance from the fuse holder surface or to monitor the dye laser output. The former arrangement enabled both the expansion velocity and temperature of the atomized cloud to be evaluated.

The ground state aluminum atom density was estimated by means of *near resonance absorption photography*.[28] In this approach a short pulse (5 nsec) from a suitably tuned nitrogen pumped dye laser is directed through the atomized cloud and photographed. If the wavelength of the laser is tuned to lie close to that of the 396.1 nm aluminum resonance line then appreciable attenuation is expected from regions of high atom density. A schematic diagram of the experimental arrangement is presented as figure 24.

The output of the nitrogen pumped dye laser was spectrally controlled by means of an intra-cavity grating and a beam expander. This system also enabled the laser line width to be narrowed to better than 0.04 nm and provided a wavelength stability of ±0.01 nm. The Exciton PBBO #04001 laser dye used had a maximum efficiency at about 396 nm and a useful tuning range of 378 to 440 nm. No measurements of the output energy were made since the only requirement for the laser energy fluence was that it be adequate to expose the film in the camera after passing through the system in the absence of the aluminum vapour.

The expansion velocity was estimated from the time delay between the emission signals obtained from the *front on* and *side viewing* photomultipliers. The latter receives light only once the atomized cloud emerges from beyond a specially positioned light baffle. This baffle was designed to prevent any extraneously scattered light from reaching the side-viewing photomultiplier prior to the expanding plasma entering its field of view. At a background pressure of 0.03 torr of nitrogen the expansion velocity, averaged over the 3.2 cm width of the light baffle, was approximately 6×10^5 cms^{-1}.

The spatially averaged electron temperature T_e of the atomized cloud was determined from the relative intensity ratio of two emission lines. If LTE prevails then it is well known, Griem,[26a] that the ratio of the two

emission signals arising from $|n\rangle$ to $|m\rangle$ and $|p\rangle$ to $|q\rangle$ transitions within the same species

$$S = A \exp(-E_{np}/kT_e) \tag{53}$$

where E_{np} represents the energy difference between the upper levels of the two transitions and A is a system constant that depends upon the photomultiplier response at the two wavelengths, and a ratio of atomic parameters, viz.,

$$A \equiv \frac{\eta(\lambda_{nm})\lambda_{pq}A_{nm}g_n}{\eta(\lambda_{pq})\lambda_{nm}A_{pq}g_p}$$

where $\eta(\lambda_{\alpha\beta})$ represents the spectral response of the photomultiplier at the wavelength $\lambda_{\alpha\beta}$ and $A_{\alpha\beta}$ represents the appropriate Einstein transition probability. g_α represents the degeneracy of the $|\alpha\rangle$ level.

It follows from (53) that the uncertainty in the temperature measurement $\Delta T_e/T_e$ can be related to the uncertainty in the signal ratio measurement by the expression

$$\frac{\Delta T_e}{T_e} = - \frac{kT_e}{E_{np}} \cdot \frac{\Delta S}{S}$$

Clearly, E_{np} should be chosen to be as large as possible compared to kT_e.

After an initial study of the aluminum spectra the 390.0 nm ($^1P^o$-^1D) and 623.2 nm ($^3P^o$-^3D) transitions of AlII were selected as both lines could be observed in spite of the 4.46 eV energy separation of their upper levels. This relatively large value for E_{np} implied that the temperature uncertainty would amount to only 22% of the signal ratio uncertainty for a temperature of around 1 eV. A preliminary measurement of the electron temperature yielded a value of (1.40±0.15) eV.

6.2 *Near Resonant Absorption Measurements of Density Gradient*

If the atomized aluminum cloud is assumed to be spherical in nature, then the optical [illegible] presented to the laser radiation at wavelength λ at distance z from the fuse holder surface, see figure 25,

$$\tau(z,\lambda) = 2 \int_{x=0}^{x=\sqrt{R^2-z^2}} k(z,x,\lambda)dx \tag{54}$$

where the absorption coefficient

$$k(z,x,\lambda) = \sigma(\lambda,r)N_1(r) \tag{55}$$

and

$$x = \sqrt{r^2-z^2}$$

R is taken as the radial location of the boundary of the expanding cloud at the instant of interest. $N_1(r)$ represents the aluminum ground state atom density at a distance r from the centre of coordinate system, which is taken to coincide with the centre of the foil strip prior to evaporation. The absorption cross section for radiation at wavelength λ at this location can be expressed in the form

$$\sigma(\lambda,r) = \frac{\lambda^4 g_2}{8\pi c\tau g_1} \mathcal{L}(\lambda,r) \tag{56}$$

where g_2/g_1 represents the degeneracy ratio, and τ the radiative lifetime for the resonance transition, c is the velocity of light and $\mathcal{L}(\lambda,r)$ represents the absorption line profile function at this location. Implicit in this analysis is the assumption that only the resonance transition closest to the laser wavelength is involved in absorption.

If we assume that over the density range of interest Stark broadening dominates, then we can write

$$\mathcal{L}(\lambda,r) = \frac{1}{\pi} \cdot \frac{\Delta\lambda_w(r)}{\{\lambda-\lambda_o+\Delta\lambda_s(r)\}^2 + \Delta\lambda_w^2(r)} \tag{57}$$

where $\Delta\lambda_s(r)$ and $\Delta\lambda_w(r)$ represent the Stark shift and width respectively. As a first approximation we shall assume that the displacement of the laser wavelength λ from the line centre wavelength λ_o is sufficiently large that we can write

$$\mathcal{L}(\lambda,r) \simeq \frac{\Delta\lambda_w(r)}{\pi\{\lambda-\lambda_o\}^2} \tag{58}$$

We shall also assume that over the density range of interest we can neglect ion broadening so that we can write

$$\Delta\lambda_w(r) \simeq \frac{2wN_e(r)}{10^{16}} \tag{59}$$

where w is given by Griem.[26b] If we also assume LTE, then the free electron density $N_e(r)$ can be determined in terms of the electron temperature T_e and the aluminum ground state density $N_1(r)$, viz.,

$$N_e(r) = \left[6\times10^{21} N_1(r)(kT_e)^{3/2} \frac{U^+(T_e)}{g_1} \exp\{-(E_I-\Delta E)/kT_e\}\right]^{1/2} \qquad (60)$$

where $U^+(T_e)$ represents the partition function of the ion, g_1 the ground level degeneracy, E_I the ionization energy of the atom and ΔE the ionization depression. Note that E_I, ΔE and kT_e are all expressed in eV units. Under the conditions of interest ΔE is expected to range between 0.4 and 0.8 and to a first approximation ΔE is set equal to 0.6 eV in (60).

In which case we can write

$$\sigma(\lambda,r) = \frac{2\sigma^A w(T_e)S(T_e)}{10^{16}\pi\{\lambda-\lambda_o\}^2} [N_1(r)]^{1/2} \qquad (61)$$

where $\sigma^A(=\lambda^4 g_2/8\pi c g_1)$ is the spectrally integrated absorption cross section and

$$S(T_e) = \left[6\times10^{21}(kT_e)^{3/2} \frac{U^+(T_e)}{g_1} \exp\{-5.36/kT_e\}\right]^{1/2} \qquad (62)$$

Under these circumstances the optical depth

$$\tau(z,\lambda) = \frac{2\times10^{-16}\sigma^A}{\pi\{\lambda-\lambda_o\}^2} \int_{x=0}^{x=\sqrt{R^2-z^2}} w(T_e)S(T_e)[N_1(r)]^{3/2}dx \qquad (63)$$

If we assume that the ground state atom density distribution

$$N_1(r) = N_o \exp\{-r^2/r_o^2\} \qquad (64)$$

and that the temperature is reasonably uniform over the expanding cloud, then

$$\tau(z,\lambda) = \frac{2\sigma^A N_o^{3/2} w(T_e)S(T_e)}{\pi\{\lambda-\lambda_o\}^2 10^{16}} \int_0^\infty \exp\left\{-\frac{3(z^2+x^2)}{2r_o^2}\right\} dx \qquad (65)$$

The *transmissivity* of the cloud,

$$T(z,\lambda) \equiv \exp\{-\tau(z,\lambda)\} \tag{66}$$

can thus be evaluated. Indeed, we can write

$$T(z,\lambda) = \exp\left[-\left\{\frac{2}{3\pi}\right\}^{1/2} \frac{2r_o\sigma^A w(T_e)S(T_e)N_o^{3/2}}{\{\lambda-\lambda_o\}^2 10^{16}} \exp\left\{-\frac{3z^2}{2r_o^2}\right\}\right] \tag{67}$$

In the case of the aluminum atom, $\lambda_o = 396.1$ nm, $\tau = 10.2$ nsec, $g_2 = g_1 = 2$ and so $\sigma^A \cong 3.2 \times 10^{-22}$ cm^3. If we use $kT_e \cong 1.4$ eV (as estimated from the line ratio measurements assumed earlier) then $S(T_e) \cong 1.23 \times 10^{10}$ and according to Griem,[26b] $w(T_e) \cong 1.65 \times 10^{-10}$ cm. Consequently,

$$T(z,\lambda) \cong \exp\left[-\frac{1.3 \times 10^{-23} r_o N_o^{3/2}}{(\Delta\lambda)^2} \exp\left\{-\frac{3z^2}{2r_o^2}\right\}\right] \tag{68}$$

where $\Delta\lambda$ corresponds to $(\lambda-\lambda_o)$ in nm-units. Transmissivity curves for various values of N_o, r_o and $\Delta\lambda$ have been computed. Two such curves for $N_o = 10^{19}$ cm^{-3}, $r_o = 0.2$ cm, $\Delta\lambda = 1.7$ nm and 3.66 nm are presented as figure 26. Also, included on this figure are the locations of the observed sudden jumps in the transmissivity corresponding to $\Delta\lambda = 1.7$, 2.44 and 3.66 nm as deduced from the near resonance laser photographs taken 3.5 μsec after the start of the plasma emission. A representative set of such photographs are presented as figure 27. The spread in the data arises from the shot-to-shot irreproducibility. In order to check that the sudden transition from light to dark on such photographs corresponded to a change in the transmissivity of about 0.1 to 0.9, a calibration experiment was undertaken using neutral density filters of known attenuation.

It is apparent from figure 25 that the aluminum atom density distribution in the expanding cloud is roughly approximated by a relation of the form

$$N(r) \sim N_o \exp\left\{-\frac{r^2}{r_o^2}\right\}$$

where $N_o \sim 10^{19}$ cm^{-3} and $r_o \sim 0.2$ cm. These results are encouraging for although they are preliminary in nature, nevertheless, they suggest

that quite steep density gradients are produced by this exploding foil technique. Indeed, the gradient for such a Gaussian distribution

$$\left|\frac{dN(r)}{dr}\right| = \frac{2r}{r_o} N_o \exp\left\{-\frac{r^2}{r_o^2}\right\} \tag{69}$$

has a maximum value given by

$$\left|\frac{dN(r)}{dr}\right|_{max} \simeq \frac{N_o}{r_o}\sqrt{\frac{2}{e}} = 0.858\,\frac{N_o}{r_o} \tag{70}$$

and occurs at a distance $r = r_o/\sqrt{2}$. In figure 28 we have plotted both $N(r)$ and $|dN(r)/dr|$ against r for the N_o and r_o values indicated above. From this figure it is evident that the atom density gradient easily exceeds the value of 7×10^{17} cm^{-4} indicated earlier as necessary for the creation of a ground level population inversion through charge exchange interactions.

Further confirmation of the steepness of the atom density gradient was obtained from a close inspection of the light to dark boundary region of the near resonance absorption photographs. Measurements undertaken with the aid of a travelling microscope reveals that the transmissivity jump (0.1 to 0.9) occurs in a distance of less than 1 mm. This can be seen to be consistent with the prediction of our calculations, see figure 26.

As indicated these results are encouraging even though they are only tentative in nature. Currently we are exploring ways of optimizing the foil explosion technique and increasing the accuracy of our diagnostics, in particular we are refining the theoretical basis for interpreting the near resonance absorption data.

ACKNOWLEDGEMENTS

The excellent theoretical and experimental contributions of Paul Cardinal, Mark Cappelli, Harald Herchen, Randy Kissack, Greg Schinn and John Bird are gratefully appreciated. This work has been supported by the U.S. AFOSR under grant No. 80-0057B. Additional support has been provided by the Natural Science and Engineering Research Council of Canada and the Ontario Graduate Scholarship Program.

REFERENCES

1. R. M. Measures, J. Quant. Spectrosc. Radiat. Transfer, 10, 107-125 (1970).
2. R. M. Measures, J. Appl. Phys., 48, 2673-2675 (1977).
3. T. B. Lucatorto and T. J. McIlrath, Phys. Rev. Letters, 37, 428-431 (1976).
4. T. J. McIlrath and T. B. Lucatorto, Phys. Rev. Letters, 38, 1390-1393 (1977).
5. C. H. Skinner, J. Phys. B: Atom. Molec. Phys., 13, 55-68 (1980).
6. F. Roussel, P. Breger, G. Spiess, C. Manus and S. Geltman, J. Phys. B: Atom. Molec. Phys. 13, L631-L636 (1980).
7. T. Stacewicz, Optics Commun. 35, 239-241 (1980).
8. C. H. Skinner, J. Phys. B: Atom. Molec. Phys. 13, L637-L640 (1980).
9. J. Krasinski, T. Stacewicz and C. R. Stroud Jr., Optics Commun. 33, 158-162 (1980).
10. D. J. Krebs and L. D. Shearer, J. Chem. Phys. 75, 3340-3344 (1981).
11. T. Stacewicz and J. Krasinski, Optics Commun. 39, 35-40 (1981).
12. B. Carré, F. Roussel, P. Breger and G. Spiess, J. Phys. B: Atom. Molec. Phys. 14, 4289-4300 (1981).
13. B. Carré, F. Roussel, P. Breger and G. Spiess, J. Phys. B: Atom. Molec. Phys. 14, 4271-4288 (1981).
14. J. L. LeGouet, J. L. Picque, F. Muilleumier, J. M. Bizau, P. Shez, P. Koch and D. L. Ederer, Phys. Rev. Lett., 48, 600-603 (1982).
15. J. Kumar, W. T. Silfvast and O. R. Wood II, J. Appl. Phys., 53, 218-222 (1982).
16. R. M. Measures and P. G. Cardinal, Physical Review A, 23, 804-815 (1981).
17. R. M. Measures, P. G. Cardinal, G. W. Schinn, J. Appl. Phys. 52, 1269-1277 (1981) and 52, 7459 (1981).
18. R. M. Measures, N. Drewell and P. G. Cardinal, Appl. Optics, 18, 1824-1827 (1979).
19. P. G. Cardinal, P. L. Wizinowich and R. M. Measures, J. Quant. Spectrosc. Radiat. Transfer, 25, 537-545 (1981).
20. R. M. Measures, J. Appl. Phys. 39, 5232-5245 (1968).
21. R. W. Boyd and D. J. Harter, Appl. Optics 9, 2660-2661 (1980).

22. M. Cappelli, UTIAS, 1982, M.A.Sc. Thesis.

23. W. Muller and I. V. Hertel, Appl. Phys. 24, 33-38 (1981).

24. A. N. Nesmeyanov, "Vapour Pressure of the Elements" (1963) (Translator J. I. Carano).

25. I. I. Sobelman, L. A. Vainshtein and E. A. Yukov, "Excitation of Atoms and Broadening of Spectral Lines", Springer-Verlag (1981).

26. (a) H. R. Griem, "Plasma Spectroscopy", McGraw Hill (1964).
(b) H. R. Griem, "Spectral Line Broadening by Plasmas", Academic Press (1974).

27. J. Grunberg, G. Coulaud, Nguyen-Hoe, Phys. Lett., 57A, 227-229 (1976).

28. J. P. Geindre, J. C. Gauthier and N. Grandjouan, J. Phys. D: Appl. Phys., 13, 1235=1242 (1980).

CUMULATIVE CHRONOLOGICAL LIST OF PUBLICATIONS (1977-PRESENT)

1. R. M. Measures and H. Herchen, "Laser Absorption Under Saturation Conditions with Allowance for Spectral Hole Burning", Accepted for J. Quant. Spectrosc. Radiat. Transfer. 27 (1982).
2. R. M. Measures, S. K. Wong, P. G. Cardinal, "The Influence of Molecular Nitrogen Upon Plasma Channel Formation by Laser Resonance Saturation", J. Appl. Physics 53, 5541-5551 (1982).
3. M. R. Arnfield and R. M. Measures, "Ion to Neutral Atom Measurements within an Ablation Plasma Through Laser Selective Excitation Spectroscopy", Physical Review A, 24, 535-539 (1981).
4. R. M. Measures, P. G. CArdinal and G. W. Schinn, "Theoretical Model of Laser Ionization of Alkali Vapours Based on Resonance Saturation", J. Appl. Phys. 52, 1269-1277 (1981).
5. P. G. Cardinal, P. L. Wizinowich and R. M. Measures, "Anomalous Laser Energy Absorption Associated with Resonance Saturation", J. Quant. Spectrosc. Radiat. Transfer 25, 537-545 (1981).
6. R. M. Measures and P. G. Cardinal, "Laser Ionization Based on Resonance Saturation - A Simple Model Description", Physical Review A, 23, 804-815 (1981).
7. R. M. Measures, P. L. Wizinowich, P. G. Cardinal, "Fast and Efficient Plasma Heating Through Superelastic Laser Energy Conversion", J. Appl. Phys., 51, 3622-3628 (1980).
8. H. S. Kwong and R. M. Measures, "Lifetime Measurements on Atoms in Compounds Embedded in Matrices Using Laser Selective Excitation and Ablation Dynamics", Appl. Optics, 19, 1025-1027 (1980).
9. R. M. Measures, N. Drewell, P. Cardinal, "Electron- and Ion-Beam Transportation Channel Formation by Laser Ionization Based on Resonance Saturation - LIBORS", J. Appl. Phys. 50, 2622-2669 (1979).
10. R. M. Measures, N. Drewell, P. Cardinal, "Laser Interaction Based on Resonance Saturation (LIBORS): An Alternative to Inverse Bremsstrahlung for Coupling Laser Energy into a Plasma", Appl. Optics, 18, 1824-1827 (1979).
11. H. S. Kwong, R. M. Measures, "Trace Element Laser Microprobe Having High Sensitivity and Freedom from Chemical Matrix Effects", Analytical Chemistry, 51, 428-432 (1979).
12. R. M. Measures, H. S. Kwong, "Development of a Trace Element Analyser Based on Laser Ablation and Selective Excited Radiation - TABLASER",

Appl. Optics, 18, 281-285 (1979).

13. R. M. Measures, N. Drewell, P. Cardinal, "Superelastic Laser Energy Conversion (SELEC)", Radiation Energy Conversion in Space (Ed. K. W. Billman), Vol. 61 of Progress in Astronautics and Aeronautics (1978).
14. R. M. Measures, "PROBE - Profile Resolution Obtained by Excitation", Applied Spectroscopy, 32, 381-388 (1978).
15. R. M. Measures, "PROBE - A New Technique for Measuring the Density Profile of a Specific Constituent Using Counter Propagating Laser Pulses", Appl. Optics, 16, 3016-3026 (1977).
16. R. M. Measures, N. Drewell, H. S. Kwong, "Atomic LIfetime Measurement Obtained by Use of Laser Ablation and Selective Excitation Spectroscopy", Phys. Rev. A, 16, 1093-1097 (1977).
17. R. M. Measures, "Efficient Laser Ionization of Sodium Vapor - A Possible Explanation Based on Superelastic Collisions and Reduced Ionization Potential", J. Appl. Phys., Vol. 48, 2673-2675 (1977).
18. R. M. Measures, "LIDAR Equation Analysis - Allowing for Target Lifetime Laser Pulse Duration and Detector Integration Period", Appl. Optics, Vol. 16, 1092-1103 (1977).

Book

R. M. Measures, "Analytical Use of Lasers in Remote Sensing", Chapter 6 of Analytical Laser Spectroscopy (Ed. N. Omenetto), J. Wiley Publications (1979).

INTERACTIONS

A paper was presented at the IEEE International Conference on Plasma Science, Ottawa, May 17-19, 1982, by R. M. Measures, P. G. Cardinal, M. Cappelli, H. Herchen, S. Wong and R. Kissack, "Laser Ionization Based on Resonance Saturation".

Professor R. M. Measures has been requested to give an "Invited Paper" at the LASER'S 82 Meeting in New Orleans, 1982, title: *Laser Resonance Saturation, An Efficient and Rapid Means of Ionization and Electron Heating.*

PROFESSIONAL PERSONNEL

Principal Investigator:

Dr. R. M. Measures (Professor of Applied Science and Engineering)

Research Assistants:

P. G. Cardinal (Ph.D. Student)

R. S. Kissack (Ph.D. Student)

S. K. Wong (Ph.D. Student)

J. D. Coles (Ph.D. Student)

J. C. Bird (M.A.Sc. Student)

M. A. Cappelli (M.A.Sc. Student)

H. Herchen (M.A.Sc. Student)

G. W. Schinn (M.A.Sc. Student)

S. D. Hanratty (M.A.Sc. Student)

NEW DISCOVERIES STEMMING FROM RESEARCH

Saturation of an atomic transition by the intense radiation field of a suitably tuned laser represents an important kind of interaction with a wide range of potential applications. The consequences of laser resonance saturation and the applications stemming from this interaction depend to a very large extent upon the period of saturation. If the resonance to ground level populations are only momentarily locked in the ratio of respective degeneracies (saturation) the principal effect is a burst of intensified spontaneous emission that can be used to diagnose the excited medium.[1,2] On the other hand an extended period of saturation (lasting for much longer than the resonance state lifetime) can lead to extensive perturbation of the medium.[3,4] Indeed, if the free electron superelastic collision time is short compared to the duration of the laser pulse near total ionization of the laser pumped species is rapidly achieved.[4-19] In the case of an ionic species extremely rapid changes of electron temperature can be produced by this means.[20]

The author was the first to recognize the importance of laser saturation and many of its possible areas of application.[1-4] Subsequent work in the author's laboratory and elsewhere have proven that laser resonance saturation does represent a significant form of interaction between laser radiation and atomic vapours or plasmas.

Momentary laser saturation represents a powerful diagnostic technique that is finding application in many areas ranging from fusion reactor studies[21] to combustion measurements.[22,23] The combination of laser ablation and laser saturation spectroscopy represents a new approach at evaluating fundamental atomic quantities such as: radiative lifetimes, branching ratios, transition probabilities and selected collision cross-sections. A preliminary paper on this subject was published by us in Physical Review.[24] This technique, as well as being convenient and accurate, is particularly well suited for measurements on short lived, highly ionized species created by laser ablation. Furthermore, it is versatile and can use multiphoton or stepwise excitation as the means of generating the bursts of intensified emission.

As a spin-off of this work we have also shown that this concept can also form the basis of a new form of trace element laser microprobe called a TABLASER.[25]

More recently, we have demonstrated in a proof of principle experiment that laser saturation spectroscopy can be used to directly measure, with both spatial and temporal resolution, the ion to neutral atom density ratio in a rapidly expanding ablation plasma.[26]

The ionization capabilities of extended laser resonance saturation have now been indisputably demonstrated with a variety of experiments.[5-17] We have developed a model of this laser ionization based on resonance saturation (LIBORS) and have shown that the interaction can be thought to proceed in four stages.[18,19] Confirmation of certain aspects of our theory has been provided by several research groups.[5-17] Recently, there has been some success in using laser resonance saturation for the purpose of creating infrared laser action.[27] Currently, our efforts are concentrating upon obtaining a better understanding of this interaction and in studying how best to employ this fast and very efficient method of coupling laser energy into a plasma for the purpose of developing an efficient short wavelength laser.

1. R. M. Measures, J. Appl. Phys. 39, 5232-5245 (1968).
2. R. M. Measures, Phys. of Fluids, 13, 1889-1890 (1970).
3. R. M. Measures, J. Quant. Spectrosc. Radiat. Transfer, 10, 107-125 (1970).
4. R. M. Measures, J. Appl. Phys., 48, 2673-2675 (1977)
5. T. B. Lucatorto and T. J. McIlrath, Phys. Rev. Letters, 37, 428-431 (1976).
6. T. J. McIlrath and T. B. Lucatorto, Phys. Rev. Letters, 38, 1390-1393 (1977).
7. C. H. Skinner, J. Phys. B: Atom. Molec. Phys., 13, 55-68 (1980).
8. F. Roussel, P. Breger, G. Spiess, C. Manus and S. Geltman, J. Phys. B: Atom. Molec. Phys., 13, L631-L636 (1980).
9. T. Stacewicz, Optics Commun. 35, 239-241 (1980).
10. C. H. Skinner, J. Phys. B: Atom. Molec. Phys., 13, L637-L640 (1980).
11. J. Krasinski, T. Stacewicz and C. R. Stroud Jr., Optics Commun 35, 158-162 (1980).
12. D. J. Krebs and L. D. Shearer, J. Chem. Phys., 75, 3340-3344 (1981).
13. T. Stacewicz and J. Krasinski, Optics Commun., 39, 35-40 (1981).

14. B. Carré, F. Roussel, P. Breger and G. Spiess, J. Phys. B: Atom. Molec. Phys., 14, 4289-4300 (1981).
15. B. Carré, F. Roussel, P. Breger and G. Spiess, J. Phys. B: Atom. Molec. Phys., 14, 4271-4288 (1981).
16. J. L. LeGouet, J. L. Picque, F. Muilleumier, J. M. Bizau, P. Shez, P. Koch and D. L. Ederer, Phys. Rev. Lett., 48, 600-603 (1982).
17. J. Kumar, W. T. Silfvast and O. R. Wood II, J. Appl. Phys., 53, 218-222 (1982).
18. R. M. Measures and P. G. Cardinal, Physical Review A, 23, 804-815 (1981).
19. R. M. Measures, P. G. Cardinal, G. W. Schinn, J. Appl. Phys., 52, 1269-1277 (1981) and 52, 7459 (1981).
20. R. M. Measures, P. L. Wizinowich and P. G. Cardinal, J. Appl. Phys., 51, 3622-3628 (1980).
21. C. H. Muller and K. H. Burrell, Phys. Rev. Lett., 47, 330-333 (1981).
22. J. D. Bradshaw, N. Omenetto, G. Zizak, J. N. Bower and J. D. Winefordner, Appl. Optics, 19, 2709-2716 (1980).
23. G. B. Boutilier, N. Omenetto and J. D. Winefordner, Appl. Optics, 19, 1838-1843 (1980).
24. R. M. Measures, N. Drewell and H. S. Kwong, Phys. Rev. A, 16, 1093-1097 (1977).
25. R. M. Measures and H. S. Kwong, Appl. Optics, 18, 281-286 (1979).
26. M. R. Arnfield and R. M. Measures, Phys. Rev. A, 24, 535-539 (1981).
27. W. Muller and I. V. Hertel, Appl. Phys., 24, 33-38 (1981).

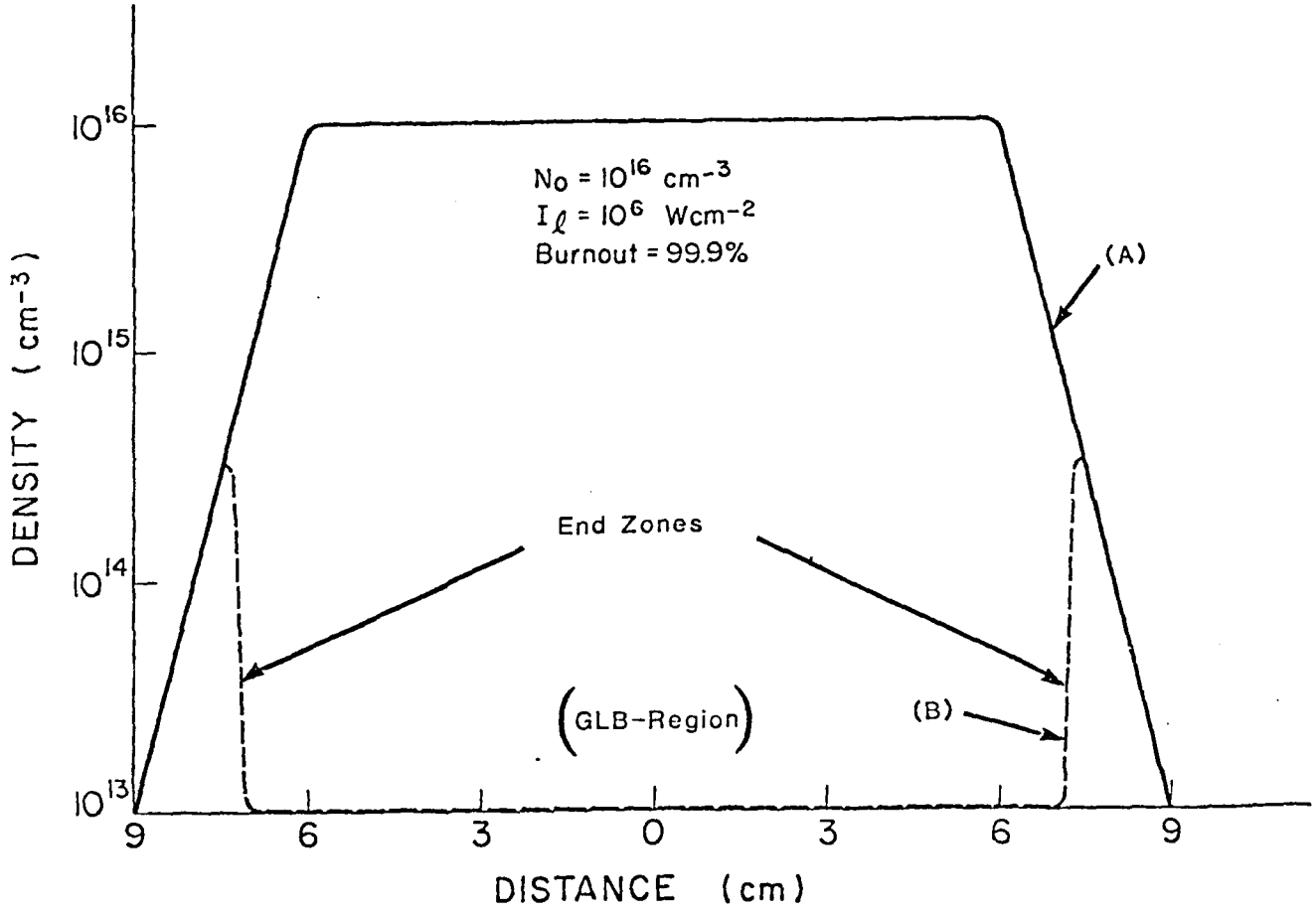

FIG. 1 RADIAL DISTRIBUTION $N_1(r)$ OF GROUND STATE SODIUM ATOMS (A) PRIOR TO LASER IRRADIATION AND (B) 750 NSEC AFTER LASER RESONANCE SATURATION COMMENCED. LASER IRRADIANCE ASSUMED TO BE 10^6 Wcm^{-2} AT ALL POSITIONS.

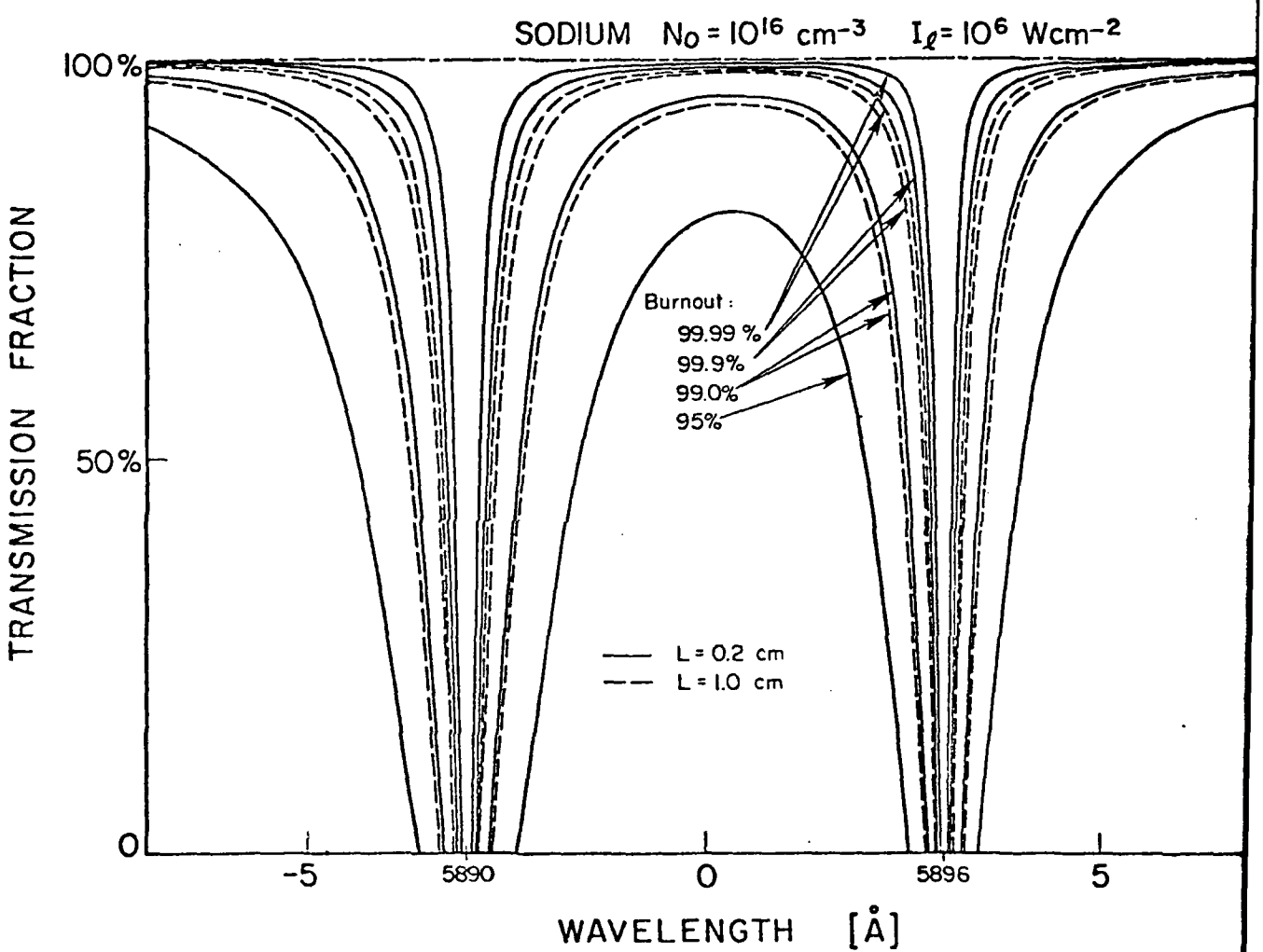

FIG. 2 % SPECTRAL TRANSMISSION CURVES FOR SPECTRALLY UNIFORM SUBSATURATING PROBE LASER RADIATION TRAVERSING A SODIUM VAPOUR DISC WITH A MAXIMUM INITIAL DENSITY OF 10^{16}CM^{-3}. THE CENTRAL REGION OF THE SODIUM VAPOUR IS ASSUMED TO HAVE ATTAINED THE GLB% SHOWN FOR TWO VALUES OF THE END ZONE SCALE LENGTH L. I_ℓ REFERS TO THE IRRADIANCE OF THE IONIZING LASER.

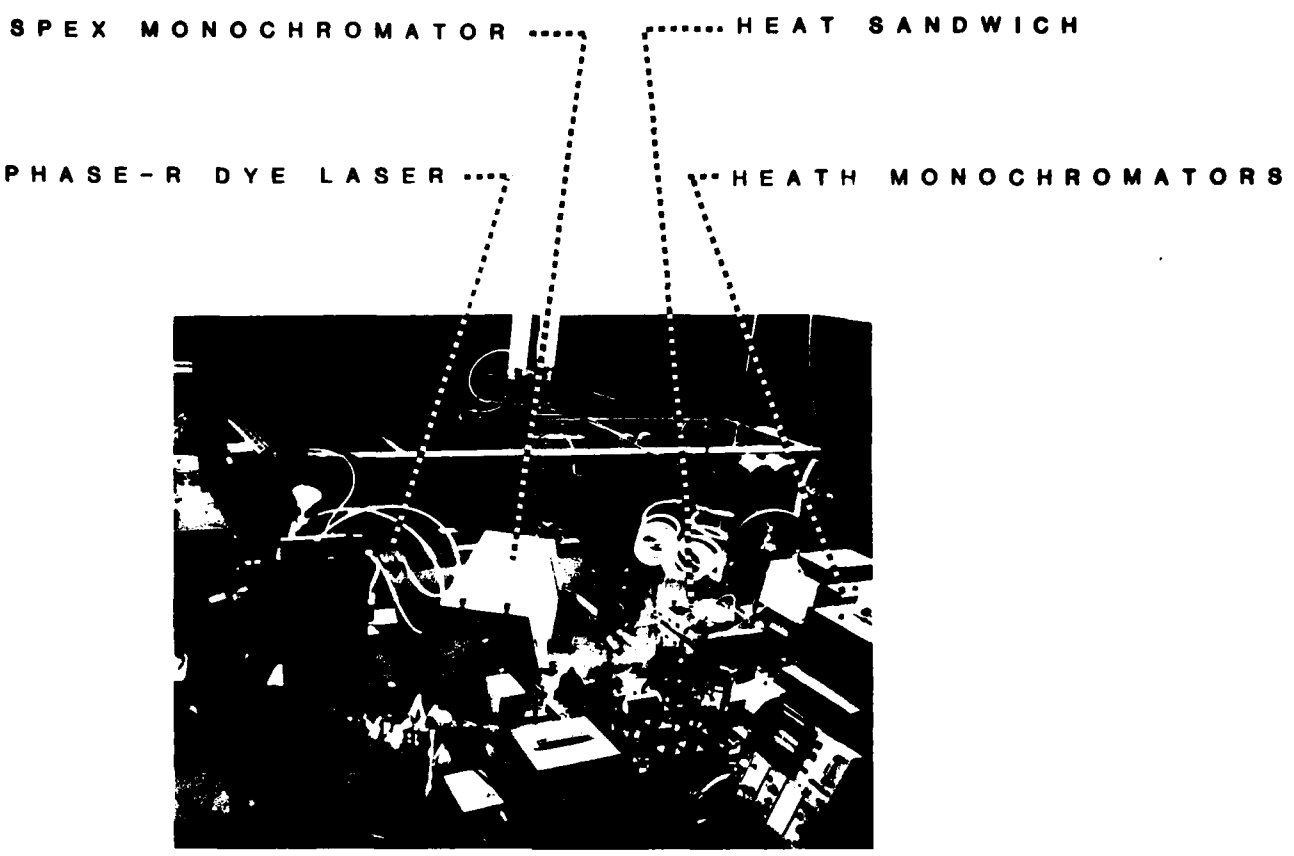

FIG. 3 OVERVIEW OF LIBORS EXPERIMENTAL FACILITY.

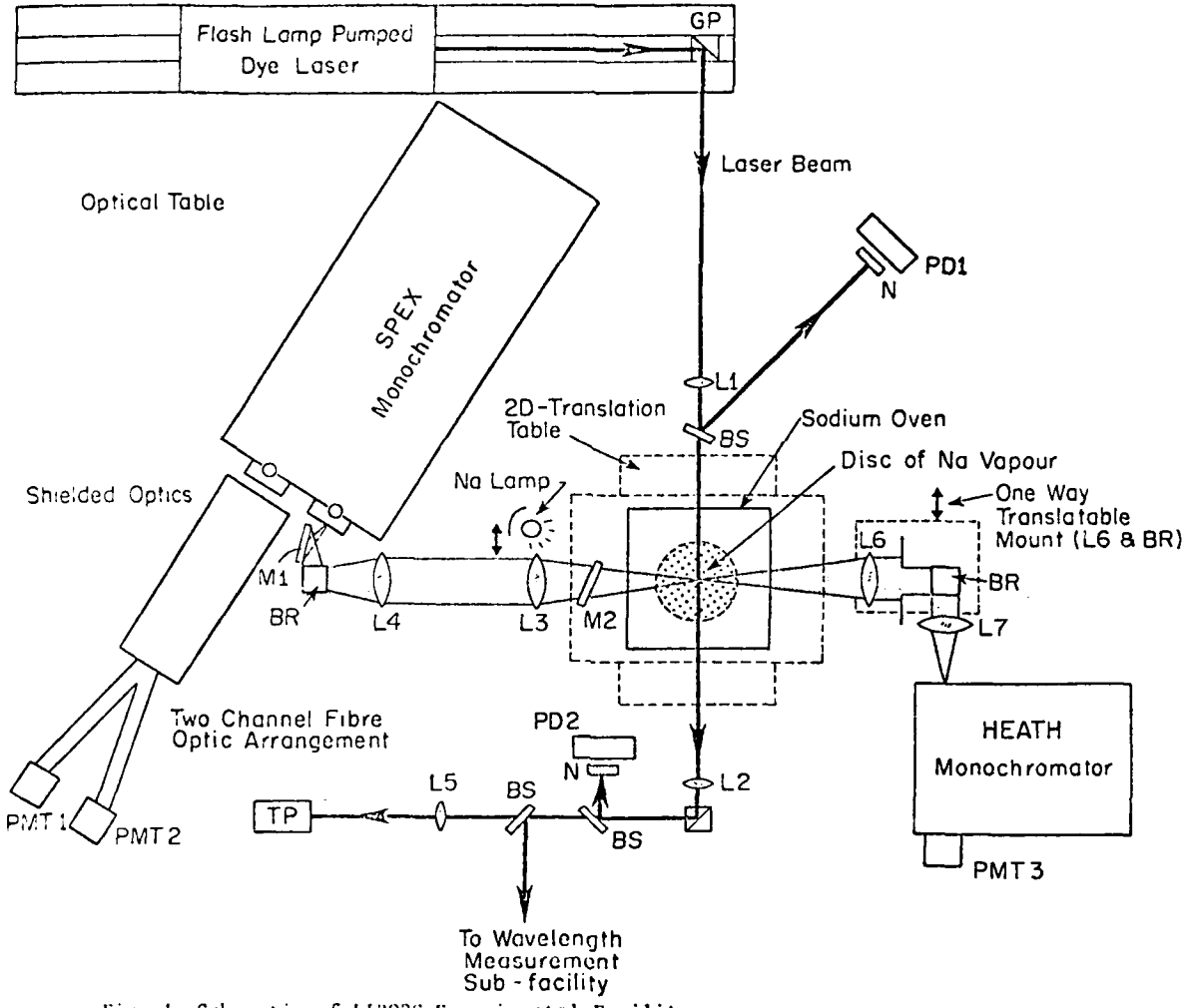

Fig. 4 Schematic of LIBORS Experimental Facility.

Key: PD photodiode detectors; L1, L2... lens; M1 mirror; BS beam splitters; BR 90° beam rotator; PMT photomultipliers; GP glass prism; N neutral density filter.

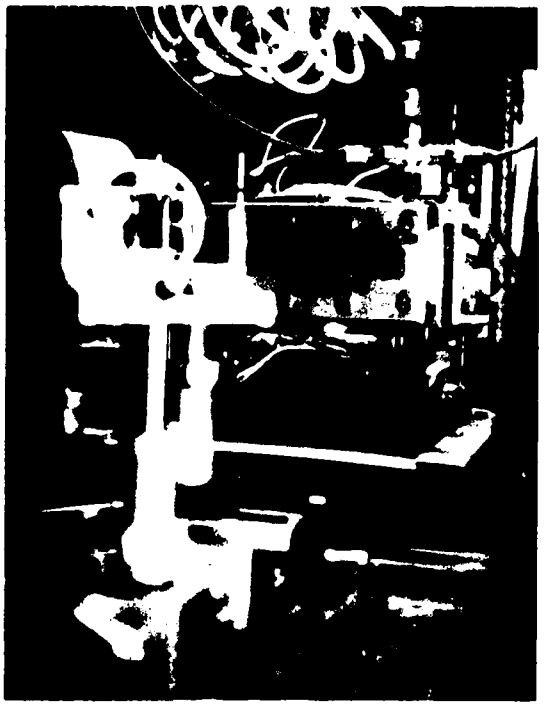

FIG. 5 CLOSEUP VIEW OF SANDWICH OVEN MOUNTED ON TRANSLATION TABLE AND SHOWING SODIUM DROPLETS.

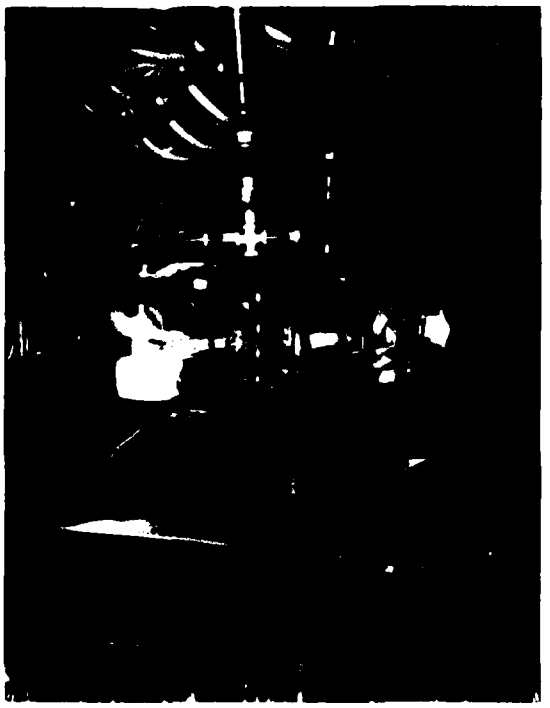

FIG. 6 CLOSEUP VIEW OF LASER PRODUCED PLASMA CREATED WITHIN SODIUM VAPOUR OF THE SANDWICH OVEN.

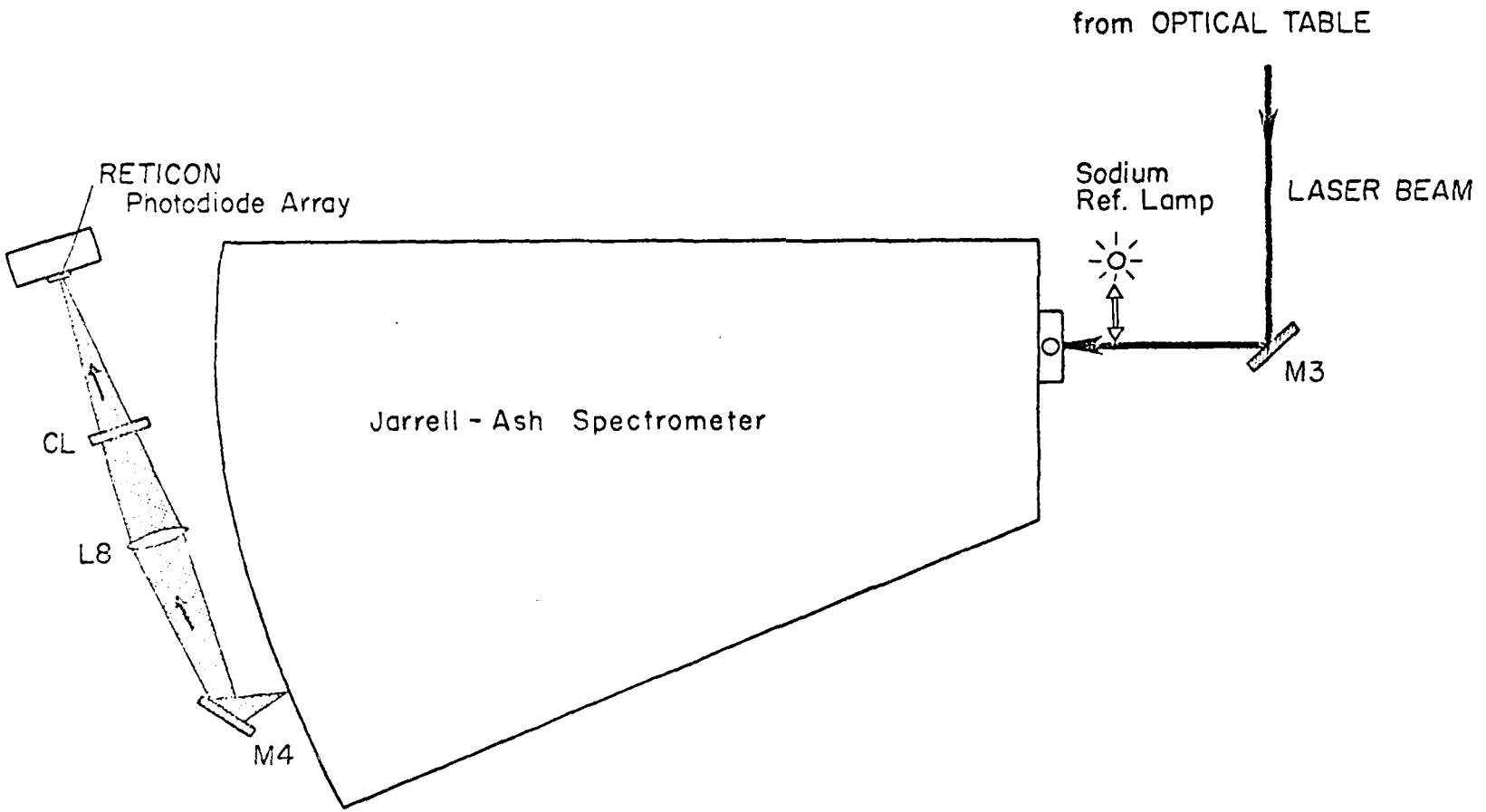

Fig. 7 Schematic of Wavelength Measurement Sub-Facility.

Key: CL is a cylindrical lens. L8 is an ordinary lens, M3 and M4 are mirrors.

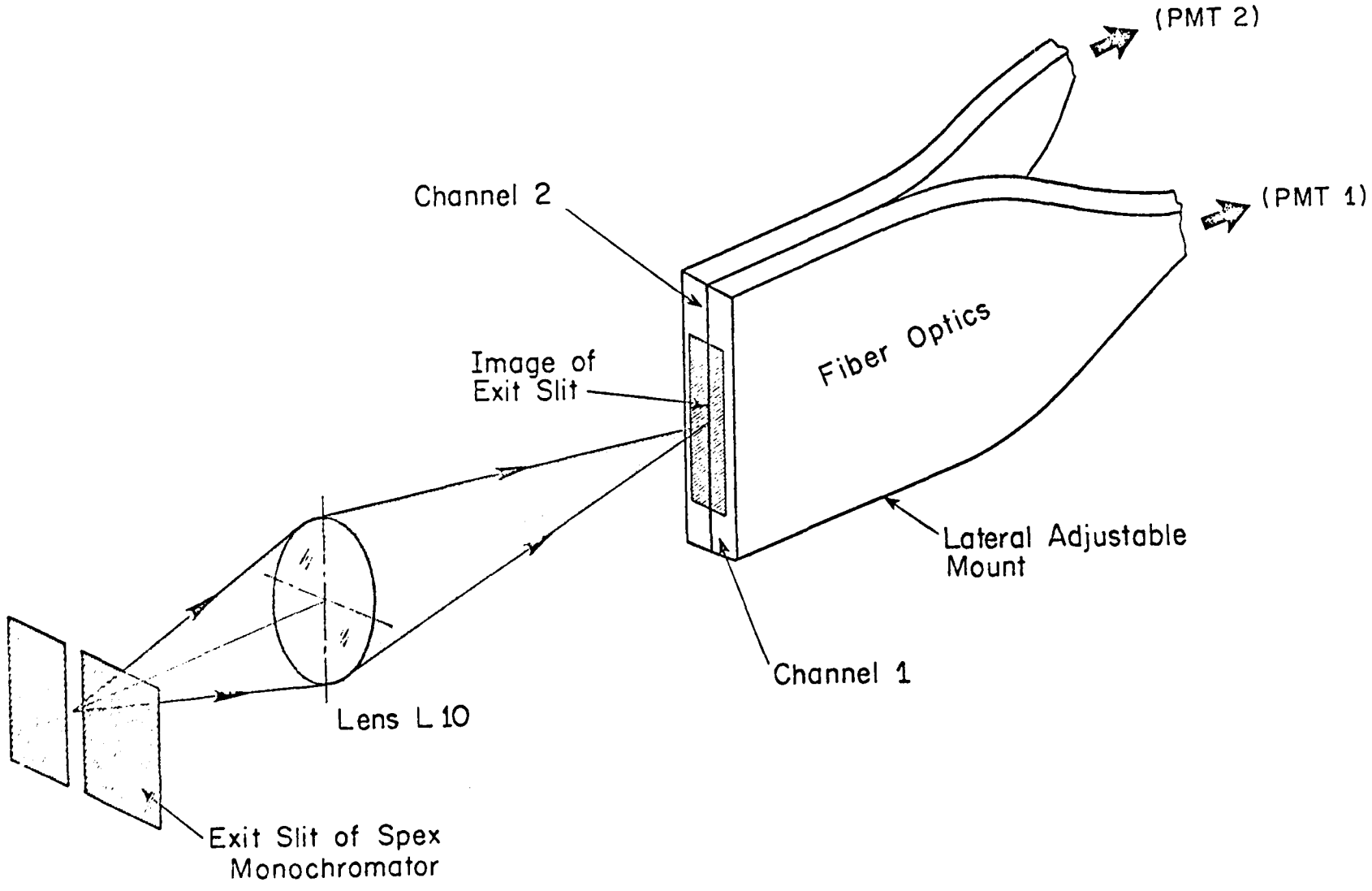

Fig. 8 Fiber Optic Array

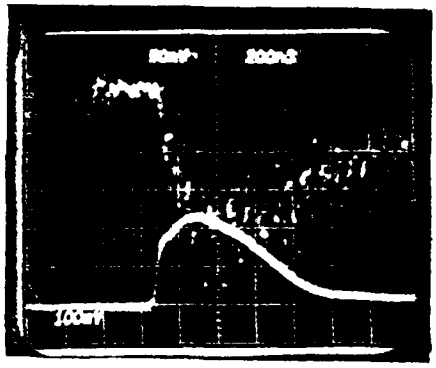

Fig. 9 Upper inverted trace displays a 3nm band of recombination radiation centred at 400nm 50mV/div ($N_a \cong 5.2 \times 10^{15} cm^{-3}$).

Lower trace shows corresponding laser pulse at 589nm ($\Delta\lambda_\ell$ = 0.2nm) as monitored on photodiode (200ns/div for both).

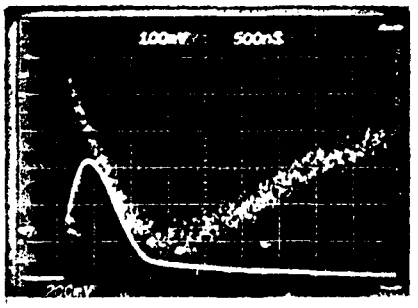

Fig. 10 Upper inverted trace displays line emission at 568.6nm, 100mV/div ($N_a \cong 9.5 \times 10^{15} cm^{-3}$).

Lower trace shows corresponding laser pulse at 589nm ($\Delta\lambda_\ell$ = 0.2nm) as monitored on photodiode (500ns/div for both).

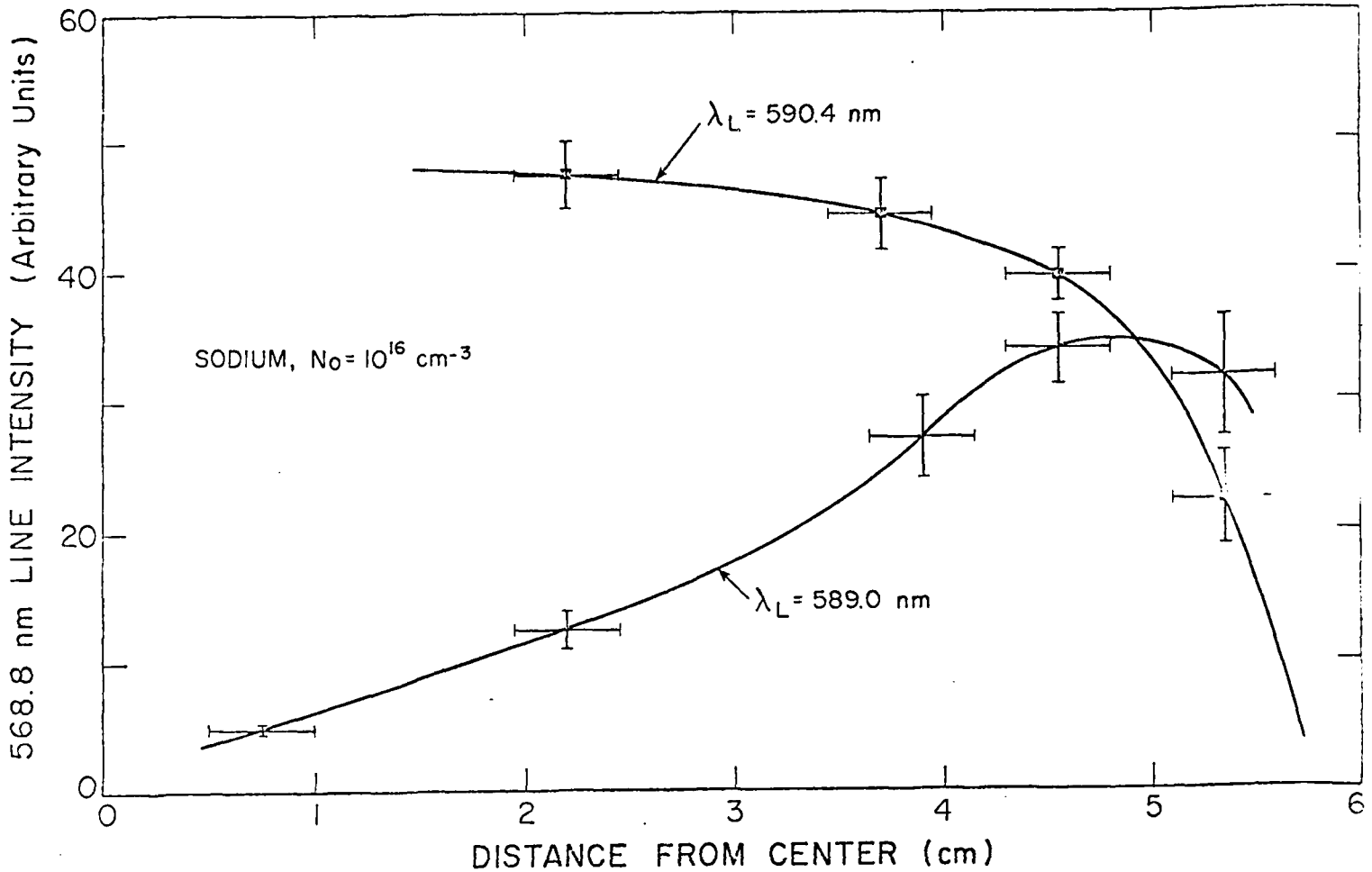

Fig. 11 Peak line emission at 568.8 nm vs heat sandwich position for both tuned and untuned laser radiation.

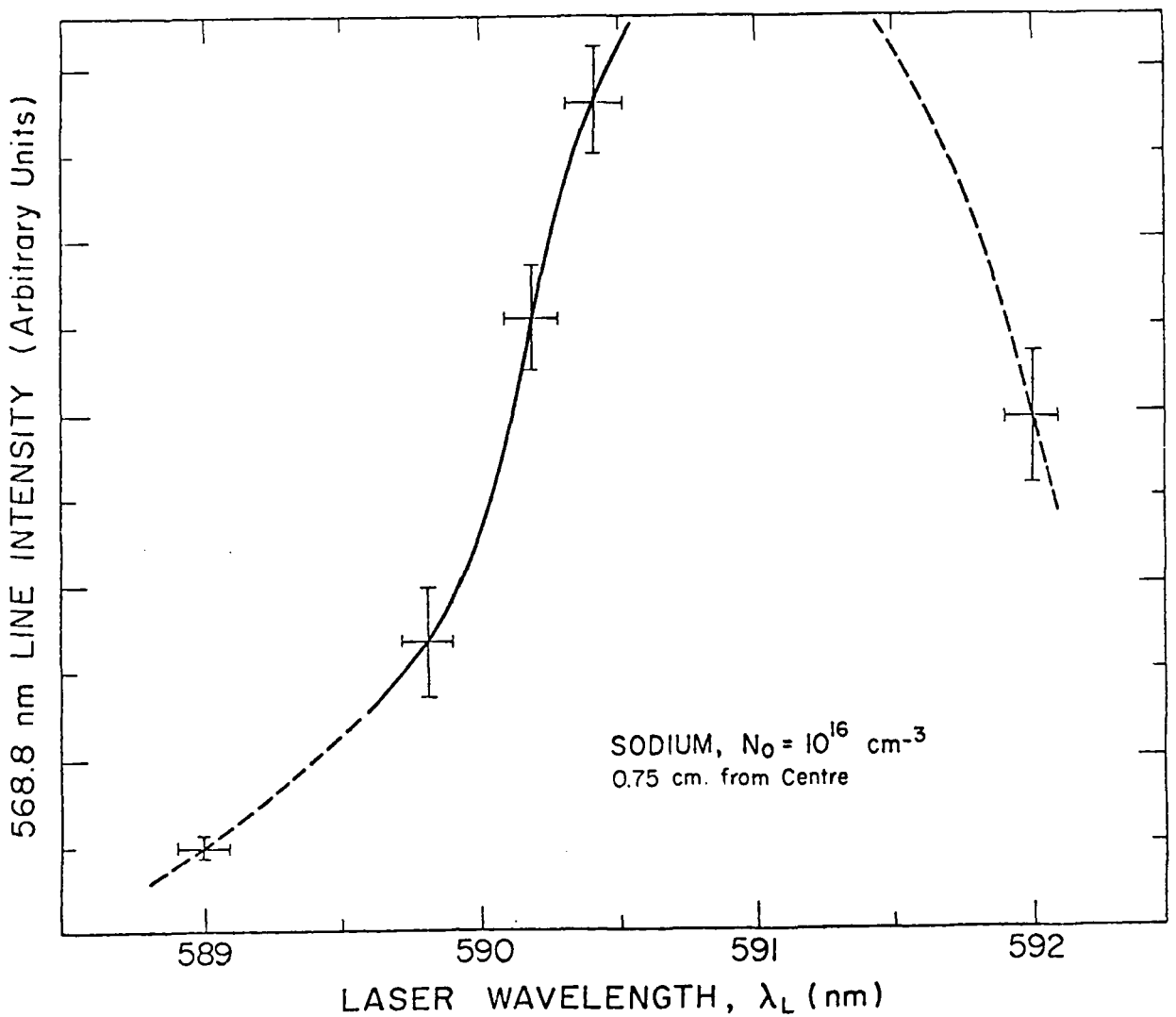

Fig. 12 Variation of peak 568.8 nm emission with laser detuning.

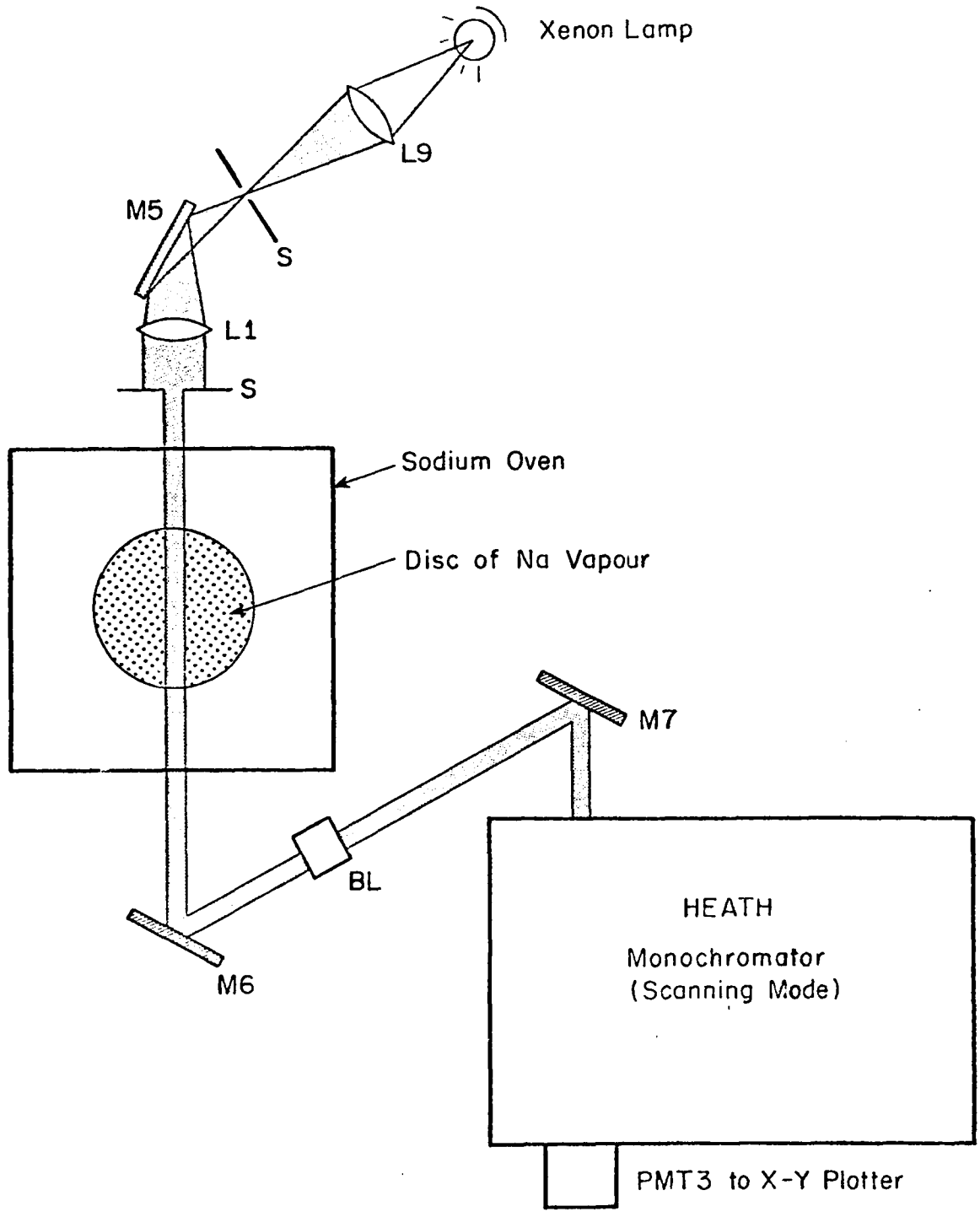

Fig. 13 Arrangement for determining the sodium vapour density by means of spectral hole technique. Key: BL beam lifter; S slit.

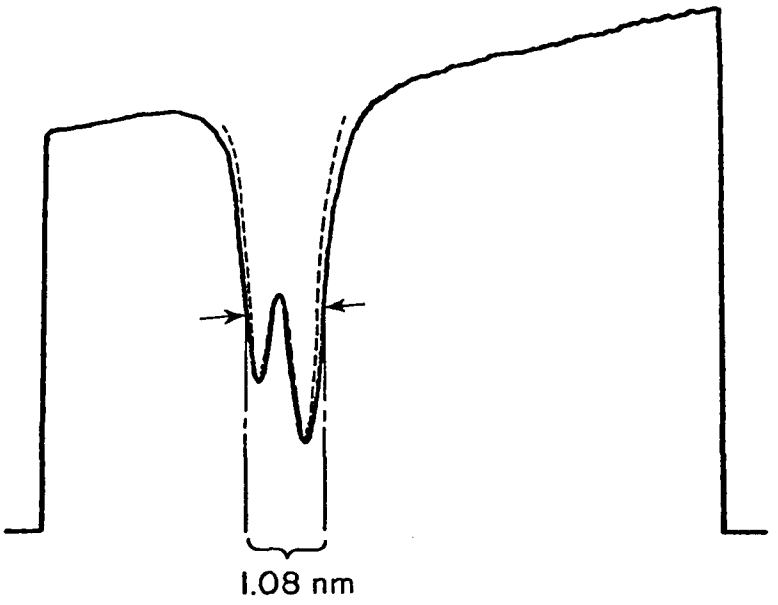

$2R \simeq 9.5$ cm, DENSITY $[Na] \simeq 9.3 \times 10^{14} cm^{-3}$, 150 μm Slit Width

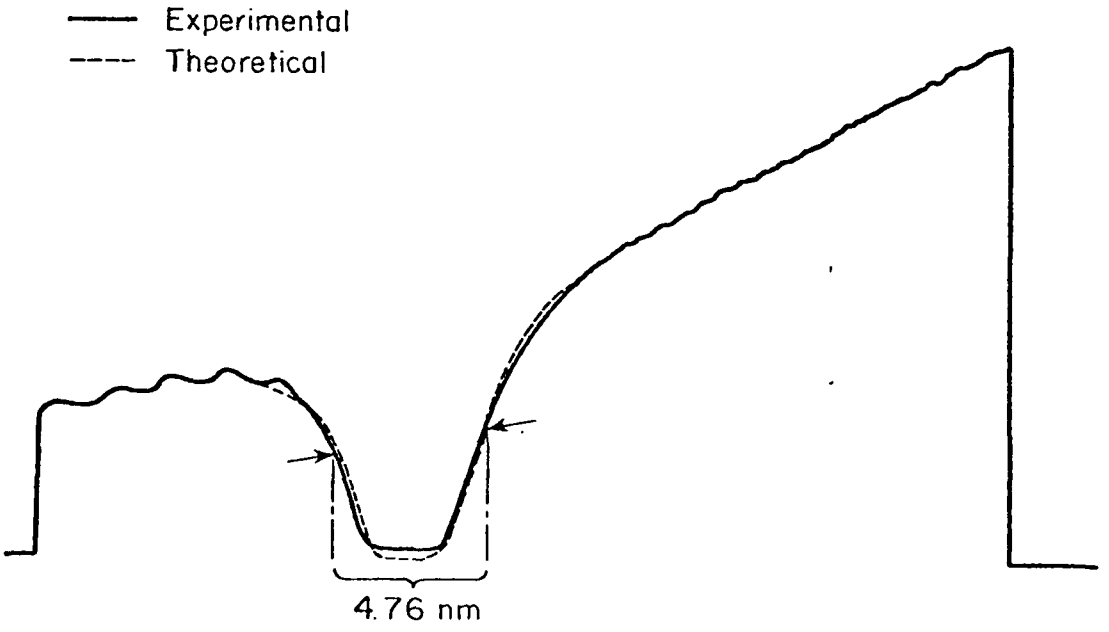

$2R \simeq 11$ cm, DENSITY $[Na] \simeq 9.5 \times 10^{15} cm^{-3}$, 150 μm Slit Width

Fig. 14 Two examples of the spectral hole measurement of the average sodium atom density in the vapour prior to laser irradiation.

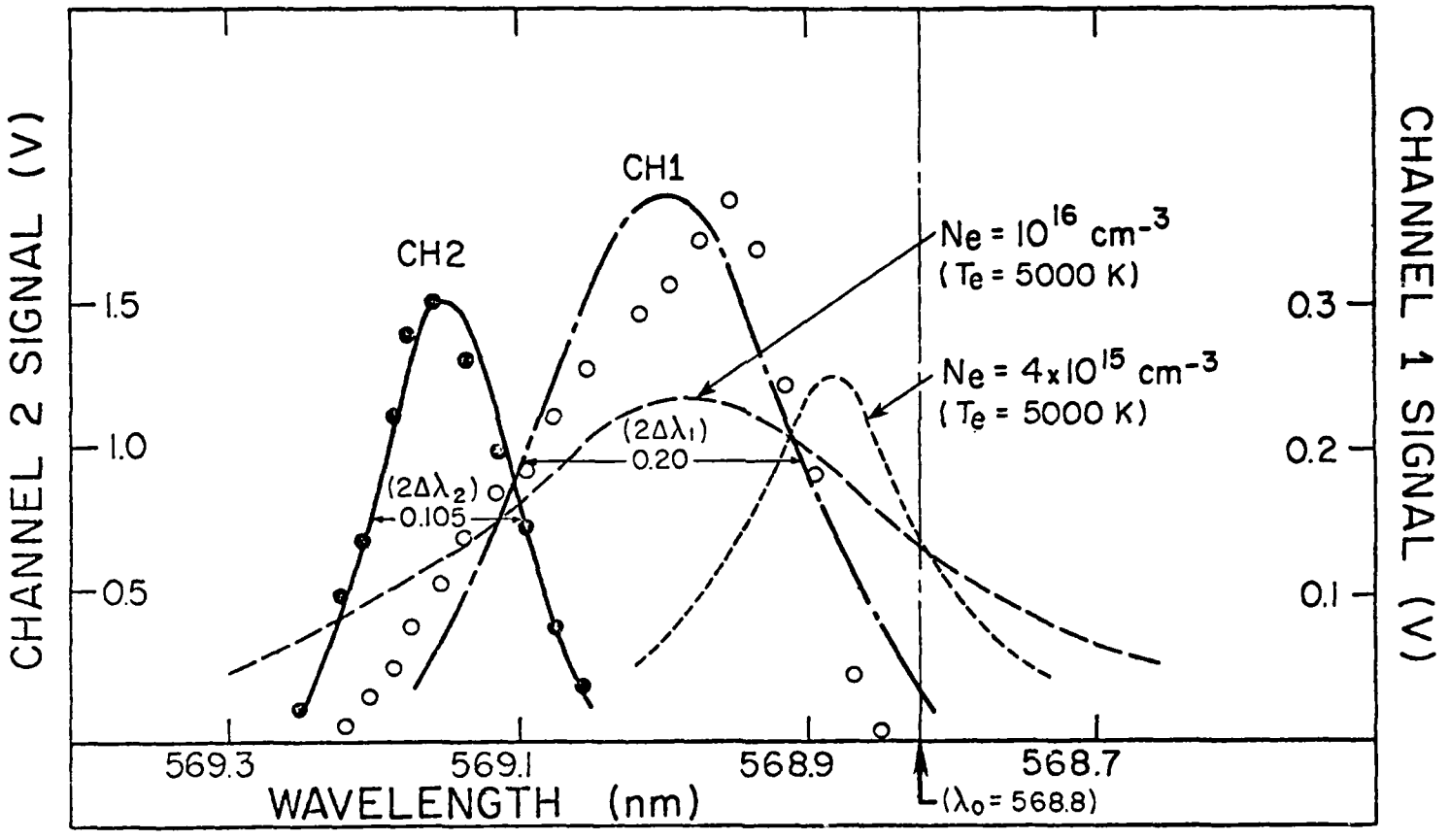

Fig. 15 Transmission functions for channels 2 and 1 (Gaussian fits —— and —·—, experimental points • and o, respectively). Method 1B, Entrance Slit 100 μmx10mm, Exit Slit 300 μm. Also shown are two calculated Stark broadened profiles.

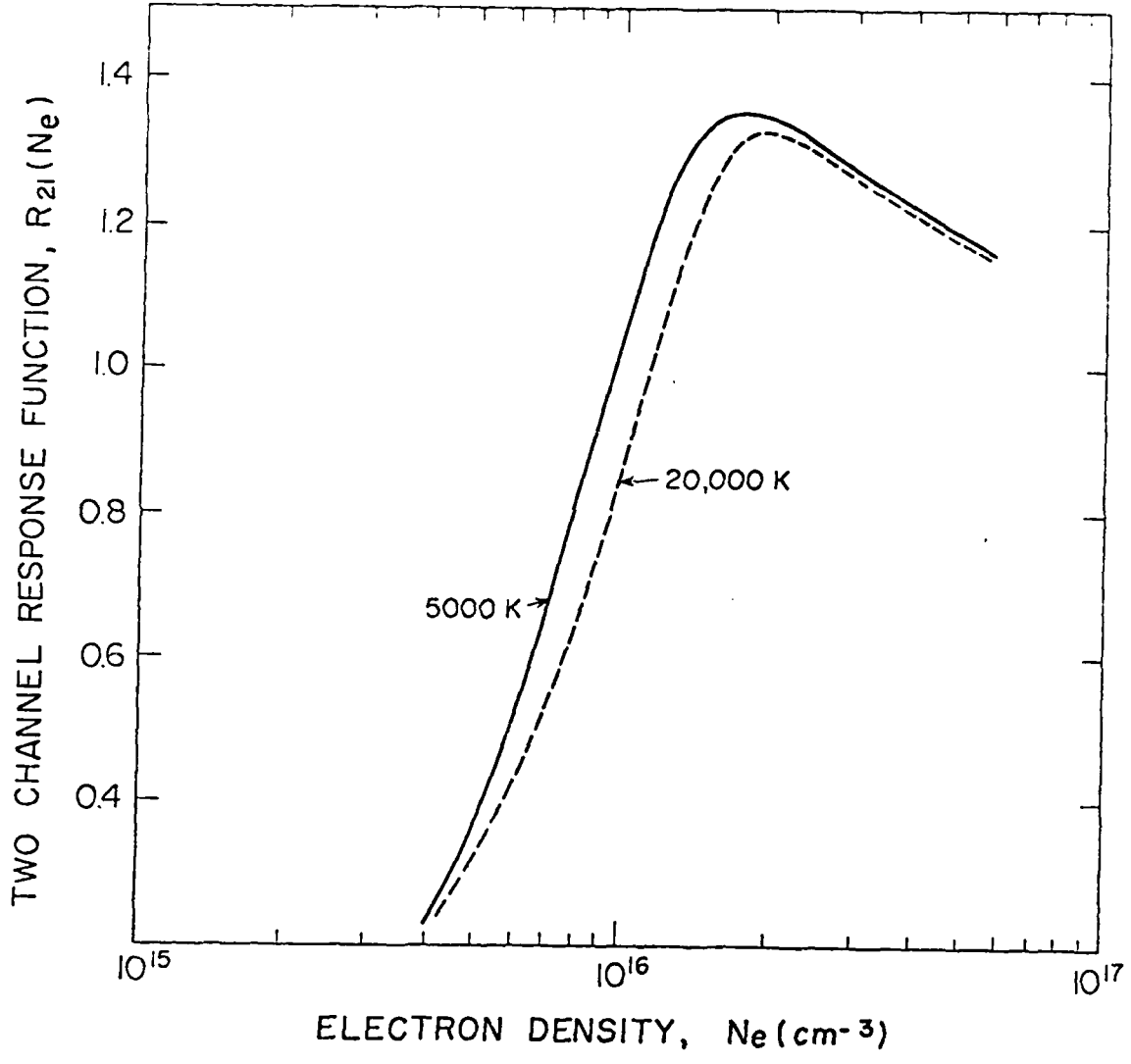

Fig. 16 Variation of two channel spectral response function $R_{21}(N_e)$ with electron density N_e (Method 1B).

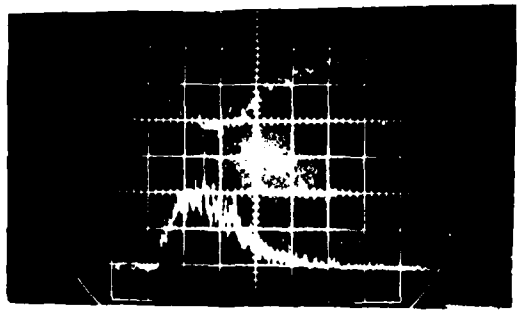

Fig. 17 Representative signals from channels 1 (inverted, 200mV/div) and 2 (500mV/div). Time scale 500ns/div.

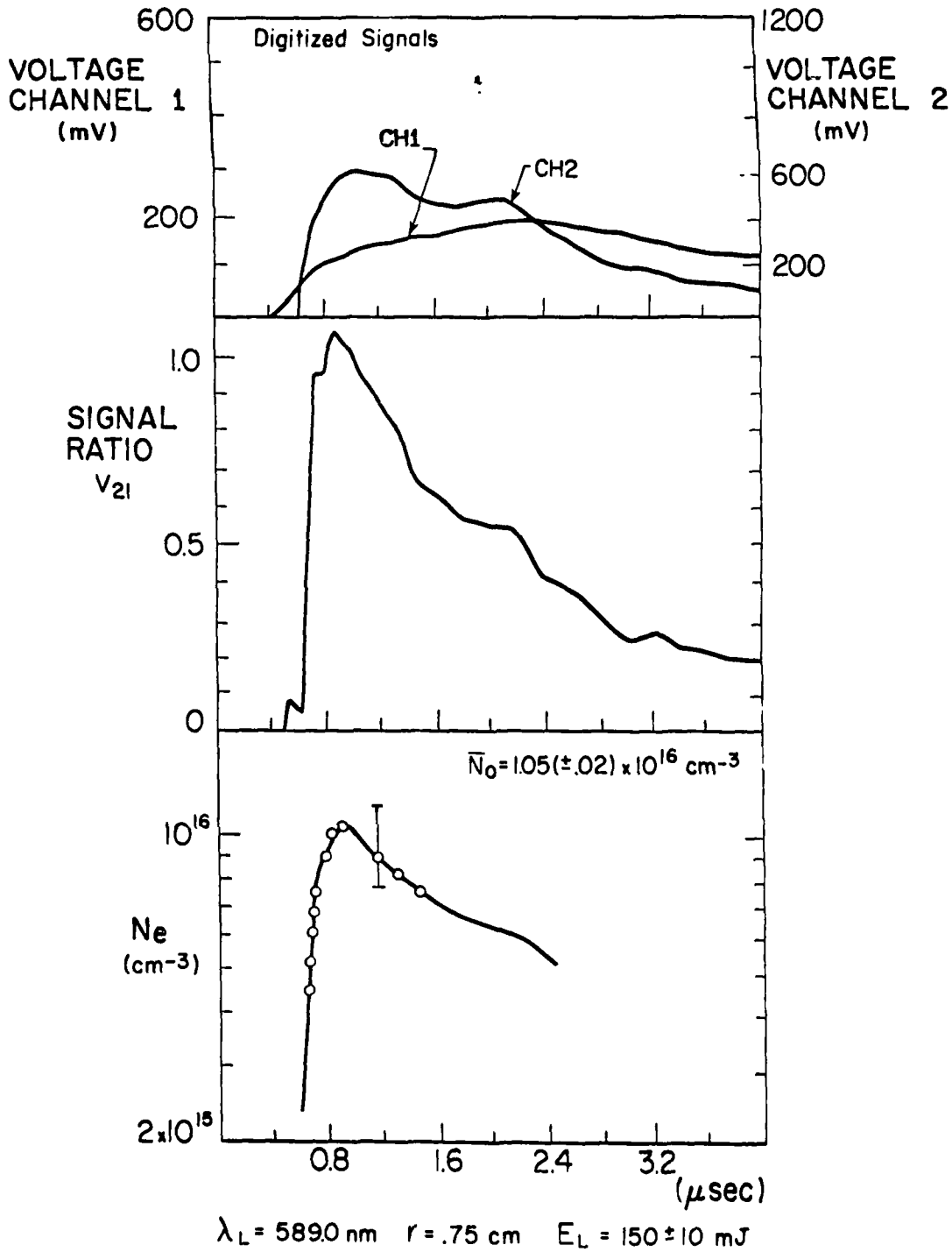

FIG. 18 REPRESENTATIVE STARK MEASUREMENTS OF ELECTRON DENSITY WITH LIBORS PLASMA.
(a) Digitized PM-voltage waveforms for channels 1 and 2.
(b) Signal ratio, V_{21} against time.
(c) Electron density time history evaluated from V_{21} using two channel response function R_{21}

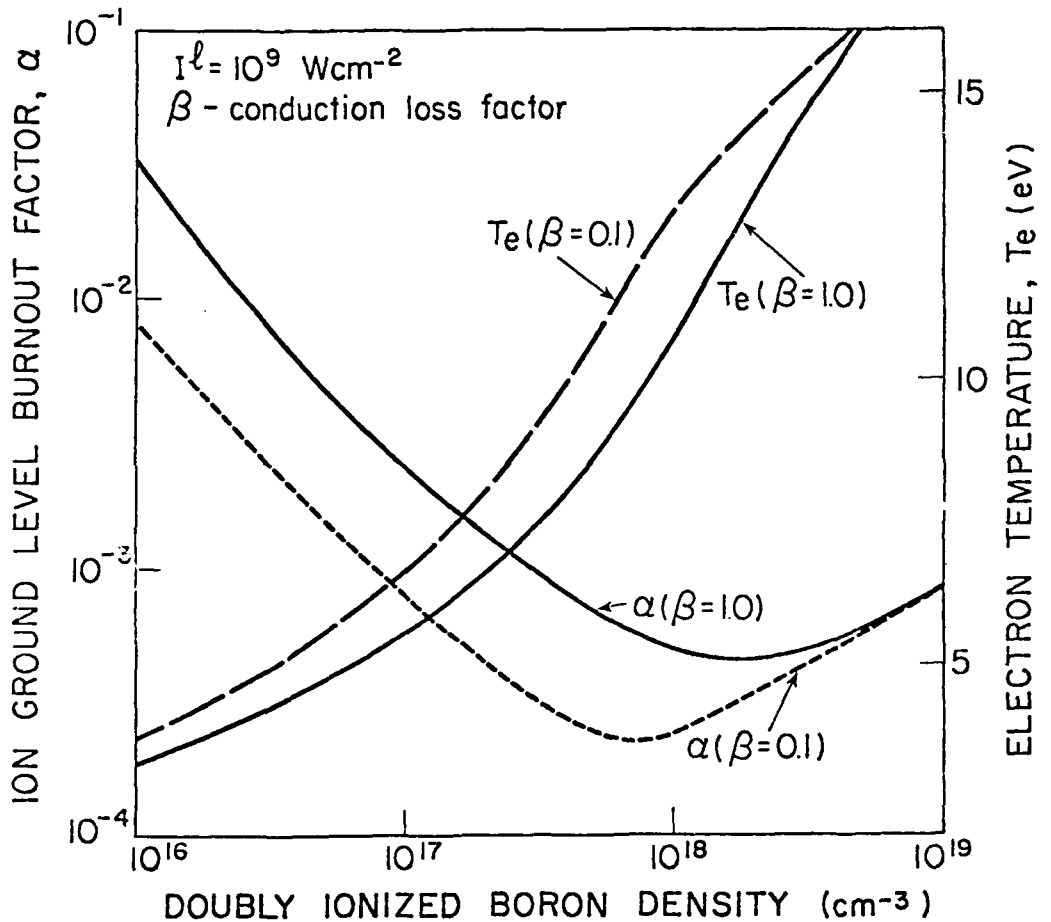

FIG. 19 VARIATION OF THE BIII GROUND LEVEL BURNOUT FACTOR α AND CORRESPONDING STEADY STATE TEMPERATURE T_e WITH INITIAL BIII ION DENSITY FOR TWO VALUES OF THE CONDUCTION LOSS FACTOR, β = 1.0 AND 0.1.

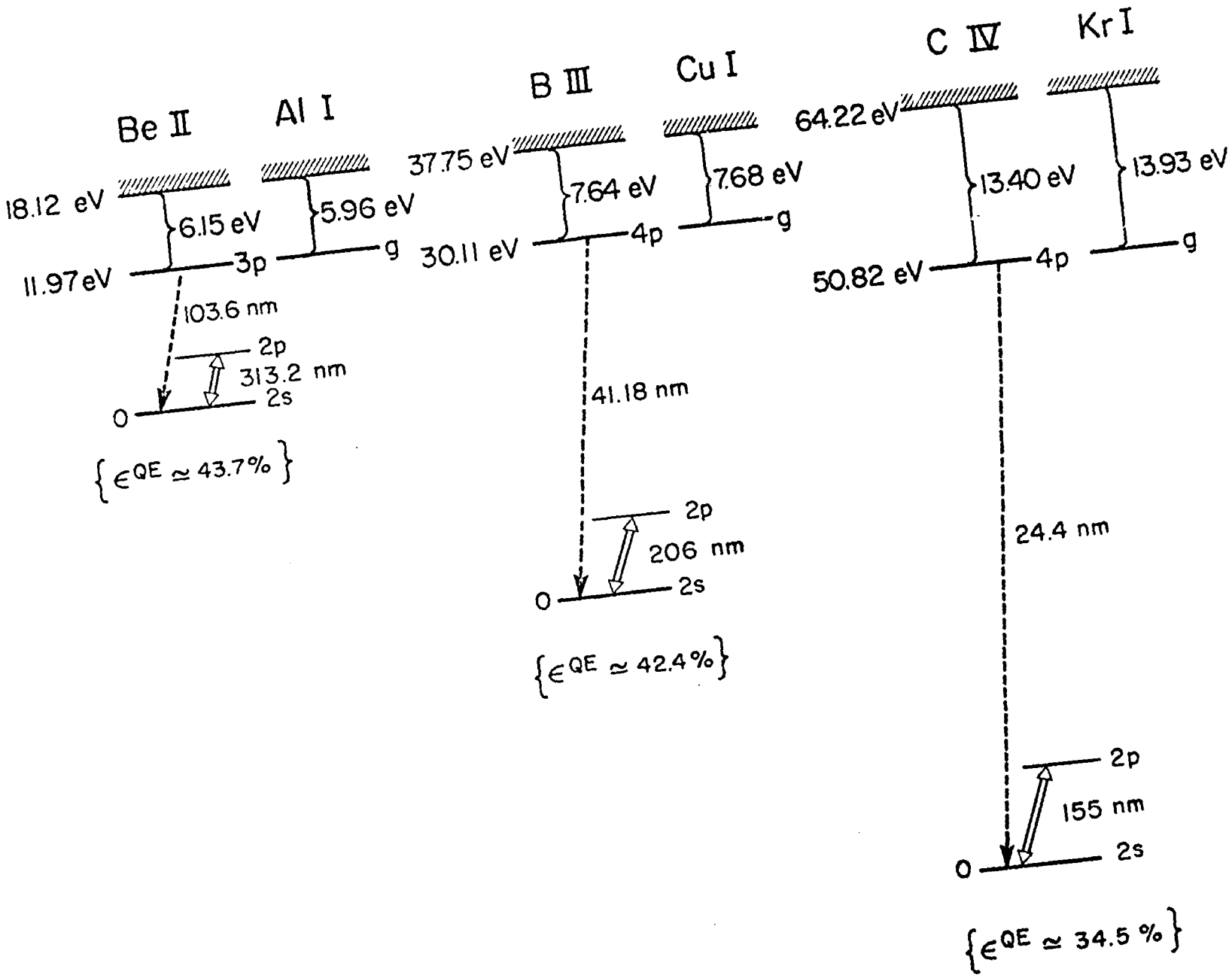

Fig. 20 Potential charge exchange pairs.

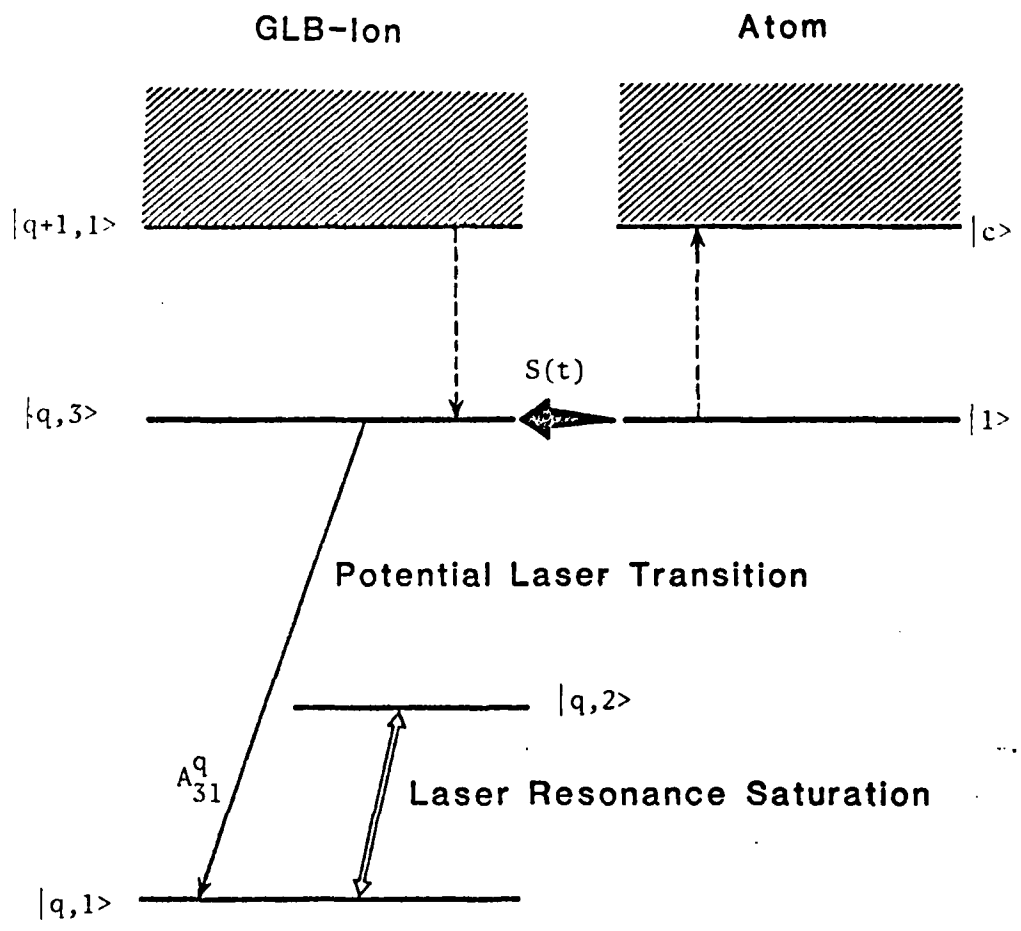

FIG. 21 SIMPLIFIED ENERGY LEVELS FOR ELECTRON DONOR ATOM AND ELECTRON ACCEPTOR (GLB-) ION INVOLVED IN RESONANCE CHARGE EXCHANGE COLLISION.

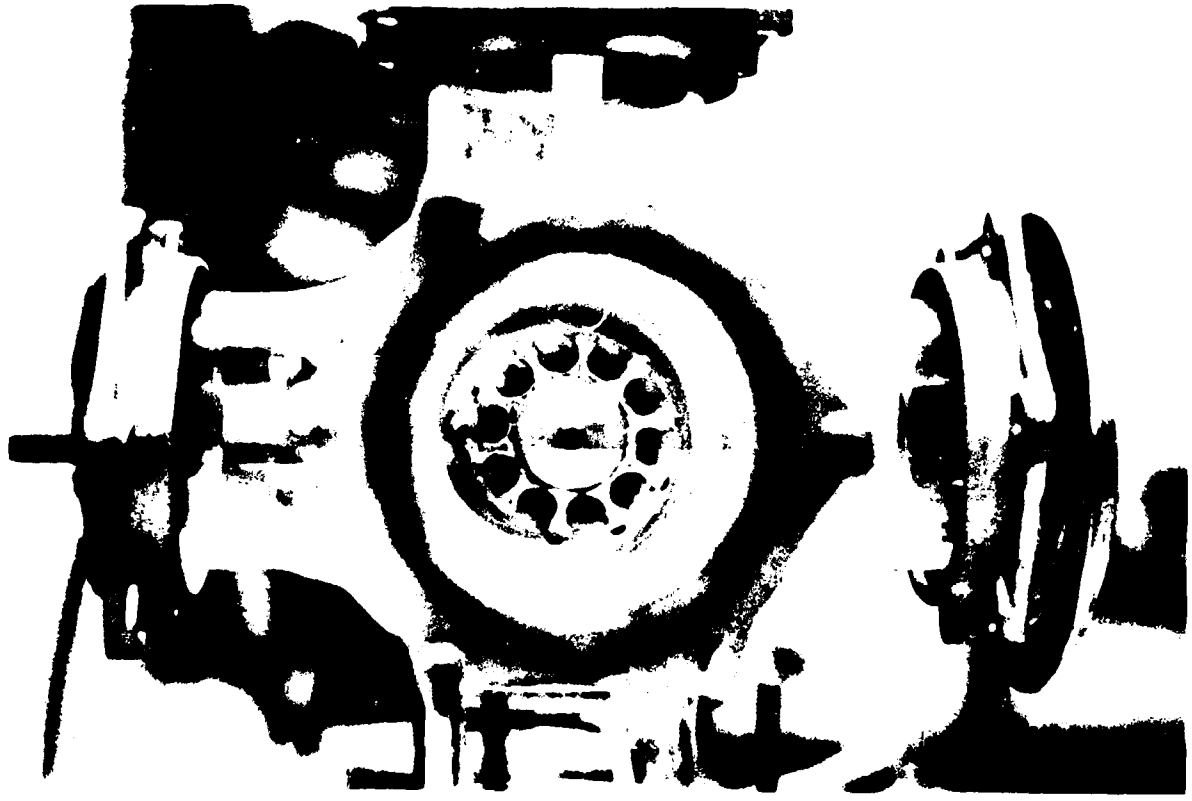

FIG. 22 MULTIPLE FOIL FUSE HOLDER SEEN WITHIN SIX-PORT VACUUM CHAMBER.

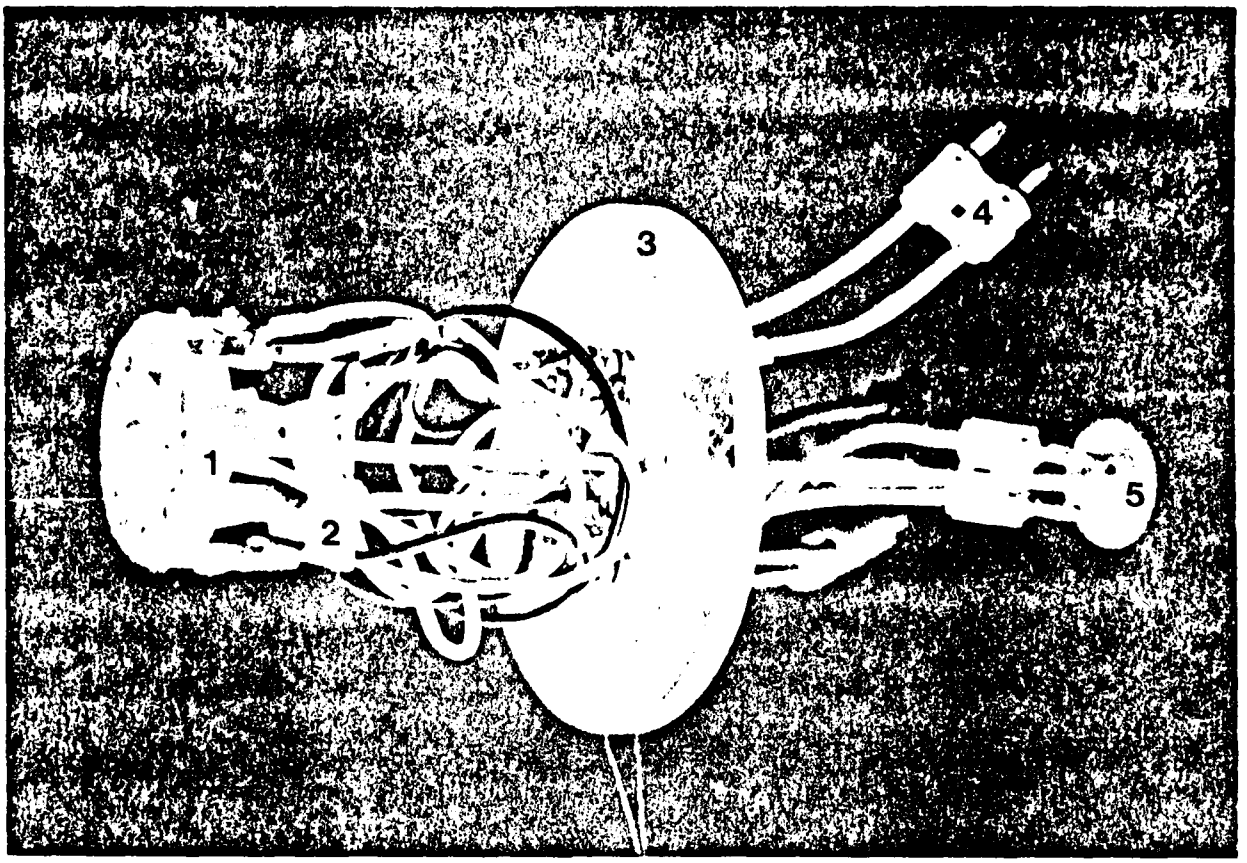

Fig. 23 Fuse holder system

1. Fuse holder
2. Connecting wires
3. Vacuum chamber port
4. Banana plugs for each fuse
5. Rotation knob

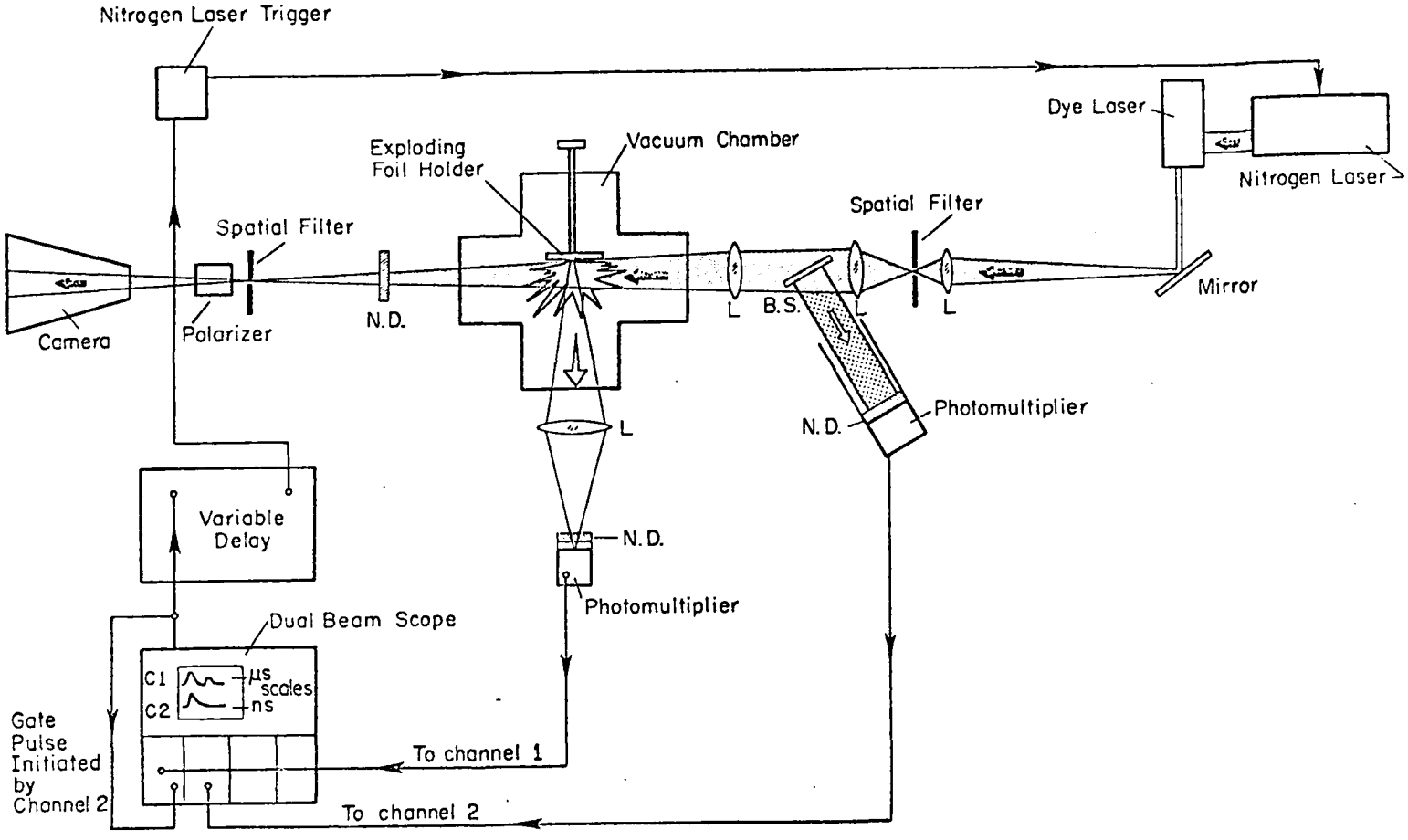

Fig. 24 Schematic of Exploding Foil Facility showing the near resonance absorption diagnostic arrangement.

Key: BS beam splitter; ND neutral density filter.

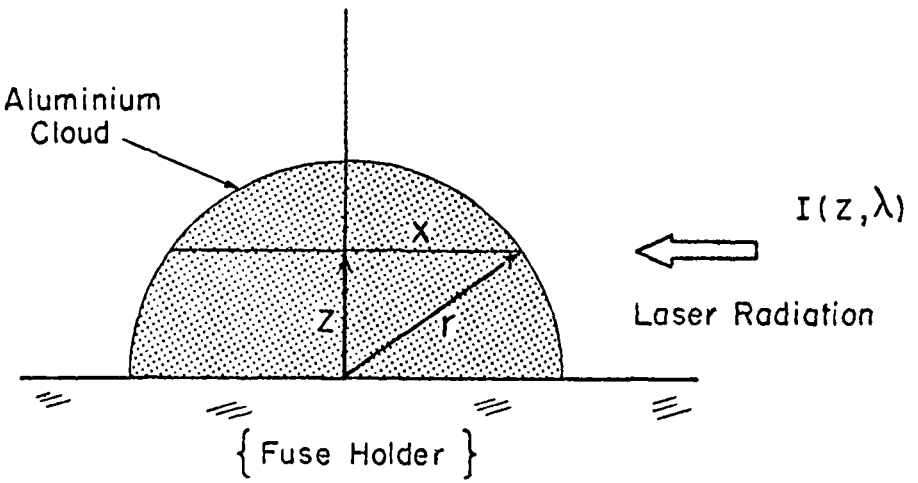

Fig. 25 Schematic for near resonance absorption technique.

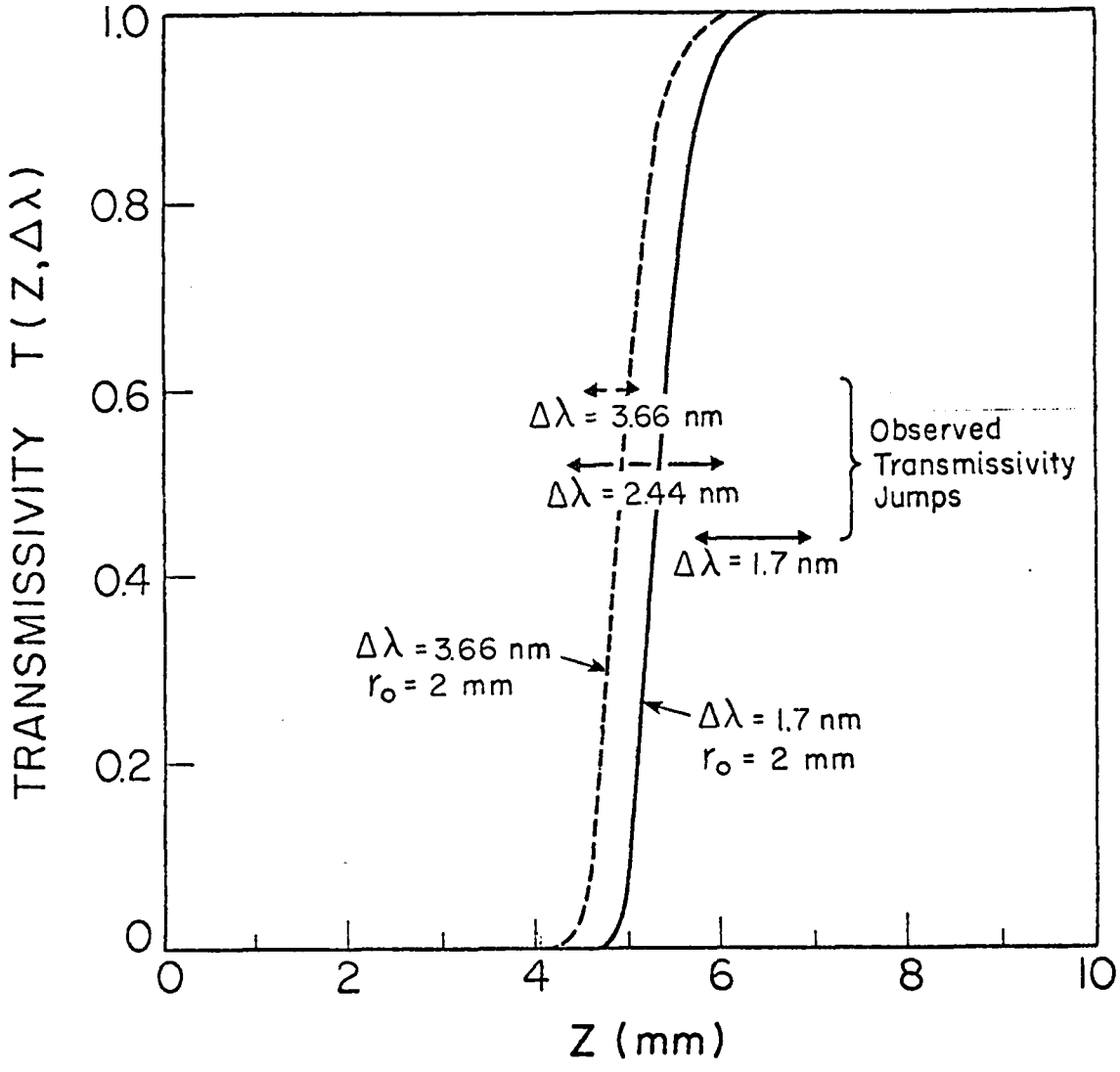

Fig. 26 Computed transmissivity variation with distance from fuse holder for two values of laser detunings, $\Delta\lambda$ = 1.7 nm and 3.66 nm. Also shown are the corresponding observed positions of the jumps in transmissivity for detunings of 1.7, 2.44 and 3.66 nm.

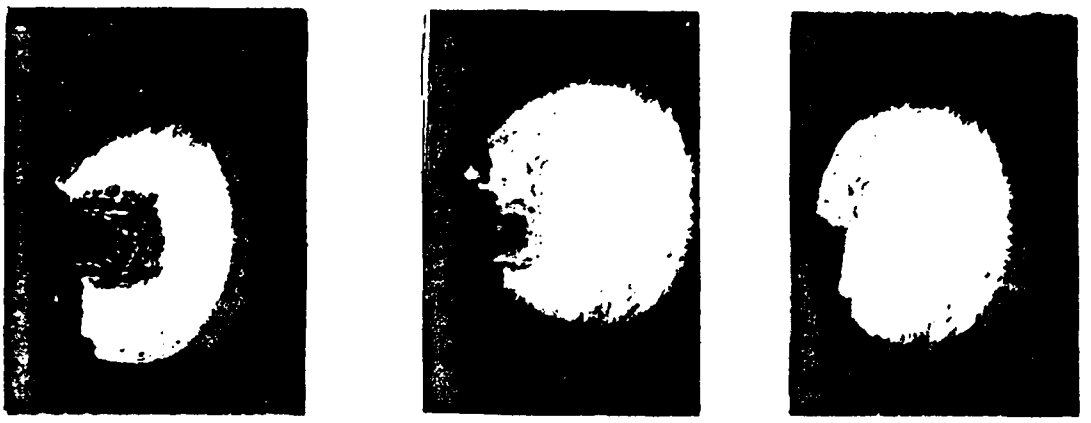

(a) (b) (c)

Fig. 27 Three representative photographs of laser light passing through exploding foil chamber. (a) Laser tuned to coincide with the 396.1 nm AlI resonance line revealing large extent of low density cloud 3.5 μsec after foil explodes. (b) Laser detuned by about 0.7 nm from 396.1 nm AlI resonance line showing much smaller extent of high density core also 3.5 μsec after foil explodes. (c) Laser fired before foil explodes.

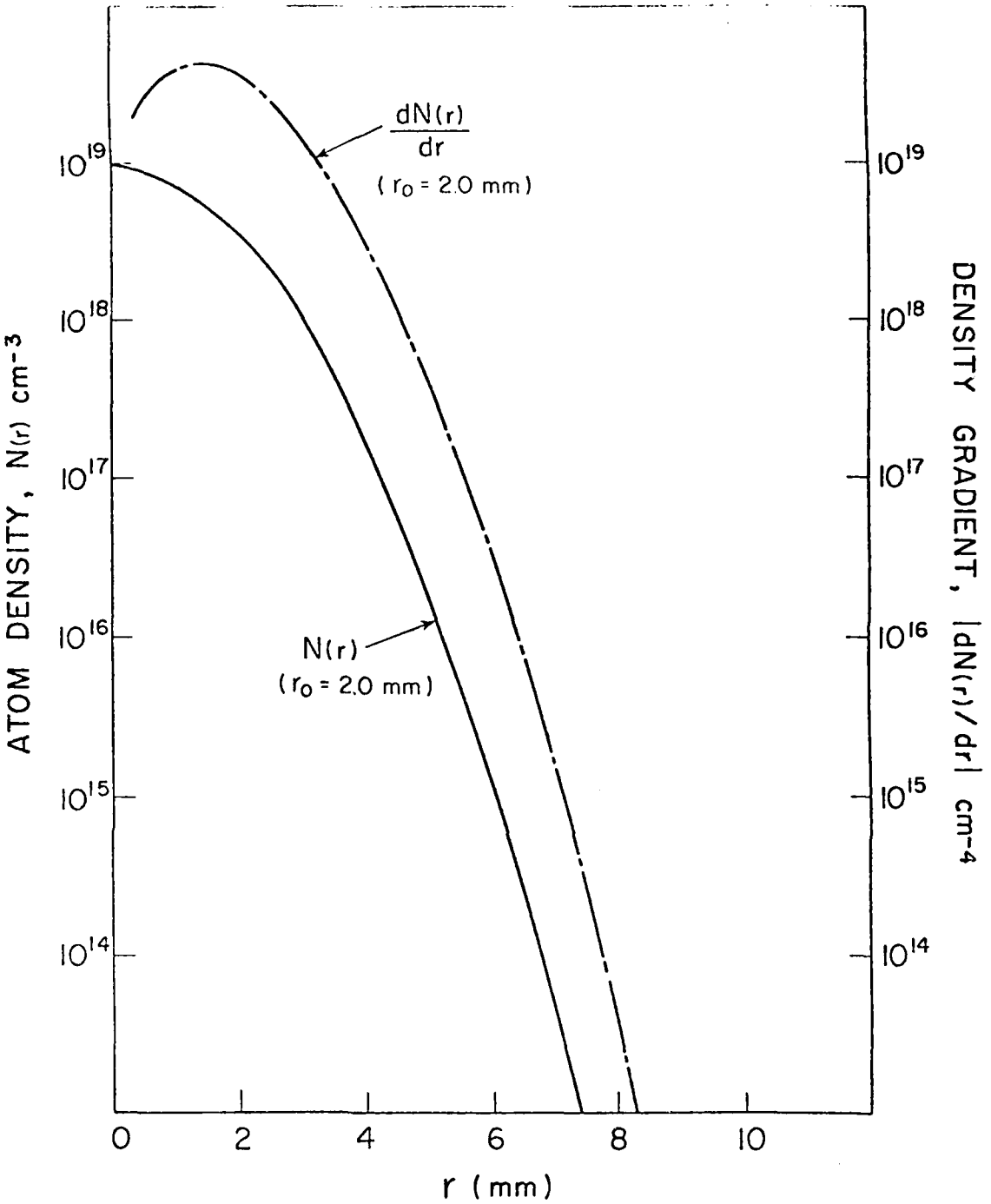

Fig. 28 Variation of both the atom density N(r) and its derivative with distance from the fuse holder according to the model $N(r)=N_0e^{-(r/r_0)^2}$ where $N_0=10^{19}$ cm^{-3} and $r_0=0.2$ cm.

APPENDIX A

LASER STIMULATED INVERSE RADIATIVE AUTOIONIZATION AS A MECHANISM FOR CREATING A GROUND LEVEL POPULATION INVERSION

R. M. Measures and R. Kissack

Abstract

We have been able to demonstrate by relatively simple equilibrium arguments that the attainment of a ground level population inversion by means of laser stimulated inverse radiative autoionization is not possible.

In many approaches towards the development of short (X and XUV) wavelength lasers, energy is stored in the ions of a plasma. The ground state of an ion of charge Z can represent an effective storage medium if, at the temperature required to ensure near complete ionization of the (Z-1) ion, there is very little excitation of the ion of charge Z. A ground level inverted population (GLIP) might then be created within such a medium if a fraction of the Z-ion ground level population could suddenly be transferred to some state that is radiatively coupled to the strongly depleted (Z-1) ion ground state. In some of the early approaches at developing an X-ray laser, rapid cooling through expansion of a dense, highly ionized plasma was thought to be capable of accomplishing this by means of three-body recombination to high lying levels[1] of the (Z-1) ion. Unfortunately, it was soon shown that the energy released by this recombination prevents the formation of a GLIP.[2,3]

In another approach at developing an X-ray laser, Harris[4] has proposed using a laser to suddenly switch the population of a storage state into a potential laser state. Although this is an attractive concept, the fact that the storage state in this approach is metastable is likely to constrain operation to low densities which in turn will severely limit the gain coefficient attainable. We felt that it might be possible to use this concept of laser switching where (in our approach) the Z ion ground state would represent the storage medium. This would avoid the limitation imposed by using a metastable state as the storage state.

In order to accomplish this we have considered the possibility of suddenly enhancing electron resonance capture into a doubly excited state of the Z-1 ion through the process of *stimulated inverse radiative autoionization*, SIRA. By this means it might be possible to momentarily create a ground level population inversion within the Z-1 ion. The feasibility of this would be greatly facilitated if the Z-1 ground level had been strongly burnt out by laser resonance saturation[5-14] prior to the sudden application of the SIRA laser pulse.

We have schematically illustrated this concept for the case of a singly charged ion in figureA1. In this illustration $|g\rangle$, $|i\rangle$ and $|d\rangle$ are taken to represent the atom ground state, the ion ground state and the atom doubly excited state, respectively. ε_p is taken as the photon energy of the stimulating laser field and ε_e the energy of the free electron that

is participating in this stimulated inverse radiative autoionization process. This interaction can be expressed as a reaction of the form

$$\text{SIRA:} \qquad |i\rangle + h\nu_L + e \rightarrow |d\rangle \tag{A1}$$

where $h\nu_L$ represents a photon of the stimulating laser field and e a free electron. Energy conservation implies that

$$\varepsilon_p + \varepsilon_e = E_{di} \tag{A2}$$

where E_{di} represents the difference in energy between $|d\rangle$ and $|i\rangle$.

The basic idea is to start with a plasma which primarily comprises ground state ions. This state of affairs can be produced by means of laser resonance saturation where a degree of ionization of close to 99.9% has been predicted. We shall assume that the electron density is high enough that just prior to switching on the SIRA laser the plasma can be thought to be in local thermodynamic equilibrium. Furthermore we shall also assume that in the absence of the SIRA laser field the dominant decay mode for the doubly excited state is radiative decay to the ground level and that during the times of interest this represents the primary mechanism for repopulating the ground level.

Under these circumstances the rate equations governing the ground and doubly excited states take the form

$$\frac{dN_g}{dt} = N_d A_{dg} \tag{A3}$$

and

$$\frac{dN_d}{dt} = N_e N_i R_{id} - N_d (R_{di} + A_{di} + A_{dg}) \tag{A4}$$

where N_g and N_d represent the density of ground and doubly excited state atoms, while N_i and N_e represent the ion and free electron densities. A_{dg} represents the Einstein spontaneous emission probability for radiative decay of $|d\rangle$ to $|g\rangle$ and A_{di} represents the spontaneous emission probability for radiative autoionization of the doubly excited state, viz.,

$$\text{RA:} \qquad |d\rangle \rightarrow |i\rangle + e + h\nu \tag{A5}$$

In the presence of the SIRA laser field the radiatively induced rate coefficients are R_{di} for stimulated radiative autoionization, viz.,

SRA: $$|d> + h\nu_L \rightarrow |i> + e + 2h\nu_L \qquad \text{(A6)}$$

and R_{id} for stimulated inverse radiative autoionization, see (A1).

For our model we can set $N_e = N_i$ and we can assume that both the electron density and its temperature are constant during the times of interest. If we further assume a step-like pulse of laser radiation then we can introduce the two constants,

$$S = N_e^2 R_{id} \qquad \text{(A7)}$$

and

$$\frac{1}{\tau} = R_{di} + A_{di} + A_{dg} \qquad \text{(A8)}$$

In which case equation (A4) takes the form

$$\frac{dN_d}{dt} = S - \frac{N_d}{\tau} \qquad \text{(A9)}$$

which has the solution

$$N_d(t) = S\tau\{1 - e^{-t/\tau}\} \qquad \text{(A10)}$$

provided $N_d(o) = 0$, which is a conservative assumption.

The population inversion density between the doubly excited state and the ground state,

$$\mathcal{N}(t) = N_d(t) - \omega N_g(t) \qquad \text{(A11)}$$

where ω represents the ratio of the statistical weights for $|d>$ and $|g>$. The appropriate rate equation for $\mathcal{N}(t)$ takes the form

$$\frac{d\mathcal{N}(t)}{dt} = S - N_d(t)\left\{\frac{1}{\tau} + \omega A_{dg}\right\} \qquad \text{(A12)}$$

If we use the above solution (A10) for $N_d(t)$, then we can write

$$\frac{d\mathcal{N}(t)}{dt} = S[(1+p)e^{-t/\tau} - p] \qquad \text{(A13)}$$

where we have introduced

$$p \equiv \omega A_{dg} \tau \tag{A14}$$

The solution of equation (A14) can be expressed in the form

$$\mathcal{N}(t) = -\omega N_g(o) - S[\tau(1+p)(e^{-t/\tau} - 1) + pt] \tag{A15}$$

where we have used the fact that $N_d(o) = 0$ in evaluating $\mathcal{N}(o)$.

To ascertain the maximum value of this population inversion density, $\mathcal{N}_{max}$, we set $d\mathcal{N}/dt = 0$. The justification for assuming that this condition corresponds to a maximum is obtained by reference to the nature of equation (A15). From equation (A13) it is apparent that $\mathcal{N}_{max}$ arises when

$$e^{-t/\tau} = p/(1+p) \tag{A16}$$

which amounts to stating that $\mathcal{N}$ is a maximum at a time

$$t_m = \tau \ln[(1+p)/p] \tag{A17}$$

Substitution of (A16) and (A17) into (A15) yields

$$\mathcal{N}_{max} = S\tau \left[1 - p \ln \left(\frac{1+p}{p} \right)\right] - \omega N_g(o) \tag{A18}$$

Clearly, a necessary condition for creating a ground level inversion, i.e., $\mathcal{N} > 0$, based on laser stimulated inverse radiative autoionization, can be expressed in the form

$$S\tau > \frac{\omega N_g(o)}{\left[1 - p \ln \left(\frac{1+p}{p} \right)\right]} \tag{A19}$$

In general, $R_{di} + A_{di} + A_{dg} \gg \omega A_{dg}$, so that $p \ll 1$ and we can restate the criterion for creating a ground level inversion through SIRA in the following manner:

$$\frac{N_e^2 R_{id}}{R_{di} + A_{di} + A_{dg}} > \omega N_g(o) \tag{A20}$$

Now R_{id} can be related to $R_{di} + A_{di}$ through the equilibrium relation

$$R_{id} = (R_{di} + A_{di})/S_d(T_e) \tag{A21}$$

where

$$S_d(T_e) \equiv \left\{ \frac{N_e^2}{N_d} \right\}^{EQUIL} = 2 \left(\frac{2\pi m_e kT_e}{h^2} \right)^{3/2} \frac{U_i(T_e)}{\omega_d} e^{E_{di}/kT_e} \tag{A22}$$

Here $U_i(T_e)$ represents the ion partition function, T_e the electron temperature and ω_d is the statistical weight of the doubly excited state. The other constants have their usual meaning.

If (A21) is substituted into (A20) we have

$$\frac{N_e^2(R_{di}+A_{di})}{(R_{di}+A_{di}+A_{dg})} > \omega N_g(o) S_d(T_e) \tag{A23}$$

In the limit of strong laser radiation (i.e., $R_{di} >> A_{di} + A_{dg}$) this amounts to requiring

$$\frac{N_e^2}{N_g(o)} \equiv S_g(T_e) > \omega S_d(T_e) \tag{A24}$$

where

$$S_g(T_e) = 2 \left(\frac{2\pi m_e kT_e}{h^2} \right)^{3/2} \frac{U_i(T_e)}{\omega_g} e^{-E_{ig}/kT_e} \tag{A25}$$

The value of T_e used in both (A22) and (A25) corresponds to the LTE value prior to irradiation with the SIRA laser. If (A22) and (A25) are used in (A24) we are able to see that the criterion for laser action can be written in the form

$$e^{-E_{ig}/kT} > e^{E_{di}/kT} \tag{A26}$$

which makes it very obvious that a ground level population can never be created by means of laser stimulated inverse radiative autoionization. It should be noted that this proof is fundamental in nature and does not require any knowledge of the cross sections involved. However, it might be worth mentioning that the plasma was assumed to be in LTE prior to irradiation by the SIRA laser pulse. Deviations from this starting condition might lead to different conclusions.

REFERENCES

1. L. I. Gudzenko and L. A. Shelepin, Sov. Phys. JETP 18, 998-1000 (1964).
2. J. M. Green and W. T. Silfvast, Appl. Phys. Lett., 28, 253-255 (1976).
3. P. Wagli and W. L. Bohn, J. Appl. Phys. 51, 3601-3603 (1980).
4. S. E. Harris, Optics Letters 5, 1-3 (1980).
5. F. Roussel, P. Breger, G. Spiess, C. Manus and S. Geltman, J. Phys. B: Atom. Molec. Phys. 13, L631-L636 (1980).
6. T. Stacewicz, Optics Commun. 35, 239-241 (1980).
7. J. Krasinski, T. Stacewicz and C. R. Stroud Jr., Optics Commun. 33, 158-162 (1980).
8. T. Stacewicz and J. Krasinski, Optics Commun. 39, 35-40 (1981).
9. B. Carré, F. Roussel, P. Breger and G. Spiess, J. Phys. B: Atom. Molec. Phys. 14, 4289-4300 (1981).
10. R. M. Measures and P. G. Cardinal, Physical Review A 23, 804=815 (1981).
11. R. M. Measures, P. G. Cardinal, G. W. Schinn, J. Appl. Phys. 52, 1269-1277 (1981) and 52, 7459 (1981).
12. T. B. Lucatorto and T. J. McIlrath, Phys. Rev. Letters, 37, 428-431 (1976).
13. T. J. McIlrath and T. B. Lucatorto, Phys. Rev. Letters, 38, 1390-1393 (1977).
14. C. H. Skinner, J. Phys. B: Atom. Molec. Phys., 13, 55-68 (1980).

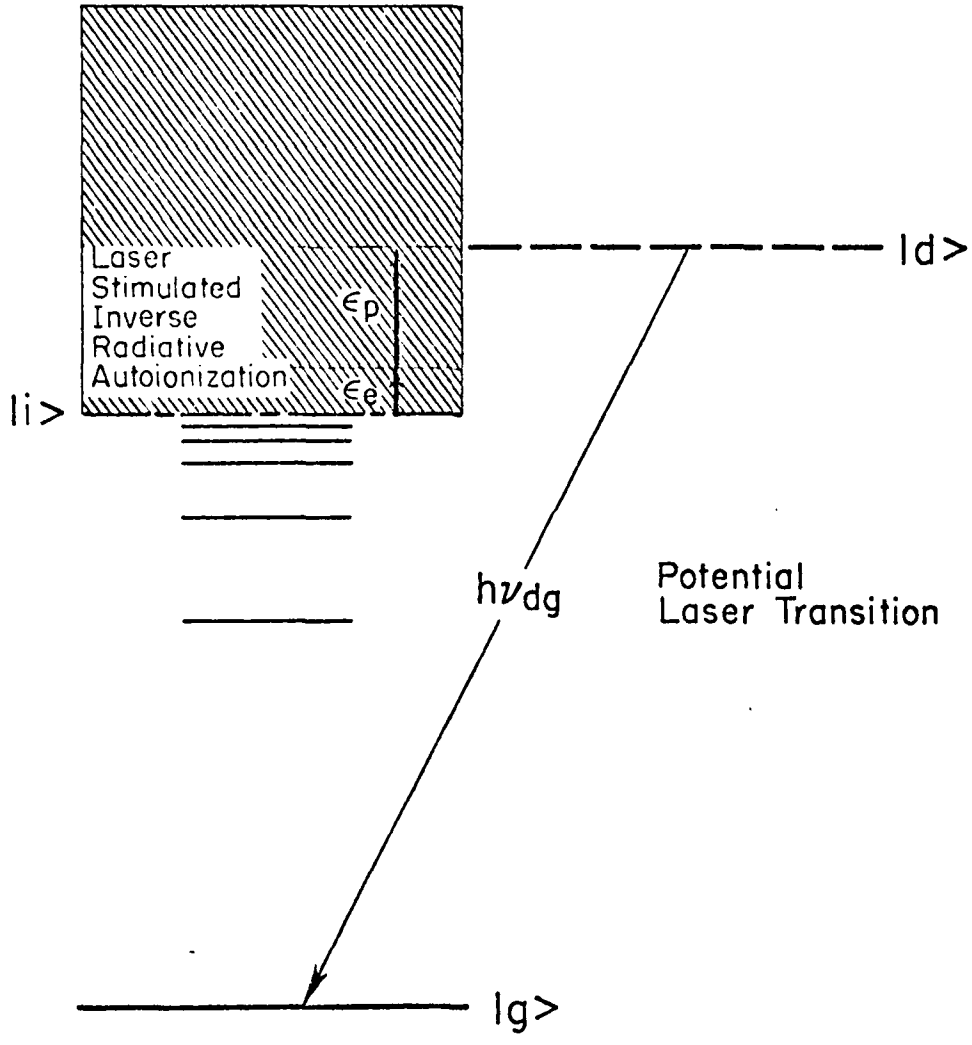

Fig. A1 Schematic of laser stimulated inverse radiative autoionization.

APPENDIX B

LASER ABSORPTION UNDER SATURATION CONDITIONS WITH ALLOWANCE FOR SPECTRAL HOLE BURNING

R. M. Measures and H. Herchen,

Institute for Aerospace Studies
University of Toronto
4925 Dufferin Street
Downsview, Ontario, Canada
M3H 5T6

Abstract

We have derived a set of equations that describe the spectral hole burning that arises in a saturating laser pulse as it propagates through a resonantly absorbing atomic vapour. The analysis has been compared with earlier experimental measurements of laser energy attenuation and found to be in excellent agreement provided little excitation or ionization occurs.

INTRODUCTION

In a recent paper, Cardinal et al[1] measured the absorption of laser energy transmitted through sodium vapour when the wavelength of the laser was adjusted to overlap the 589 nm resonance transition of the sodium atoms. A spectrally integrated radiation transport analysis was undertaken in this paper in an attempt to account for the observed dependence of this absorption upon the sodium vapour density and the incident laser energy. This simple radiation transport theory appears to have been adequate to account for the experimental results at modest values of incident laser energy but underestimated the amount of attenuation observed at higher values of laser energy. Cardinal et al[1] suggested that this anomalous absorption could be explained in terms of excitation and ionization of the sodium vapour, as first observed by Lucatorto and McIlrath,[2] and theoretically discussed by Measures and Cardinal[3] and Measures et al.[4]

In the present paper, we have extended the calculations on the transport of laser radiation through an atomic vapour by taking account of both the transition absorption profile and the finite bandwidth of the laser pulse. Our analysis reveals that spectral hole burning is likely to have been quite severe in the experiments reported earlier.[1] We also compare the predictions of this more complete analysis with that of the simplified theory and with experimental results.[1]

FORMULATION OF RADIATION TRANSPORT PROBLEM

In formulating the radiative transfer equation appropriate to the transmission of a pulse of laser energy tuned to one of the resonance transitions within an atomic vapour, we shall assume that the atoms can be treated as a two-level system and that the speed of light is infinite.

We shall also neglect multiphoton interactions and laser-induced collisions as these were shown[1] to be negligible in our experiments. If we neglect lateral variations in the laser beam and assume the vapour to be homogeneous, we can write the one-dimensional radiative transfer equation as

$$\frac{\partial}{\partial z} I(z,t,\nu) = \frac{1}{4\pi} \{N_2(z,t) - gN_1(z,t)\} B_{21} I(z,t,\nu) \mathcal{L}_a(\nu) h\nu , \qquad (1)$$

where $I(z,t,\nu)$ represents the spectral irradiance at z and t, $g(\equiv g_2/g_1)$ represents the ratio of the degeneracies for the ground $|1\rangle$ and resonance $|2\rangle$ levels, B_{21} represents the Milne stimulated emission coefficient for the resonance transition, N_2 and N_1 represent the population densities of the resonance and ground states respectively, and $\mathcal{L}_a(\nu)$ represents the resonance line profile function.

If we can neglect excitation beyond the resonance level, that is to say we adhere strictly to a two-level system, continuity requires that

$$N_1 + N_2 = N_o , \qquad (2)$$

where N_o represents the atomic number density prior to laser illumination. Substitution of Eq. (2) into Eq. (1) with the introduction of

$$G \equiv g/(1+g), \qquad (3)$$

$$n \equiv N_2/GN_o , \qquad (4)$$

$$\sigma_a \equiv (1+g) h\nu \frac{B_{21}}{4\pi} \mathcal{L}_a(\nu_o), \qquad (5)$$

$$L(\nu) \equiv \mathcal{L}_a(\nu)/\mathcal{L}_a(\nu_o), \qquad (6)$$

and

$$x \equiv GN_o \sigma_a z \qquad (7)$$

yields

$$\frac{\partial}{\partial x} I(x,t,\nu) = \{n(x,t) - 1\} L(\nu) I(x,t,\nu) , \qquad (8)$$

where ν_o represents the centre frequency for the resonance line, σ_a the peak absorption cross section and x is the optical depth of the vapour at the centre frequency prior to laser irradiation.

If we neglect coherency effects, which is justified because of the large assumed laser bandwidth, then the temporal variation in the resonance state population can be described by a rate equation of the form

$$\frac{\partial}{\partial t} N_2(z,t) = \{gN_1(z,t) - N_2(z,t)\} \frac{B_{21}}{4\pi} \int_{-\infty}^{\infty} I(z,t,\nu) \mathcal{L}_a(\nu) d\nu - \frac{N_2(z,t)}{\tau_{21}} ,$$

where τ_{21} represents the lifetime of the resonance level population. In the absence of collisional quenching,

$$\tau_{21} = 1/\gamma_{21} A_{21} , \qquad (10)$$

where A_{21} represents the Einstein spontaneous transition probability for the resonance line and γ_{21} is the effective radiation trapping constant. If we introduce the nondimensional time

$$\tau \equiv t/\tau_{21} \qquad (11)$$

and the saturated irradiance

$$I_s = h\nu/\sigma_a\tau_{21}, \tag{12}$$

then Eq. (9) can be rewritten in the nondimensional form

$$\frac{\partial}{\partial x} n(x,\tau) = [1 - n(x,\tau)]\mathcal{J}(x,\tau) - n(x,\tau), \tag{13}$$

where we have introduced the new nondimensional irradiance variable

$$\mathcal{J}(x,\tau) = \frac{1}{I_s}\int_{-\infty}^{\infty} I(x,\tau,\nu)L(\nu)d\nu. \tag{14}$$

If we further assume that the laser irradiance changes slowly in the times of interest, then we can set $(\partial/\partial\tau)n(x,\tau) = 0$, which leads to a pseudo-steady-state nondimensional resonance level density given by

$$n(x,\tau) = \mathcal{J}(x,\tau)/[1 + \mathcal{J}(x,\tau)]. \tag{15}$$

If we now combine Eqs. (8) and (15), we can eliminate $n(x,\tau)$ and obtain

$$\frac{\partial}{\partial x} I(x,\tau,\nu) = -\frac{I(x,\tau,\nu)L(\nu)}{1 + \mathcal{J}(x,\tau)}. \tag{16}$$

The solution of Eq. (16) can be expressed in the form

$$I(x,\tau,\nu) = I(o,\tau,\nu)\exp\left[-L(\nu)\int_0^x \frac{dx^*}{1 + \mathcal{J}(x^*,\tau)}\right], \tag{17}$$

which can then be used in the definition of $\mathcal{J}(x,\tau)$ to yield the transcendental equation

$$\mathcal{J}(x,\tau) = \frac{1}{I_s}\int_{-\infty}^{\infty} I(o,\tau,\nu)L(\nu)\exp\left[-L(\nu)\int_0^x \frac{dx^*}{1 + \mathcal{J}(x^*,\tau)}\right]d\nu. \tag{18}$$

The laser spectral energy fluence transmitted through the vapour to a depth x is given by

$$E(\nu,x) = \tau_{21}\int_0^{\tau_\ell} I(x,\tau,\nu)d\tau, \tag{19}$$

where τ_ℓ represents the laser pulse duration. The corresponding total laser energy fluence is

$$E(x) = \tau_{21}\int_0^{\tau_\ell}\int_{-\infty}^{\infty} I(x,\tau,\nu)d\nu d\tau. \tag{20}$$

If we integrate Eq. (16) over all frequencies, we can write the radiative transfer equation for the laser irradiance as

$$\frac{\partial}{\partial x} I(x,\tau) = -\left[\frac{\mathcal{J}(x,\tau)}{1 + \mathcal{J}(x,\tau)}\right] I_s. \tag{21}$$

The solution of which takes the form

$$I(x,\tau) = I(o,\tau) - I_s\int_0^x \frac{\mathcal{J}(x^*,\tau)dx^*}{1 + \mathcal{J}(x^*,\tau)}. \tag{22}$$

This equation has to be solved in conjunction with Eq. (18) and does not in general lend itself to analytical solutions. There are, however,

two limiting cases where simple analytical solutions are possible. In the intense field limit, $\mathcal{J}(x,\tau) >> 1$, and

$$I(x,\tau) \sim I(o,\tau) - xI_s, \tag{23}$$

which amounts to linear attenuation of the laser beam as suggested by Measures.[5] At the other extreme, in the weak field limit, $\mathcal{J}(x,\tau) << 1$, and Eq. (22) becomes

$$I(x,\tau) = I(o,\tau) - \int_0^x \int_{-\infty}^{\infty} I(o,\tau,\nu)L(\nu)\exp\{-L(\nu)x^*\}d\nu dx^*. \tag{24}$$

Reversing the order of integration in Eq. (24) is permitted and yields

$$I(x,\tau) = \int_{-\infty}^{\infty} I(o,\tau,\nu)\exp\{-L(\nu)x\}d\nu, \tag{25}$$

which is the Beer-Lambert law of attenuation.

PARTICULAR SOLUTIONS

If the laser bandwidth is very narrow compared to that of the absorbing atoms,

$$I(x,\tau,\nu) = I(x,\tau)\delta(\nu-\nu_\ell), \tag{26}$$

where $\delta(\nu-\nu_\ell)$ represents a delta function and ν_ℓ the effective laser frequency. If we also assume that the resonance line profile function is Lorentzian, then

$$\mathcal{L}_a(\nu) = \frac{1}{\pi} \cdot \frac{\Delta_c}{(\nu-\nu_o)^2 + \Delta_c^2}, \tag{27}$$

where Δ_c represents the collision HWHM of the absorbing atoms. Under these circumstances, Eq. (17) takes the form

$$I(x,\tau) = I(o,\tau)\exp\left[-\int_0^x \frac{\Delta_c^2 dx^*}{(\nu_\ell-\nu_o)^2 + \Delta_c^2)\left\{1 + \frac{1}{I_s}\int_{-\infty}^{\infty} I(x,\tau)\,\frac{\Delta_c^2\delta(\nu-\nu_\ell)d\nu}{(\nu-\nu_o)^2 + \Delta_c^2}\right\}}\right]. \tag{28}$$

This reduces to

$$I(x,\tau) = I(o,\tau)\exp\left[-\int_0^x \frac{\Delta_c^2 dx^*}{(\nu_\ell-\nu_o)^2 + \Delta^2(x,\tau)}\right], \tag{29}$$

which can be interpreted as Beer-Lambert attenuation for atoms suffering power broadening under the influence of the radiation field such that their effective absorption HWHM

$$\Delta(x,\tau) = \Delta_c(1 + I(x,\tau)/I_s)^{1/2}. \tag{30}$$

For the earlier experimental work,[1] the laser bandwidth was quite substantial in terms of the resonance line bandwidth and a better approximation to the incident laser spectral irradiance is a Gaussian distribution of the form

$$I(o,\tau,\nu) = \frac{I(o,\tau)}{\beta_\ell\sqrt{\pi}} \exp\left[-\left(\frac{\nu-\nu_\ell}{\beta_\ell}\right)^2\right], \tag{31}$$

where $I(o,\tau)$ is the incident laser irradiance, β_ℓ represents the experimental bandwidth of the laser field, and ν_ℓ is the centre-frequency of the distribution.

Using Eqs. (27) and (31) in Eq. (18),

$$\mathcal{J}(x,\tau) = \frac{I(o,\tau)}{I_s\sqrt{\pi}} \int_{-\infty}^{\infty} L(\nu)\exp\left[-\left(\frac{\nu-\nu_\ell}{\beta_\ell}\right)^2 - L(\nu)\int_o^x \frac{dx^*}{1+\mathcal{J}(x^*,\tau)}\right] d\nu, \quad (32)$$

where

$$L(\nu) = \frac{\Delta_c^2}{(\nu-\nu_o)^2 + \Delta_c^2}. \quad (33)$$

In many experiments, especially those reported by Cardinal et al,[1] the laser is tuned to overlap the resonance line and so it is reasonable to set $\nu_\ell = \nu_o$. If we then introduce the nondimensional parameters

$$\eta = (\nu-\nu_o)/\beta_\ell, \quad (34)$$

$$\mathcal{I}(o,\tau) = I(o,\tau)/I_s, \quad (35)$$

$$A = (\beta_\ell/\Delta_c)^2, \quad (36)$$

Eq. (32) becomes

$$\mathcal{J}(x,\tau) = \frac{\mathcal{I}(o,\tau)}{\sqrt{\pi}} \int_{-\infty}^{\infty} \frac{\exp\left[-\eta^2 - \frac{f(x,\tau)}{1+A\eta^2}\right] d\eta}{1+A\eta^2}, \quad (37)$$

where

$$f(x,\tau) = \int_o^x \frac{dx^*}{1+\mathcal{J}(x^*,\tau)}. \quad (38)$$

The most important experimental parameters are the transmitted laser irradiance

$$I(x,\tau) = I(o,\tau) - I_s\int_o^x \frac{\mathcal{J}(x^*,\tau)dx^*}{1+\mathcal{J}(x^*,\tau)}, \quad (39)$$

the transmitted laser spectral energy fluence

$$E(\nu,x) = \tau_{21}\int_o^{t_p} I(o,\tau,\nu)\exp[-L(\nu)f(x,\tau)]d\tau, \quad (40)$$

and the total laser energy transmitted

$$\mathcal{E}(x) = \pi r_o^2\tau_{21}\int_o^{\tau_\ell}\int_{-\infty}^{\infty} I(o,\tau,\nu)\exp[-L(\nu)f(x,\tau)]d\nu d\tau, \quad (41)$$

where r_o represents the effective radius of the laser pulse. Clearly, evaluation of any or all of these parameters requires computing $\mathcal{J}(x,\tau)$ as given by Eq. (37). In general, this can only be achieved through numerical techniques. In the next section, we show the results of our calculations and indicate how they relate to our previous work.[1] The details of these calculations will not be included here but are available[6] on request.

COMPUTATIONAL RESULTS AND CONCLUSIONS

In the case of the laser pulses used in the experiments of Cardinal et al[1] the incident laser irradiance can be approximated by an expression of the form

$$I(o,\tau) = 1.1\times10^{7}E_{\ell}\,\frac{1}{10\gamma_{21}}\left\{1-\frac{\tau}{72.6\gamma_{21}}\right\}\exp\left(-\frac{\tau}{5\gamma_{21}}\right)\ (W\text{-}cm^{-2}), \tag{42}$$

where E_ℓ is the incident laser energy in J and the beam radius was measured to be about 0.2 cm. For sodium, the collision FWHM of the 589 nm resonance line[7] is

$$\Delta_c = 1.2 \times 10^{-7}\ N_o \quad (Hz), \tag{43}$$

where N_o is the sodium atom density in cm^{-3}. The corresponding saturated irradiance is

$$I_s = 0.193\ \Delta_c\gamma_{21} \quad (Wcm^{-2}). \tag{44}$$

The optical depth corresponding to a vapour length z (cm) and a density N_o (cm^{-3}) is

$$x = 8.22 \times 10^{-3} z\ N_o/\Delta_c = 6.95 \times 10^{4} z; \tag{45}$$

for the 40-cm vapour length used in the earlier experiments,[1]

$$x_L = 2.74 \times 10^{6}. \tag{46}$$

Clearly, the vapour was extremely optically thick at the resonance line centre frequency ν_o. The laser linewidth was about 0.6 Å which corresponds to $\beta_\ell = 5.2 \times 10^{10}$ Hz.

In Figs. 1 and 2, the incident and transmitted laser spectral irradiance half-profiles (normalized by the peak value of the incident laser spectral irradiance) are presented in terms of the off-resonance frequency parameter n for two values of sodium vapour density ($N_o = 2.9 \times 10^{15}$

and 1.5×10^{16} cm^{-3}). The corresponding normalized sodium 589 nm absorption half-profiles are also presented for comparison. It is quite evident that the width of the spectral hole burned into the transmitted laser profile is much greater than the width of the absorption line in both cases. In Fig. 3, we present the full frequency profiles of the laser spectral energy fluence (normalized by the peak value of the incident laser spectral energy fluence) for several vapour lengths at the two sodium densities $N_o = 2.9 \times 10^{15}$ and 1.5×10^{16} cm^{-3}. The laser energy for both densities was taken to be 0.4J. The difference in the shape of the spectral hole burned into the laser spectral energy fluence profile for the two densities is apparent and should provide a good test for the theory in future experiments.

There are three characteristic ratios that could be used for this purpose: the full width at half depth of the hole compared to that of the incident FWHM δ_A/δ_L, the height of the transmitted laser profile at the centre frequency compared to that of the incident laser pulse $\mathcal{L}_L^o(z)/\mathcal{L}_L^o$, and the height of the peak in the transmitted laser profile compared to the height at the centre frequency of the incident laser profile $\mathcal{L}_L^p(z)/\mathcal{L}_L^o$. These characteristic lengths are indicated on the representative laser profiles shown in Fig. 4. In Fig. 5, we have plotted the variation of these ratios as a function of the vapour length for the two specified sodium densities.

In order to compare this more complete theoretical analysis of the attenuation of a laser pulse as it propagates through an absorbing atomic vapour with our earlier experiments and theory,[1] we have evaluated the absorption expected for the same range of density and incident laser energy conditions. The results are presented as Fig. 6 and are surprising. It appears that making allowance for spectral hole burning

makes almost no difference to the predicted energy absorbed. This result suggests that absorption in the broad Lorentzian wing of the resonance line is the primary mechanism of attenuation for the laser pulse. This idea is strengthened by additional computations that we have undertaken[6] in which the resonance line was assumed to be Doppler-broadened. In this instance, the attenuation was very much less than with a Lorentz profile due to the low wing absorption of a Gaussian profile.

We have derived a set of equations that describe the attenuation of a saturating laser pulse as it propagates through a resonantly absorbing atomic vapour, provided little or no excitation or ionization occurs. These equations predict that appreciable spectral hole burning can arise if the optical depth of the vapour is large enough. In the event that the spectral details are unimportant, our analysis indicates that the simpler relation[1]

$$I(y) + I_s \ell nI(y) = I(o) + I_s \ell nI(o) - yI_s$$

is adequate to describe the attenuation of the laser irradiance under a wide range of conditions. Here, $I(y)$ represents the laser irradiance at an effective optical depth $y = x \times \pi\Delta_c/\Delta\nu_\ell$, where $\Delta\nu_\ell$ represents the effective bandwidth of the laser, $I(o)$ is the corresponding incident laser irradiance, and I_s is the saturated irradiance of the relevant transition.

ACKNOWLEDGEMENTS

Work supported by USAF/AFOSR (under Grant No. 80-0057B) and the Natural Science and Engineering Research Council of Canada. The authors would like to thank Prof. Alkemade for remarks that prompted this analysis.

REFERENCES

1. P. G. Cardinal, P. L. Wizinowich and R. M. Measures, JQSRT, 25, 537 (1981).
2. T. B. Lucatorto and T. J. McIlrath, Phys. Rev. Letts. 37, 428 (1976).
3. R. M. Measures and P. G. Cardinal, Phys. Rev. A 25, 804 (1981).
4. R. M. Measures, P. G. Cardinal and G. W. Schinn, J. Appl. Phys. 52, 1269 (1981); 52, 7459 (1981).
5. R. M. Measures, JQSRT 10, 107 (1970).
6. H. Herchen, University of Toronto, Institute for Aerospace Studies, M.A.Sc. Thesis, 1982.
7. Hans R. Griem, Plasma Spectroscopy, McGraw-Hill Book Co. (1964).

FIGURE CAPTIONS

1. Incident and transmitted laser spectral irradiance half-profiles of a saturating laser pulse propagating through a 40-cm column of sodium vapour with an atom density of 2.9×10^{15} cm^{-3}. The centre frequency of the laser radiation was assumed to coincide with that of the 589 nm resonance line of sodium. The sodium atom's absorption half-profile is also presented. τ_{max} refers to the instant of maximum irradiance.

2. Incident and transmitted laser spectral irradiance half-profiles of a saturating laser pulse propagating through a 40-cm column of sodium vapour with an atom density of 1.5×10^{16} cm^{-3}. The centre frequency of the laser radiation was assumed to coincide with that of the 589 nm resonance line of sodium. The sodium atom's absorption half-profile is also presented. τ_{max} refers to the instant of maximum irradiance.

   Incident and transmitted laser spectral energy fluence profiles of a saturating laser pulse propagating through various lengths of sodium vapour for atom densities of 2.9×10^{15} and 1.5×10^{16} cm^{-3}.

4. Representative laser spectral energy fluence profiles for representative incident and transmitted laser pulses.

5. Variations of the characteristic ratios with vapour length at two densities.

6. Comparison of the present calculations with the original[1] theoretical and experimental variations of absorbed laser energy as functions of incident laser pulse energy, for three sodium atom densities.

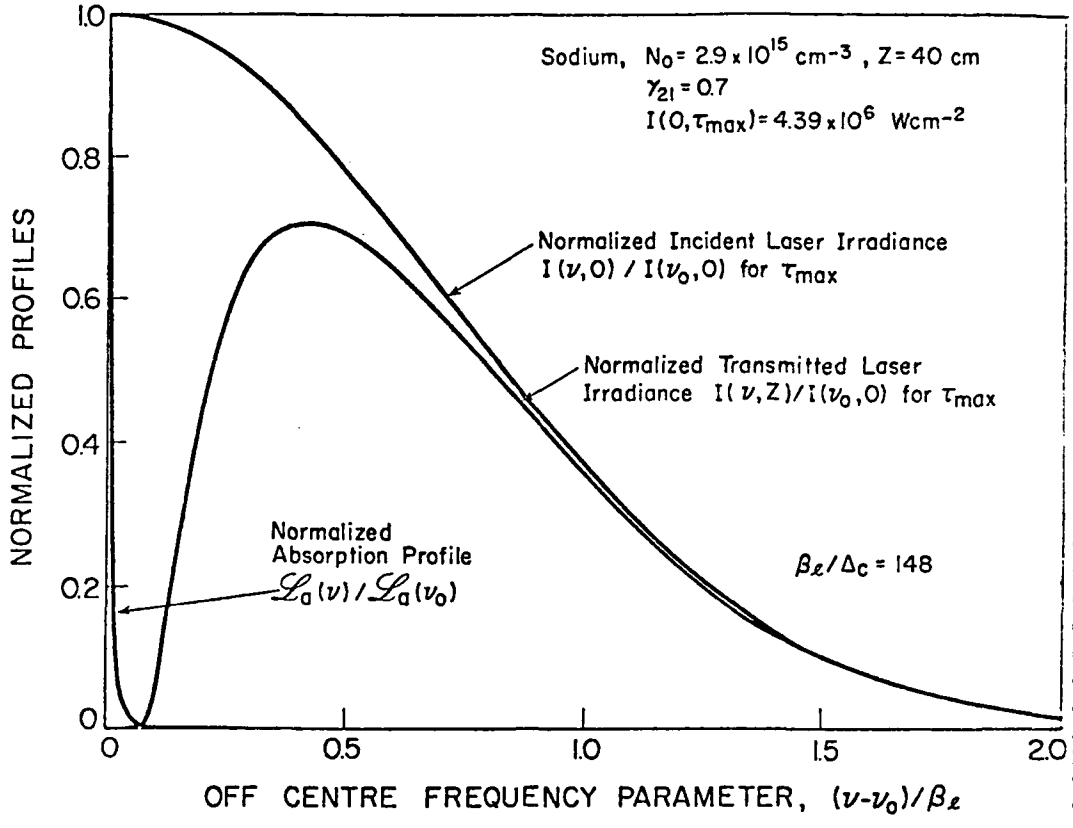

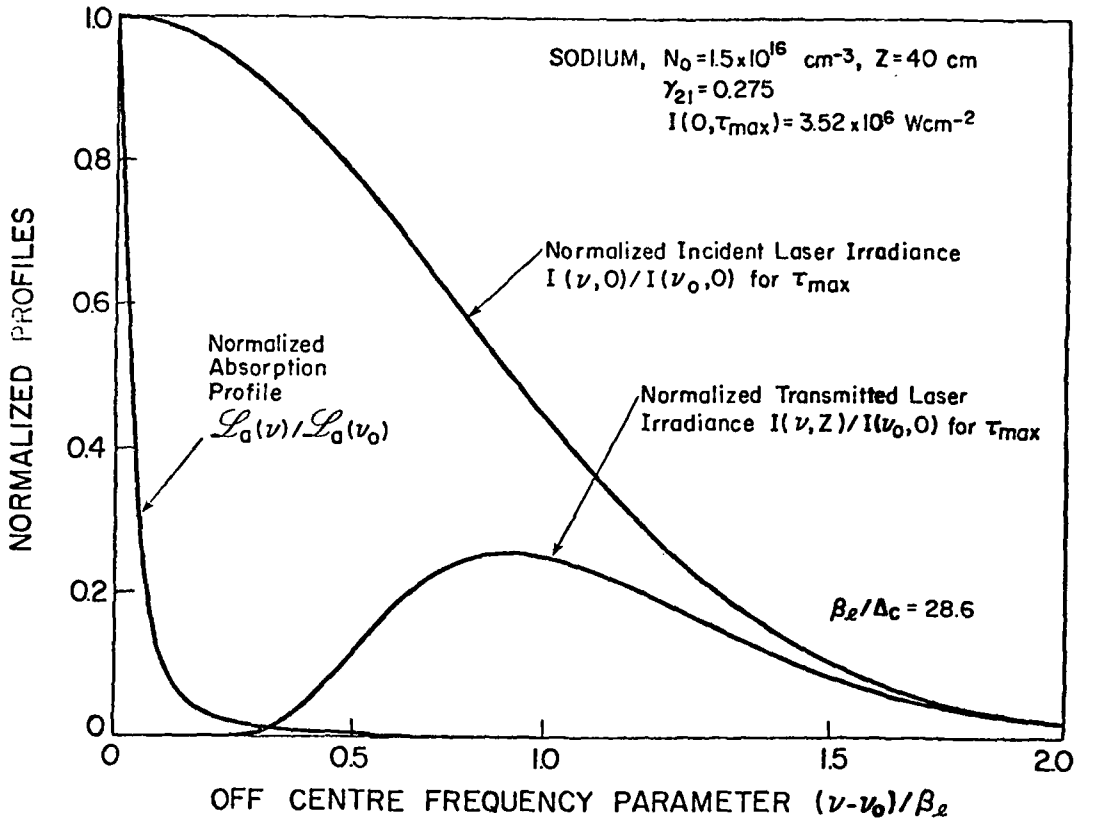
SODIUM, $N_0 = 1.5 \times 10^{16}$ cm^{-3}, Z = 40 cm
$\gamma_{21} = 0.275$
$I(0,\tau_{max}) = 3.52 \times 10^6$ Wcm^{-2}
Normalized Incident Laser Irradiance
$I(\nu,0)/I(\nu_0,0)$ for τ_{max}
Normalized Absorption Profile
$\mathscr{L}_a(\nu)/\mathscr{L}_a(\nu_0)$
Normalized Transmitted Laser Irradiance $I(\nu,Z)/I(\nu_0,0)$ for τ_{max}
$\beta_\ell/\Delta_C = 28.6$
NORMALIZED PROFILES
OFF CENTRE FREQUENCY PARAMETER $(\nu-\nu_0)/\beta_\ell$
0
0.2
0.4
0.6
0.8
1.0
0.5
1.5
2.0

FIG 2

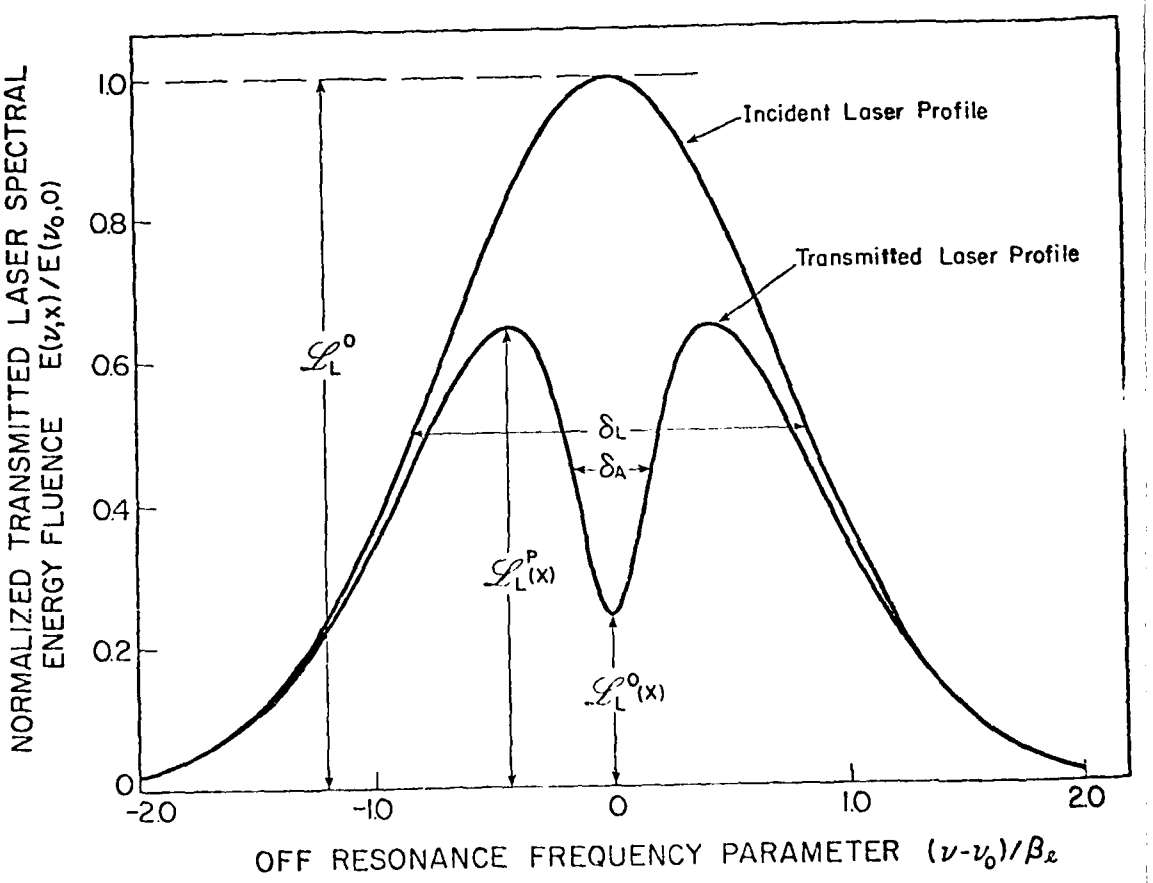
Incident Laser Profile
Transmitted Laser Profile
$\mathscr{L}_L^0$
δ_L
δ_A
$\mathscr{L}_L^{P}(X)$
$\mathscr{L}_L^0(X)$
NORMALIZED TRANSMITTED LASER SPECTRAL ENERGY FLUENCE $E(\nu,x)/E(\nu_0,0)$
OFF RESONANCE FREQUENCY PARAMETER $(\nu-\nu_0)/\beta_\ell$
0
0.2
0.4
0.6
0.8
1.0
-2.0
-1.0
1.0
2.0

FIG 3

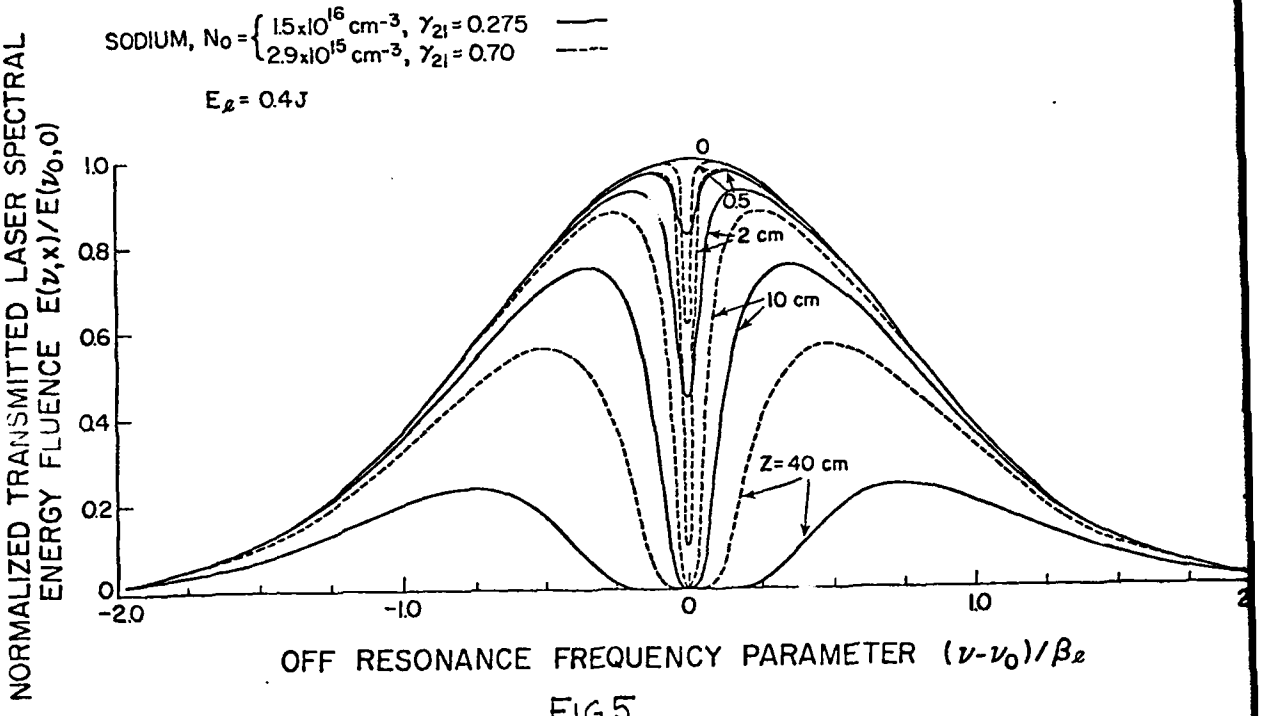
SODIUM, N_0 = { 1.5×10^{16} cm^{-3}, γ_{21} = 0.275 ; 2.9×10^{15} cm^{-3}, γ_{21} = 0.70
E_ℓ = 0.4J
NORMALIZED TRANSMITTED LASER SPECTRAL ENERGY FLUENCE $E(\nu,x)/E(\nu_0,0)$
0
0.5
2 cm
10 cm
Z=40 cm
1.0
0.8
0.6
0.4
0.2
0
-2.0
-1.0
0
1.0
OFF RESONANCE FREQUENCY PARAMETER $(\nu-\nu_0)/\beta_\ell$

FIG 5.

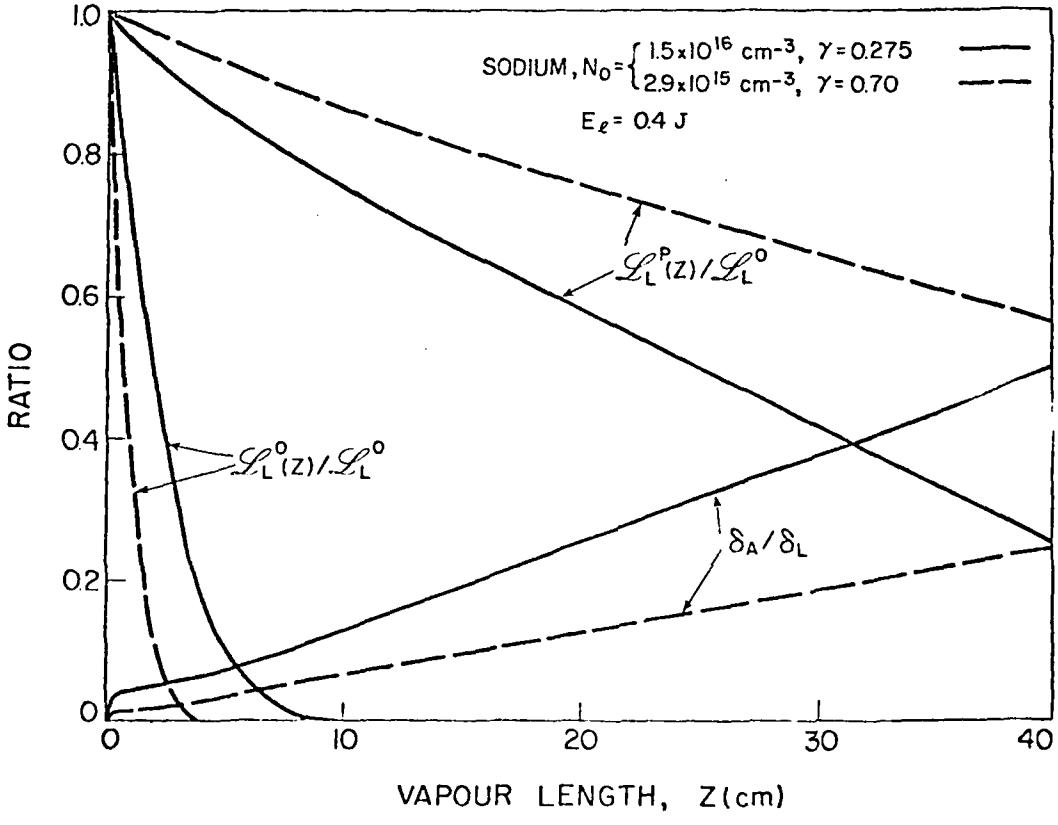
SODIUM, N_0 = { 1.5×10^{16} cm^{-3}, γ = 0.275 ; 2.9×10^{15} cm^{-3}, γ = 0.70
E_ℓ = 0.4 J
$\mathscr{L}_L^P(Z)/\mathscr{L}_L^0$
$\mathscr{L}_L^0(Z)/\mathscr{L}_L^0$
δ_A/δ_L
RATIO
1.0
0.8
0.6
0.4
0.2
0
0
10
20
30
40
VAPOUR LENGTH, Z(cm)

FIG 4.

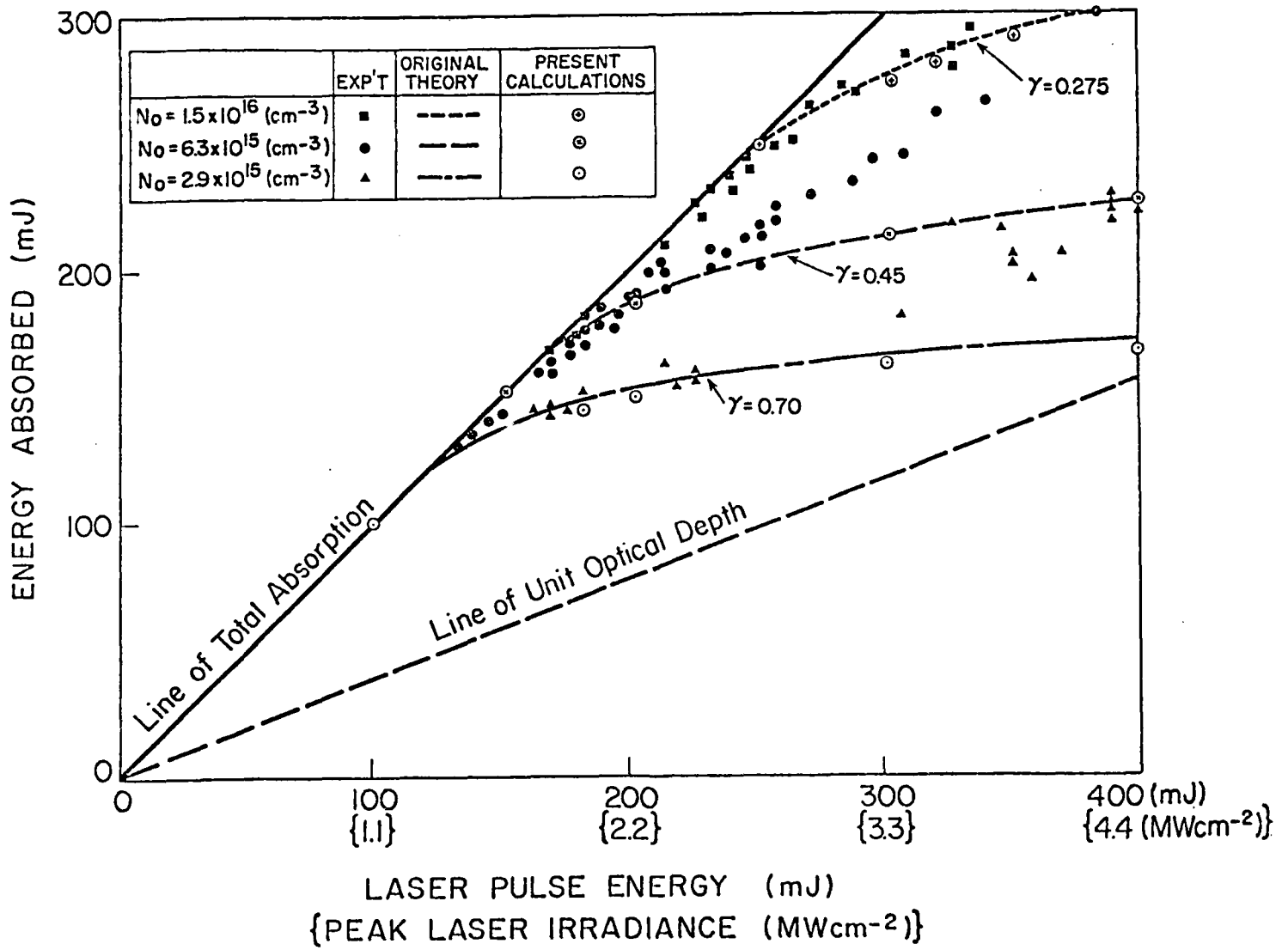
EXP'T
ORIGINAL THEORY
PRESENT CALCULATIONS
No = 1.5x10^16 (cm^-3)
No = 6.3x10^15 (cm^-3)
No = 2.9x10^15 (cm^-3)
γ=0.275
γ=0.45
γ=0.70
Line of Total Absorption
Line of Unit Optical Depth
ENERGY ABSORBED (mJ)
300
200
100
0
0
100 {1.1}
200 {2.2}
300 {3.3}
400 (mJ) {4.4 (MWcm^-2)}
LASER PULSE ENERGY (mJ)
{PEAK LASER IRRADIANCE (MWcm^-2)}

The influence of molecular nitrogen upon plasma channel formation by laser resonance saturation

R. M. Measures, S. K. Wong, and P. G. Cardinal
Institute for Aerospace Studies, University of Toronto, 4925 Dufferin Street, Downsview, Ontario, Canada M3H 5T6

(Received 7 July 1981; accepted for publication 27 October 1981)

Laser resonance saturation of alkali vapors represents a very attractive method of creating the extended plasma channels of interest in light ion beam fusion. We have undertaken a preliminary study of the influence of molecular nitrogen upon this laser ionization technique. Our results indicate that the electron cooling, resonance quenching, and the increase in the laser energy requirement are acceptable, providing that the alkali seeding exceeds 0.5%.

PACS numbers: 52.50.Jm, 52.20.Fs, 52.25.Ps

I. INTRODUCTION

A fusion reactor based upon *multiple light ion beam drivers* promises to be less expensive and more efficient than other inertial confinement reactor schemes. The light ion beam approach to fusion also lends itself to methods of minimizing the wall loading of such a reactor by employing a large reactor cavity and using an atmosphere that will absorb most of the energy liberated (other than that released in the form of fast neutrons) when the fuel pellet undergoes fusion. A *stand off* distance of several meters may be required in order to protect the array of ion diodes from the microexplosion, and this will necessitate the development of an efficient mode of ion beam transport across the reactor chamber.

There is a reasonable body of experience that has demonstrated that light ion beams can be efficiently transported for distances of at least one meter by means of current carrying plasma channels.[1-3] These plasma channels provide both charge and beam current neutralization and sufficient azimuthal magnetic field to confine and guide the ions. Recent experiments have also shown that these discharge channels can be initiated and guided by laser heating of a molecular gas.[4,5] In this work a CO_2 laser is used to vibrationally excite ammonia molecules, thereby creating a low density, very weakly ionized channel for guiding the discharge. Although this approach may be adequate for testing the concept it is unlikely to be a candidate for a fusion power reactor, where the ambient temperature could be in excess of 1000 °K.

We have proposed[6] that saturating a strong transition within one of the gaseous constituents (such as lithium vapor) of a fusion reactor with an appropriately tuned laser represents an almost ideal method of creating the multiple electrical discharge guide paths. In regard to this task the advantages inherent in our proposed *laser ionization based on resonance saturation*—LIBORS technique are

(1) *High Efficiency* due to the large cross sections involved in directly converting the laser energy into ionization and electron energy;

(2) *Complete Ionization* ($>95\%$) of laser pumped species along the path of the laser beam, even for relatively modest values of laser irradiance;

(3) *Uniform Plasma Channels* should be formed due to the linear rate of energy deposition along the path of the laser beam;

(4) *Superelastic Heating* of the free electrons to provide high conductivity channels;

(5) *Rapid Formation* of the plasma channels through exponential growth of ionization;

(6) *Minimum Pellet Preheat* by the laser radiation due to the modest demand of laser energy;

(7) *Compatibility* of the constituent (such as lithium vapor), that is amenable to LIBORS, with the proposed operating conditions within a fusion reactor; and

(8) *Resonance Line Lasers* currently under development[7] could lead to a simplification of the design and operation of the lasers required for LIBORS.

In our initial study[6] we have shown that a laser pulse of less than 1 J would be required to create a plasma channel with an electron density of close to 10^{15} cm^{-3} over a 5-m path in the case of a 0.1-Torr sodium atmosphere. Furthermore, we can say, based on our recent development of a simple model of LIBORS,[8,9] that this estimate would also apply to a similar lithium atmosphere. This can be seen by reference to Fig. 1, where the variation in the 95% ionization burnout time with laser irradiance is presented for lithium, sodium, potassium, and rubidium. Although these ionization times were estimated on the basis of a spatially uniform, step-like laser pulse, we have recently shown[9] that in the case of sodium, allowance for a realistic laser pulse (both spatially and temporally) should lead only to a doubling of the *observed* ionization time. By way of illustration, in Fig. 2, we present the time history of the growth in the *free electron line density*, $N_e(t)$ for three kinds of laser pulse.

An analysis[10] of the radiant heat pulse, from the fusion created fireball within the atmosphere of a light ion beam reactor, has suggested that it might lead to excessive loading of the reactor walls. A more recent analysis[11] has found that seeding this argon atmosphere with as little as 0.2% of sodium vapor could degrade this heat pulse to a more satisfactory level. Thus it would appear that the alkali vapor could serve two useful purposes within the reactor. The possibility of using a molecular gas as the main constituent of the reactor cavity atmosphere has also been suggested.[12]

In this paper, we report on an initial study of the influence a of molecular gas upon the plasma channel formation potential of LIBORS. Nitrogen was chosen as a representa-

 0021-8979/82/085541-11$02.40

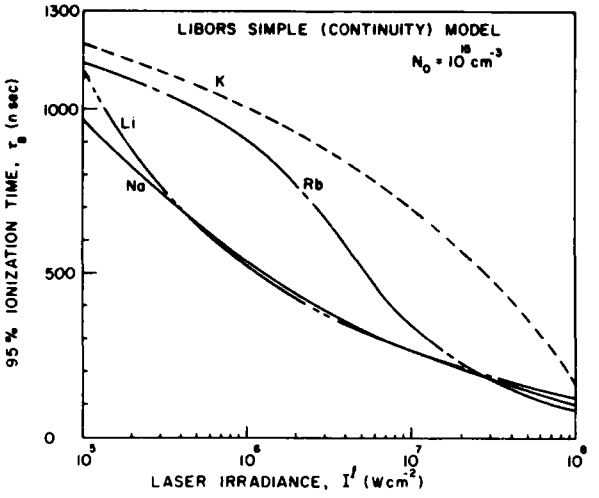

FIG. 1. Variation of 95% ionization burnout times τ^B with laser irradiance I^l, as predicted by simple model for lithium, sodium, potassium, and rubidium, corresponding to initial density $N_0 = 10^{15}$ cm^{-3}.

tive molecular gas with no obvious disadvantage. In particular, we set out to see if laser resonance saturation of sodium vapor could still lead to the formation of a plasma channel with an electron density of close to 10^{15} cm^{-3}, in a time of less than 1 μsec in the presence of molecular nitrogen at a density of at least 2×10^{17} cm^{-3}. In addition, we have evaluated the increase in the minimum laser energy required for the creation of such channels by this background gas. Where possible we have made simplifying assumptions that are strongly conservative and we therefore expect that our results will, if anything, overpredict the laser energy required to create these plasma channels. Even so, our analysis is encouraging because it indicates that LIBORS still represents an efficient and low energy method of producing the discharge guide path necessary for ion beam transport.

II. LASER IONIZATION WITH NITROGEN BACKGROUND GAS

The presence of an appreciable background density of a molecular gas such as nitrogen will invariably have a detrimental effect on the laser ionization process. Clearly the large number of internal energy states associated with a molecule will represent an effective sink for the energy of both the free electrons and the laser excited species. The most serious of these are considered below.

A. Potential influence of nitrogen

(i) Free electron cooling through excitation, dissociation, and ionization of the nitrogen molecules, viz.,

$e^- + N_2 \rightarrow N_2^+ + 2e^- - (15.58\text{ eV})$ *ionization*,

$e^- + N_2 \rightarrow N^+ + N + 2e^- - (14.54\text{ eV})$ *dissociative ionization*,

$e^- + N_2 \rightarrow N + N + e^- - (9.76\text{ eV})$ *dissociation*.

The group of interactions shown above are all expected to be unimportant due to the relatively low electron temperature found in LIBORS of the alkali metal vapors (typically $\lesssim 1$ eV). In the case of

$e^- + N_2 \rightarrow N_2^* + e^- - (>6.2\text{ eV})$ *electronic excitation*,

the energy spacing between the ground state ($X\,^1\Sigma_g^+$) of N_2 and its first excited electronic state ($A\,^3\Sigma_g^+$) is about 6.2 eV and so electronic excitation of N_2 should also be relatively unimportant unless the alkali seeding drops below 0.1%.

Thus, the primary cooling mechanism for the free electrons has been assumed to result from

$e^- + N_2 \rightarrow N_2 + e^- - (\approx 0.01\text{ eV})$ *rotational excitation*,

and $e^- + N_2(w) \rightarrow N_2(u) + e^- - (\epsilon_u - \epsilon_w)$ *vibrational excitation*,

of the nitrogen molecules, where $\Delta\epsilon_{uw} \equiv \epsilon_u - \epsilon_w \approx (u-w)\times 0.29$ eV). ϵ_w represents the energy of vibrational state described by the w-vibrational quantum number and $u > w$.

(ii) Quenching of the laser excited resonance state through vibrational excitation of nitrogen molecules

$$Na(3p) + N_2(w) \rightarrow Na(3s) + N_2(u) + [E_{21} - \Delta\epsilon_{uw}],$$

where E_{21} represents the sodium resonance energy (equal to the laser photon energy).

We see that for each resonance state atom quenched by collision with a nitrogen molecule, the excess energy between the resonance energy and that required to vibrationally excite the molecule from w to u, goes into translational energy of the colliding species, thereby heating the gaseous mixture.[13]

(iii) Depletion of the alkali seed atoms through the formation of nitrides has been assumed to be negligible due to the low decomposition temperature of these compounds (e.g., NaN_3 decomposes for $T > 300$ °K).

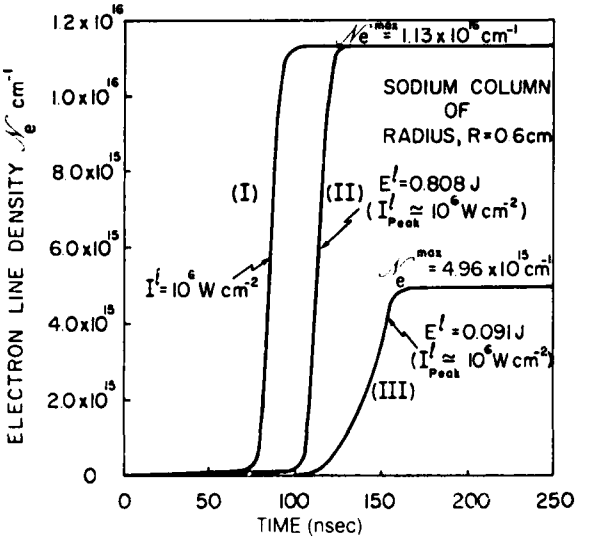

FIG. 2. Comparison of the temporal variation of the *free electron line density*, $\mathcal{N}_e$ of a sodium column evaluated to a radius of 0.6 cm for the three cases. (i) Steplike, flat laser pulse for $I^l = 10^6$ W cm^{-2}; (ii) Laser pulse is assumed to have realistic temporal variation but uniform radial distribution out to 0.6 cm. Energy in the pulse is set to be 0.808 J corresponding to a peak irradiance of 10^6 W cm^{-2}; (iii) Laser pulse is assumed to have both a realistic temporal variation and a Gaussian radial distribution with an exponential radius of 0.20 cm and an energy of 0.091 J, giving a peak irradiance of 10^6 W cm^{-2}.

(iv) Removal of low energy electrons through the formation of N_2^- appears to be negligible due to the negative electron affinity of N_2.[14]

It is apparent that the two most important interactions to be considered are electron cooling and direct resonance level quenching, through vibrational excitation of the nitrogen molecules. We shall now consider each in turn.

B. Electron cooling through vibrational excitation of nitrogen

The total electron-nitrogen scattering cross section is found to peak just in the energy range of interest.[15] The magnitude and structure of this cross section is associated with a resonance interaction that leads to the vibrational excitation of N_2 through the momentary formation of N_2^- according to Herzenberg[16] and Birtwistle and Herzenberg.[17] The absence of an electric dipole moment for N_2 ensures that the probability of direct vibrational excitation is small.[15]

The LIBORS energy equation[8] for the free electrons in the presence of nitrogen molecules can be written in the form

$$\begin{aligned}\frac{d}{dt}(N_e\epsilon_e) = {} & N_2 N_e K_{21} E_{21} + (2E_{21} - E_{c2}) N_2 \sigma_{2c}^{(2)} F^2 \\ & + \tfrac{1}{2}(2E_{21} - E_A) N_2^2 \sigma_A v \\ & + \tfrac{1}{2}(3E_{21} - E_{cl}) N_2^2 \sigma_L F v \\ & + \sum_{n>2} (E_{21} - E_{cn}) N_n \sigma_{nc}^{(1)} F \\ & - N_e \sum_{n>1} N_n K_{nc} E_{cn} - N_e C \\ & - N_e^2 H_{ei} - N_e N H_{ea} + N_e^3 \sum_{n>1} K_{cn} E_{cn} \\ & - N_e^2 \epsilon_e \sum_{n>1} \beta(n) + N_e \sum_{u>w} \sum \langle \sigma v \rangle_{uw}^{e} n_u \Delta\epsilon_{uw} \\ & - N_e \sum_{u>w} \sum \langle \sigma v \rangle_{wu}^{e} n_w \Delta\epsilon_{uw}, \end{aligned} \tag{1}$$

where $\epsilon_e(J)$ represents the mean translation energy and N_e the density of the free electron. *Note* N_2 in this equation represents the sodium resonance state population density and N_n (cm^{-3}) represents the population density of the n level in sodium. n_u and n_w represent the respective nitrogen population densities in the u and w vibrational states of the ground electronic state.

The first term on the RHS of Eq. (1) represents the superelastic heating term for the free electrons arising from electron collision quenching of the laser sustained resonance level population. $E_{mn}(J)$ represents the energy separation between levels m and n of the *laser pumped species*, LPS. E_{cn} represents the ionization energy of level n of LPS and K_{cn} represents the three-body recombination rate coefficient for level n. The next three terms of Eq. (1) represent the contribution to the free electron energy from the three most likely electron seed creation processes. In the case of sodium: (i) resonance state two-photon ionization $Na(3p) + 2h\nu \rightarrow Na^+ + e^- + KE$ (≈ 1.17 eV), (ii) associative ionization $Na(3p) + Na(3p) \rightarrow Na_2^+ + e^- + KE$ (≈ 0.04 eV), (iii) laser-induced penning ionization $Na(3p) + Na(3p) + h\nu \rightarrow Na^+ + Na(3s) + e^- + KE$ (≈ 1.17 eV).

Na(3p) and Na(3s) represent a resonance and ground state atom, respectively. $h\nu$ represents the laser photon energy and corresponds to the energy difference between the resonance and ground states E_{21}. $\sigma_{2c}^{(2)}$ (cm^4 sec) represents the two-photon ionization rate coefficient (sometimes referred to as the generalized cross section) for the resonance level; σ_A and E_A represent, respectively, the cross section and ionization energy corresponding to associative ionization; σ_L (cm^4 sec) represents the cross section for laser-induced Penning ionization, v represents the mean velocity of the LPS.

$\sigma_{nc}^{(1)}$ (cm^2) represents the single photon ionization cross section for level n, and the sum extends over all levels $n > 2$ for which ionization by a single laser photon can be achieved, F (photons cm^{-2} sec^{-1}) represents the appropriate photon flux per unit area of the laser beam, i.e.,

$$h\nu F \equiv \int I^l(\nu)\, d\nu.$$

C represents the loss of energy per electron due to the net collisionally induced upward movement of bound electrons (exclusive of the resonance superelastic term) and is given by

$$C = \sum_{n=1} \sum_{m>n} (N_n K_{nm} - N_m K_{mn}) E_{mn} + N_2 K_{21} E_{21},$$

where $N_2 K_{21} E_{21}$ represents the laser-induced superelastic heating term for the free electrons. H_{ei} represents the rate of elastic energy transfer to ions through Coulomb scattering collisions, and if the electrons and ions have Maxwellian velocity distributions H_{ei} takes the form[18]

$$H_{ei} = \frac{e^4}{m_i}\left(\frac{8\pi m_e}{kT_e}\right)^{1/2}\left(\frac{T_e - T_i}{T_e}\right)\ln\left(\frac{9(kT_e)^3}{8\pi N_e e^6}\right),$$

where T_e (K) and T_i (K) represent the respective electron and ion temperatures [viz., $\epsilon_e = (3/2)kT_e$) and m_e (g)] and m_i (g) their respective masses, e is the electronic charge (esu). N (cm^{-3}) represents the total neutral atom density, and H_{ea} represents the rate of elastic energy coupling between the free electrons and the neutral atoms. We can approximate H_{ea} by

$$H_{ea} \approx \left(\frac{8kT_e}{m_e}\right)^{1/2}(T_e - T_a)\sigma_{ea}\frac{4km_e}{m_a},$$

where σ_{ea} represents the electron atom elastic scattering cross section. $\beta(n)$ represents the radiative recombination rate coefficient for level n of the LPS.

The last two terms of Eq. (1) take account of the energy gained and lost to the free electrons through vibrational de-excitation and excitation respectively. $\langle \sigma v \rangle_{wu}^{e}$ represents the electron collisional excitation rate coefficient for excitation from w to u.

The electron energy equation can be divided into two equations, one taking account of the rate of change of the electron density and the other giving the rate of change of the mean electron translational energy. If we assume that the free electrons are described by a Maxwellian velocity distribution corresponding to an electon temperature T_e, then we

can write for $\epsilon_e = (3/2)kT_e$,

$$\frac{3}{2}k\frac{dT_e}{dt} = \frac{1}{N_e}\left[\frac{d}{dt}(N_e\epsilon_e) - \epsilon_e\frac{dN_e}{dt}\right], \tag{2}$$

where

$$\frac{dN_e}{dt} = N_e\sum_{n>1}N_nK_{nc} + \sum_{n>2}N_n\sigma_{nc}^{(1)}F + N_2\sigma_{2c}^{(2)}F^2 + \frac{1}{2}N_2^2\{\sigma_A v + \sigma_L vF\} - N_e^2\sum_{n>1}\beta(n) - N_e^3\sum_{n>1}K_{cn}, \tag{3}$$

and $d(N_e\epsilon_e)/dt$ is given by Eq. (1).

We see that the influence of the nitrogen molecules is felt through their effect on T_e, and subsequently on the various electron collisional rate coefficients. In order to determine the extent of this influence we need to solve not only the atomic population rate equations and energy equations, but also the appropriate set of nitrogen vibrational state population rate equations,

$$\frac{dn_u}{dt} = N_e\left\{\sum_{w\neq u}n_w\langle\sigma v\rangle_{wu}^e - n_u\sum_{w\neq u}\langle\sigma v\rangle_{uw}^e\right\} + \langle\sigma v\rangle^E\Big[\sum_{w\neq u}\{n_wn_uP(u+1,u,w,w+1) + n_wn_{u-1}P(u-1,u,w,w-1) - n_{w+1}n_uP(u,u+1,w+1,w) - n_{w-1}n_uP(u,u-1,w-1,w)\}\Big]. \tag{4}$$

The first two summation terms in Eq. (4) take account of the electron induced rates of excitation and de-excitation of the ground electronic state having a vibrational quantum number "u". The subsequent four summation terms are concerned with the rate of creation and rate of destruction of the population in this u-vibrational state through vibration-vibration energy exchange collisions between nitrogen molecules. Thus $\langle\sigma v\rangle^E$ represents the elastic (gas kinetic) collision rate coefficient between nitrogen molecules.
$P(u+1,u,w,w+1)$ represents the probability that in a collision between two nitrogen molecules there will be a vibrational exchange of energy equal to one quanta of vibration energy, i.e., the molecule that was in state-$(u+1)$, drops to u, while the molecule that was in state-w is raised to $w+1$.

For a harmonic oscillator it can be shown that[19]

$$P(u+1,u,w,w+1) = P(u,u+1,w+1,w) = (u+1)(w+1)P(1,0,0,1), \tag{5}$$

and

$$P(u,u-1,w-1,w) = P(u-1,u,w,w-1) = uwP(1,0,0,1). \tag{6}$$

If we further introduce the total nitrogen density,

$$n_I \equiv \sum_u n_u, \tag{7}$$

and the average vibrational quanta

$$\bar{V} \equiv \sum_u wn_w/n_I, \tag{8}$$

then we can write

$$\frac{dn_u}{dt} = N_e\left\{\sum_{w\neq u}n_w\langle\sigma v\rangle_{wu}^e - n_u\sum_{w\neq u}\langle\sigma v\rangle_{uw}^e\right\} + \frac{1}{\tau_v}[(u+1)(\bar{V}+1)n_{u+1} - \{u+(2u+1)\bar{V}\}n_u + u\bar{V}n_{u-1}], \tag{9}$$

where

$$\tau^V \equiv [\langle\sigma v\rangle^E n_T P(1,0,0,1)]^{-1} \tag{10}$$

represents the effective relaxation time for vibrational exchange.

A set of equations of the form given by Eq. (9) needs to be solved in conjunction with the normal set of LIBORS equations and the amended electron energy equation [Eq. (2)]. In general the rate of electron excitation from the lowest vibrational state is larger, or of the same order of magnitude, than that from any of the higher vibrational states. In addition a molecule in an excited vibrational state can be collisionally de-excited and heat the free electrons. Consequently, if we assume that essentially all of the nitrogen molecules are in their lowest vibrational state, the rate of electron cooling will be as large as possible and we will invariably underestimate T_e. This in turn will lead to a *conservative* estimate of the lengthening of the ionization time associated with the molecular background gas. With the assumption that all the nitrogen molecules are in the lowest vibrational state we avoid having to solve the set of vibrational rate equations, and can write for the electron energy equation

$$\frac{3}{2}k\frac{dT_e}{dt} = \text{LIBORS terms} - n_0\sum_{w>0}\langle\sigma v\rangle_{0w}^e\Delta\epsilon_{w0}, \tag{11}$$

where n_0 is set equal to the total nitrogen density and the LIBORS terms of Eq. (11) refer to all the terms of Eq. (2) exclusive of those involving nitrogen.

It should also be noted that $\langle\sigma v\rangle_{0w}^e$ decreases as w increases and so in our preliminary work we have summed to $w = 8$ in Eq. (11). These rates were numerically evaluated from the cross-sectional data available in the literature.[20] It should be noted that these cross sections include both rotational and vibrational excitations. The subsequent vibrational cooling term in Eq. (11) is dependent upon the electron temperature and is fitted by an expression of the form $n_0AT_e^B\exp(C/T_e)$ in our LIBORS code, where $A = 8.685\times10^{-4}$, $B = -0.9678$, $C = -2.359\times10^4$, and T_e is in K.

C. Resonance quenching through vibrational excitation of nitrogen

In addition to cooling the electrons the nitrogen molecules will also quench the resonance state sodium atoms through the following interaction

$$Na(3p) + N_2(w) \rightarrow Na(3s) + N_2(u) + (E_{21} - \Delta\epsilon_{uw}).$$

Here again $N_2(w)$ and $N_2(u)$ represent nitrogen molecules in the w and u vibrational states, respectively. In such a quenching collision the vibration energy of the nitrogen molecule is increased and the difference between the atom resonance energy and the gain in vibrational energy will appear

in the form of increased translational energy of the collision partners. This form of heating will be considered later.

Each time a sodium resonance atom is returned to its ground level by a quenching collision, an additional laser photon is required to elevate the atom back to its resonance state. In effect this raises the value of the *saturated spectral irradiance* $I_s(\nu)$. As was first shown by the author[21] the resonance and ground level populations of the laser excited atoms are only locked in the ratio of their degeneracies g, if $I^l(\nu) \gg I_s(\nu)$, where $I^l(\nu)$ is the laser spectral irradiance (assumed broadband compared to the atomic linewidth). The *saturated spectral irradiance*

$$I_s(\nu) \equiv \frac{8\pi h\nu^3}{c^2(1+g)}\left\{\frac{\tau^{rad}}{\tau}\right\}, \tag{12}$$

where $h\nu$ is the laser photon energy, c is the velocity of light, ν is the frequency of the laser radiation, τ^{rad} is the radiative lifetime of resonance level and τ is the actual lifetime in the presence of quenching collisions.

In the case of the sodium resonance transition,

$$I_s(\nu) \approx 6.07 \times 10^{-10} \text{ W cm}^{-2} \text{ Hz}^{-1},$$

in the absence of collisional quenching. If the laser bandwidth is about 0.1 nm (or 86 GHz) this corresponds to stating that for saturation

$$I^l \gg 52 \text{ W cm}^{-2}.$$

In general we can write

$$\frac{1}{\tau} = A_{21} + N_e\left\{K_{21} + K_{12} + \sum_{n>2} K_{2n}\right\} + \sum_u n_u \sum_w \langle \sigma v\rangle^Q_{uw}, \tag{13}$$

where $\langle \sigma v\rangle^Q_{uw}$ is the nitrogen collision quenching rate involving vibrational transitions from u to w and A_{21} represents the Einstein spontaneous transition probability for the resonance to ground transition. If we assume as before that the majority of the nitrogen molecules are in the lowest vibrational level of ground electronic state then we can write

$$\frac{1}{\tau} = A_{21} + N_e\left\{K_{21} + K_{12} + \sum_{n>2} K_{2n}\right\} + C^Q_{21}, \tag{14}$$

where

$$C^Q_{21} \approx n_0 v^Q \sum_w \sigma^Q_{0w}, \tag{15}$$

and σ^Q_{0w} is the effective cross section for vibrational excitation from 0 to w through quenching with Na($3p$),

$$v^Q = \left\{\frac{8\,kT}{\pi\mu}\right\}^{1/2}.$$

T is the gas temperature, and μ is the reduced mass for the sodium-nitrogen collision.

In Table I we present estimates[22,23] of the Na($3p$)-N_2 quenching cross sections and the corresponding energy defects E_{21}-$\Delta\epsilon_{0w}$. In the absence of nitrogen the electron superelastic quenching leads to a minimum resonance state lifetime of about 12.5 nsec (compared to $\tau^{rad} \approx 15.9$ nsec) for a sodium atom density of 5×10^{15} cm^{-3}, corresponding to a vapor temperature of 670 K.[24] The presence of 2×10^{17} cm^{-3} of nitrogen molecules further reduces this lifetime to about 2.2 nsec, which in turn increases the requirement for laser saturation, from Eq. (12)

$$I^l \gg 295 \text{ W cm}^{-2}.$$

This poses no problem as the values of laser irradiance throughout our analysis considerably exceeds this value.

The power extracted per unit volume from the laser field resulting from these nitrogen quenching collisions can be expressed in the form

$$Q^l_{n_0} = n_0 N_2 v^Q E_{21} \sum_w \sigma^Q_{0w}, \tag{16}$$

and is included in the LIBORS code to allow for the additional laser power density absorbed in the presence of nitrogen. N_2 is again the sodium resonance state density.

For times somewhat less than the ionization time we can approximate Eq. (16) by the form

$$Q^l_{n_0} = G n_0 N_0 v^Q E_{21} \sum_w \sigma^Q_{0w}, \tag{17}$$

where we have assumed laser saturation which gives[21]

$$N_2 = G N_0 \tag{18}$$

with

$$G = \frac{g}{1+g}. \tag{19}$$

For $N_0 = 5\times10^{15}$ cm^{-3}, $n_0 = 2\times10^{17}$ cm^{-3} we have $Q^l_{n_0} \approx 6.76\times10^4$ W cm^{-3} using the values of σ^Q_{0w} given in Table I. This represents a fairly large rate of laser energy deposition into the nitrogen gas. Indeed, the rate of translationally heating the nitrogen molecules (ϵ_{n_0} is mean thermal energy of a nitrogen molecule) is given by the expression

$$\frac{d\epsilon_{n_0}}{dt} = G N_0 v^Q \sum_w \sigma^Q_{0w}\{E_{21} - \Delta\epsilon_{0w}\}. \tag{20}$$

At $N_0 = 5\times10^{15}$ cm^{-3} and $n_0 = 2\times10^{17}$ cm^{-3} Eq. (20) gives $d\epsilon_{n_0}/dt \approx 6.50\times10^5$ eV sec^{-1} molecule^{-1}, and leads to an increase in temperature of 503 K for each 100 nsec of laser irradiation (until appreciable ionization occurs).

This gas heating would invariably lead to thermal depopulation of the vibrational ground state and as indicated earlier would reduce the electron cooling rate. This would mean that T_e would be higher and the ionization time reduced. This is consistent with our statement that our calculations would be conservative. That is to say, our estimate of the increase in laser energy required in the presence of N_2 will be larger than required in reality.

We have also omitted the ion-nitrogen translation ener-

TABLE I. Sodium/nitrogen resonance quenching cross sections and energy defects.

Vibrational excitation	σ^Q_{0w} (Å^2)	$E_{21} - \Delta\epsilon_{0w}$ (eV)
0 → 3	3.74	1.23
0 → 4	5.86	0.94
0 → 5	7.81	0.65
0 → 6	6.03	0.36
0 → 7	1.9	0.07

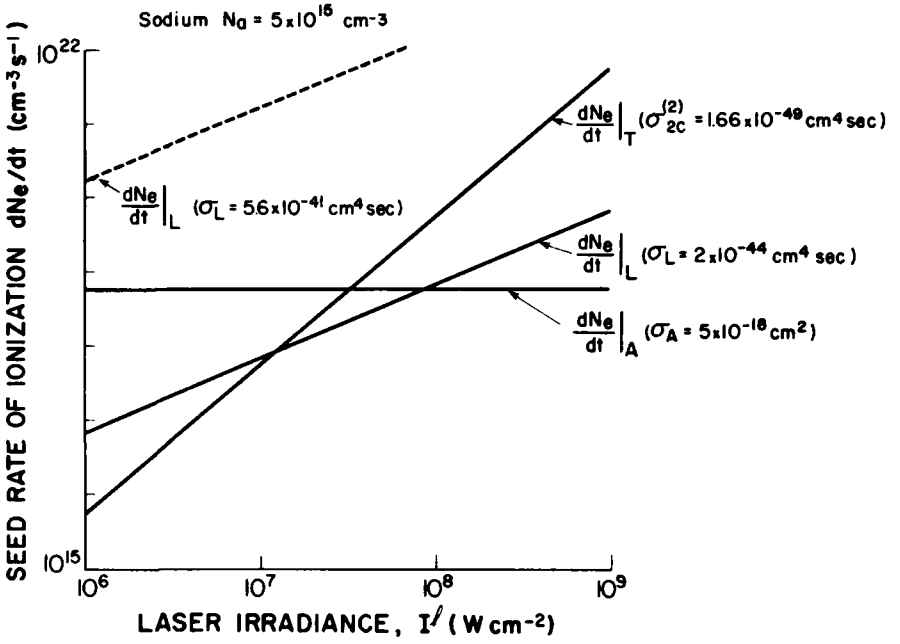

FIG. 3. Variation of three primary seed ionization rates with laser irradiance for sodium at 5×10^{15} cm^{-3}. $(dN_e/dt)|_A$— associative ionization rate, $(dN_e/dt)|_L$— laser induced penning ionization rate and $(dN_e/dt)|_T$— two photon resonance state ionization.

gy exchange terms from the ion energy equation. Such a term would, in effect, tend to prevent the ion temperature from rapidly rising towards the electron temperature and thereby mean that the electron-ion energy loss term [$N_e^2 H_{ei}$ of Eq. (1)] would remain large for a longer period. This should not affect the ionization time and in order to test this we ran one case where the ion temperature was forced to stay at room temperature (an extreme example). The results of this run confirmed our justification for avoiding the complexity of including the ion-nitrogen energy exchange terms.

D. LIBORS computer code results with and without nitrogen

In order to see which of the *seed ionization processes* is likely to dominate at any given value of laser irradiance, we have evaluated the ionization rate for each as a function of I^l assuming a $N_0 = 5\times10^{15}$ cm^{-3}. The results (for the cross sections used in most of our code runs) are presented as the full lines in Fig. 3. It is evident that associative ionization will dominate for $I^l \lesssim 2\times10^7$ W cm^{-2}, while two photon ionization of the resonance level will be the primary seed ionization process for higher values of laser irradiance.

Recent experiments[25] have suggested that the laser induced Penning cross section σ_L could be as large as 5.6×10^{-41} cm^4 sec, and so we have added this result (broken curve) to Fig. 3. Clearly, if this is correct, laser induced penning ionization is likely to be the dominant seed electron creation process over the I^l range of interest. Nevertheless, most of our LIBORS code runs used the smaller value of 2×10^{-44} cm^4 sec for σ_L. It is evident that if we had used the larger value of σ_L the ionization time would have been somewhat shorter and this would have had the effect of reducing the amount of laser energy required to form a plas-

TABLE II. LIBORS code results with and without nitrogen. $I^l = 10^6$ W cm^{-2}; $\sigma_L = 2\times10^{-44}$ cm^4 sec; $\sigma^{(2)}_{2c} = 1.66\times10^{-49}$ cm^4 sec; $\sigma_A = 5\times10^{-18}$ cm^2.

Sodium density N_0 (cm^{-3})	Nitrogen density n_0 (cm^{-3})	Computer run time (nsec)	Electron density achieved N_e^{max} (cm^{-3})	Electron temperature at end of run T_e (K)
1×10^{15}	0	606	9.988×10^{14}	6275
3×10^{15}	0	218	2.993×10^{15}	6930
5×10^{15}	0	220	4.982×10^{15}	6889
1×10^{16}	0	120	9.957×10^{15}	7581
1×10^{15}	2×10^{17}	1000	1.051×10^{11}	4293
3×10^{15}	2×10^{17}	804	2.500×10^{15}	3787
5×10^{15}	2×10^{17}	430	4.284×10^{15}	4060
1×10^{16}	2×10^{17}	225	8.836×10^{15}	4500
1×10^{15}	3×10^{18}	1000	2.284×10^{11}	2758
3×10^{15}	3×10^{18}	1000	3.505×10^{11}	3226
5×10^{15}	3×10^{18}	1000	1.144×10^{15}	3365
1×10^{16}	3×10^{18}	527	5.105×10^{15}	3508

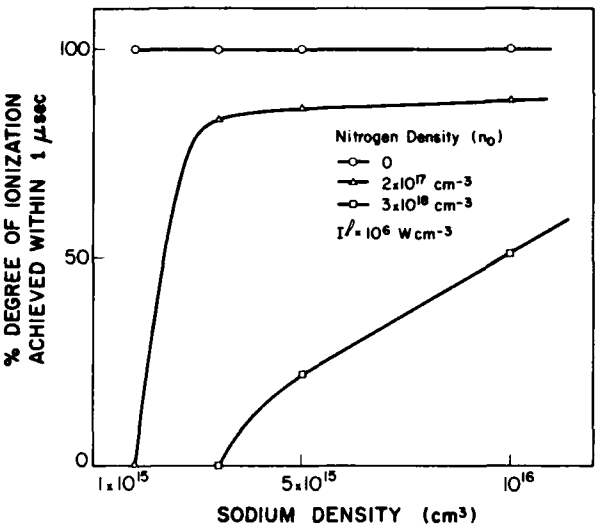

FIG. 4. Percentage degree of ionization achieved within one microsecond for several sodium/nitrogen atmospheres assuming a laser irradiance of 10^6 W cm^{-2}.

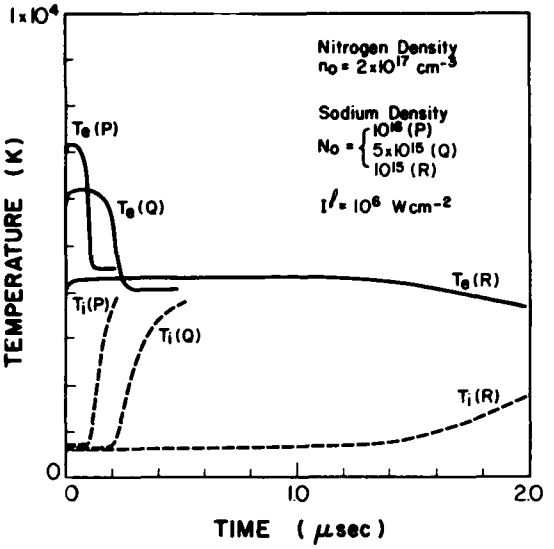

FIG. 5. Dependence of electron and ion temperature time histories on sodium density assuming 10^6 W cm^{-2} laser irradiance and a nitrogen density of 2×10^{17} cm^{-3}.

ma channel of a given length. We have proved this to be the case for one set of conditions where the ionization burnout time was indeed reduced by about a factor of 3. This reaffirms our assertion that our predictions will be conservative.

In Table II we present the results of a broad series of LIBORS code runs used to gauge the likely conditions of interest. These runs were also used to ascertain the degree of ionization achievable within 1 μsec at a laser irradiance of 1 MW cm^{-2}. The results are presented in Fig. 4 and from these we can see that in order to obtain an appreciable degree of ionization (i.e., $\alpha > 50\%$), the sodium doping density $N_0 \gtrsim 3\times10^{15}$ cm^{-3} for a nitrogen density $n_0 \simeq 2\times10^{17}$ cm^{-3}. It might, however, be noted from Table II that if a plasma channel with an electron density of 10^{13} cm^{-3} is acceptable, then a sodium vapor density as low as 10^{15} cm^{-3} is adequate even with a nitrogen background density of 2×10^{17} cm^{-3} provided a laser irradiance of at least 10^6 W cm^{-2} is maintained for a 1 μsec period along the path of the beam.

Since the presence of nitrogen leads primarily to a cooling of the electrons we decided to check the variation of this cooling with sodium density for a given laser irradiance and nitrogen density. The results are presented in Fig. 5 where it is evident that both the plateau and minimum values of the electron temperature decrease with decreasing sodium density for a given nitrogen density. The corresponding variation in ionization burnout time can be seen by reference to Fig. 6. Clearly, the ionization time increases and the final electron density achieved decreases with decreasing N_0. It is evident from these results that plasma channel formation with an electron density of about 10^{15} cm^{-3} should be attainable within 1 μsec provided $N_0 \gtrsim 5\times10^{15}$ cm^{-3}, $I' \gtrsim 10^6$ W cm^{-2} and $n_0 \lesssim 2\times10^{17}$ cm^{-3}. The value of 2×10^{17} cm^{-3} for the nitrogen density is in keeping with current thinking about the likely atmospheric conditions within a light ion beam fusion reactor.[12]

We can gauge directly the influence of a nitrogen atmosphere of about 13 Torr upon the maximum electron density, peak electron temperature and ionization burnout time attained with $I' = 10^6$ W cm^{-2}, for $N_0 = 5\times10^{15}$ cm^{-3} by reference to Fig. 7. The full lines correspond to laser ionization in the absence of nitrogen, while the broken curves refer to the case where $n_0 = 2\times10^{17}$ cm^{-3}. It can be seen that the presence of the nitrogen reduces both the peak and the final electron temperature by about a third and this, in effect, doubles the ionization time and prevents full ionization ($\alpha = 84\%$ as opposed to 99.9% for $n_0 = 0$) from being attained.

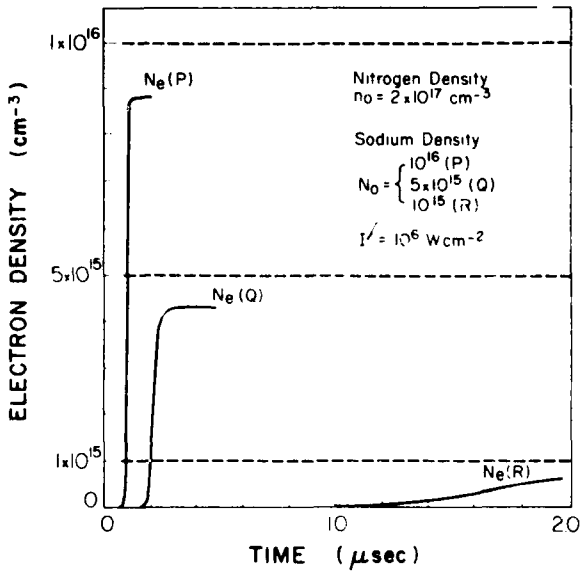

FIG. 6. Dependence of electron density time histories on sodium density assuming a laser irradiance of 10^6 W cm^{-2} and a nitrogen density of 2×10^{17} cm^{-3}.

AD-A126 366 THE APPLICATION OF LASER RESONANCE SATURATION TO THE DEVELOPMENT OF EFFIC..(U) TORONTO UNIV DOWNSVIEW (ONTARIO) INST FOR AEROSPACE STUDIES R M MEASURES 2/2

UNCLASSIFIED SEP 82 AFOSR-TR-83-0134 AFOSR-80-0057 F/G 20/5 NL

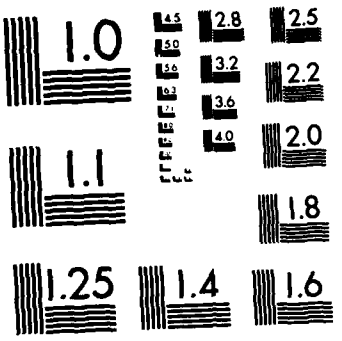

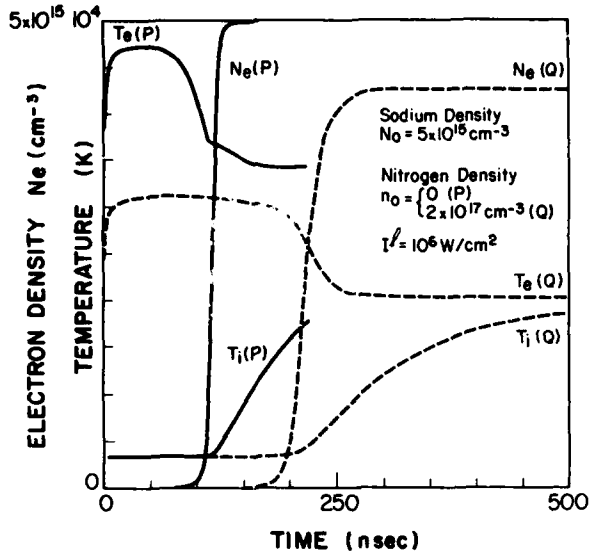

FIG. 7. A comparison of the temporal variation in electron density N_e, electron temperature T_e and ion temperature T_i, with (2×10^{17} cm^{-3}) and without nitrogen, assuming a laser irradiance of 10^6 W cm^{-2} and a sodium density of 5×10^{15} cm^{-3}.

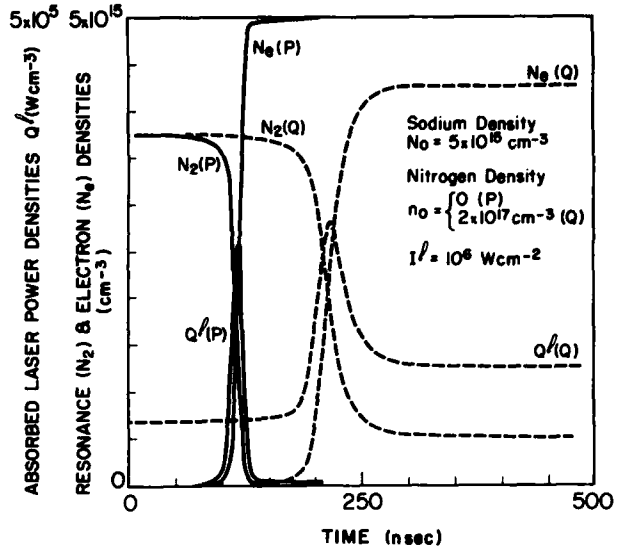

FIG. 8. A comparison of the temporal variation in the electron density, the resonance state density and the absorbed laser power density Q^l(W cm^{-3}), with (2×10^{17} cm^{-3}) and without nitrogen assuming a laser irradiance of 10^6 W cm^{-2} and a sodium density of 5×10^{15} cm^{-3}.

The difference in the power density extracted from the laser field Q^l, under these same conditions, can also be seen from Fig. 8, where the temporal variation in Q^l is presented with that of both the resonance state N_2 and electron densities N_e. Clearly, although Q^l reaches a peak where the product N_2N_e is a maximum for both $n_0 = 0$ and $n_0 = 2\times10^{17}$ cm^{-3}, implying that electron superelastic quenching always dominates the peak absorption. It is quite apparent that the presence of the nitrogen significantly increases the laser power density required before and after this peak. We shall return to this point in the next section.

In Fig. 9, we present the variation of the 75% ionization time τ_B with laser irradiance for $N_0 = 5\times10^{15}$ cm^{-3}, $n_0 = 0$ (● points) and $n_0 = 2\times10^{17}$ cm^{-3} (○ points). The full and broken curves are respective fits to these data by a relation of the form

$$\tau_B = \frac{1}{a + b\{I^l\}^x}. \tag{21}$$

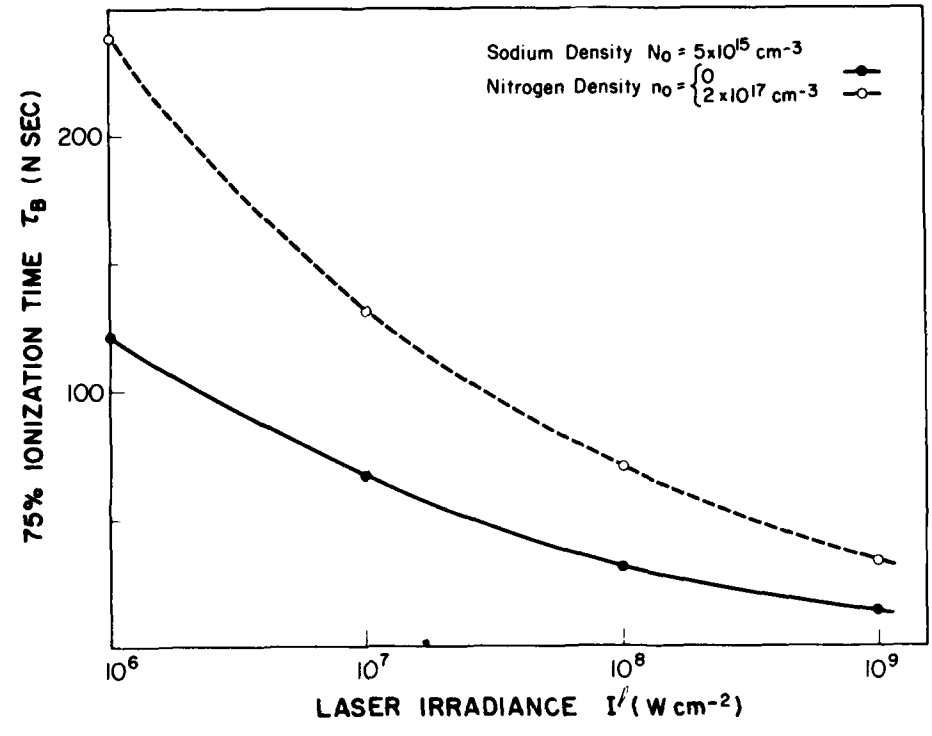

FIG. 9. Variation of the 75% ionization time with laser irradiance for sodium density 5×10^{15} cm^{-3} assuming a zero and 2×10^{17} cm^{-3} density of nitrogen. LIBORS code points (●) for $n_0 = 0$ and (○) for $n_0 = 2\times10^{17}$ cm^{-3}. Curves are analytical fits to the points of the form $\tau_B = [a + b\{I^l\}^x]^{-1}$.

We can see from Fig. 9 that for values of laser irradiance ranging from 10^6 to 10^9 W cm^{-2}, the sodium vapor ionization time is roughly doubled in the presence of 13 Torr of nitrogen as a result of electron cooling.

E. Nitrogen effects on laser requirements for plasma channel creation

We shall now proceed to estimate the energy density of the laser pulse needed to create a plasma channel of length L in sodium vapor of initial atom density, $N_0 = 5\times10^{15}$ cm^{-3} in the absence of any nitrogen background gas. We shall then recalculate the energy density required in the presence of 13 Torr of nitrogen (i.e., $n_0 = 2\times10^{17}$ cm^{-3}). As previously shown[6] the ionization time increases with depth because as the laser pulse burns its way through the sodium vapor its irradiance decreases. This will mean that, even if the original laser pulse were step-like, its temporal nature will change with penetration into the vapor column. Although we are currently working on this complex problem the analysis included in this report assumes that we are always dealing with a step-like laser pulse. We therefore assume that the laser energy density required to create a plasma channel can be written in the form

$$E_0^l \approx I_0^l \tau_B^l, \tag{22}$$

where I_0^l(W cm^{-2}) represents the incident laser irradiance and τ_B^l (sec) represents the 75% ionization time after a penetration depth L (cm). Under condition of laser saturation it has been shown[6] that the laser irradiance at the end of the channel length

$$I_f^l = I_0^l - Q^l L. \tag{23}$$

This relation assumes that the laser power density absorbed is independent of the laser irradiance (and therefore position). This is not strictly true for $I^l \gtrsim 10^7$ W cm^{-2}, as can be seen from Fig. 10. The deviation from constant Q^l is due primarily to the growing importance of single photon ionization at the higher values of laser irradiance. Thus to be conservative we shall in fact write

$$I_f^l = I_0^l - Q_{\max}^l L, \tag{24}$$

where $Q_{\max}^l$ is taken to be the peak value of Q^l corresponding to the $I^l = 10^8$ W cm^{-2} runs, i.e.,

$$Q_{\max}^l = Q_{\max}^l(N_0, n_0, I^l = 10^8). \tag{25}$$

The *ionization burnout time* from Eq. (21) becomes

$$\tau_B^l(N_0,n_0,I_0^l,L) = (a(N_0,n_0) + b(N_0,n_0)\{I_0^l - Q_{\max}^l L\}^{x(N_0,n_0)})^{-1}, \tag{26}$$

and from Eq. (22)

$$E^l(N_0,n_0,I_0^l,L) = \frac{I_0^l}{a(N_0,n_0) + b(N_0,n_0)\{I_0^l - Q_{\max}^l L\}^{x(N_0,n_0)}}. \tag{27}$$

The values of a, b, and x were obtained for the two sets of runs shown in Fig. 9, and

$$Q_{\max}^l = \begin{cases} 2.9\times10^5 \text{ W cm}^{-3} & \text{for } n_0 = 0 \\ 3.0\times10^5 \text{ W cm}^{-3} & \text{for } n_0 = 2\times10^{17} \text{ cm}^{-3}. \end{cases}$$

Equations (26) and (27) were used to show the variation

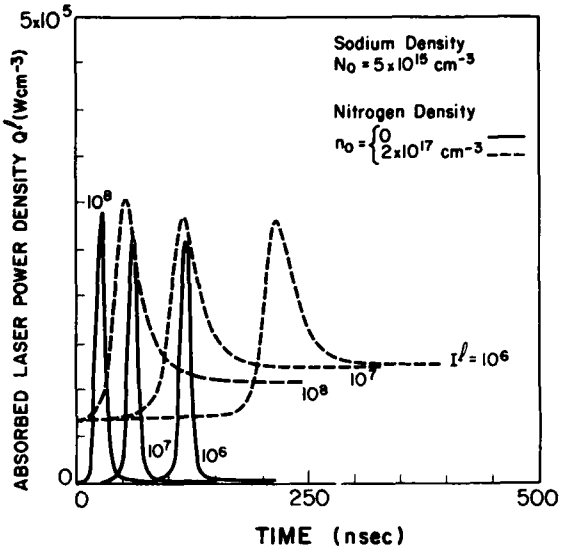

FIG. 10. Dependence of laser absorbed power density Q^l time history upon laser irradiance for sodium density of 5×10^{15} cm^{-3} assuming zero (full curves) and 2×10^{17} cm^{-3} nitrogen (broken curves).

of the laser energy with laser pulse length (chosen to achieve at least 75% ionization along a 5 m long channel of 1 cm^2 cross sectional area) and the results presented in Fig. 11. The full curve assumes $N_0 = 5\times10^{15}$ cm^{-3} and $n_0 = 0$, while the broken curve assumes $N_0 = 5\times10^{15}$ cm^{-3} and $n_0 = 2\times10^{17}$ cm^{-3}. Clearly the former situation leads to a minimum laser energy density $E_{\min}^l = 7.4$ J cm^{-2}, a corresponding laser pulse duration $\tau^l = 35$ nsec and $I_0^l = 2.11\times10^8$ W cm^{-2},

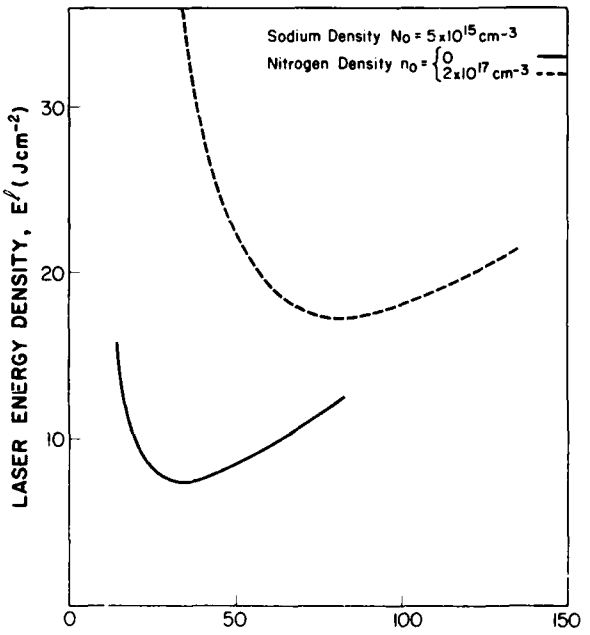

FIG. 11. Variation of laser energy density E^l(J cm^{-2}) with laser pulse duration necessary to achieve 75% ionization at the end of a 5 m channel in sodium vapor at 5×10^{15} cm^{-3} and in sodium/nitrogen (5×10^{15} cm^{-3}/2×10^{17} cm^{-3}) atmosphere

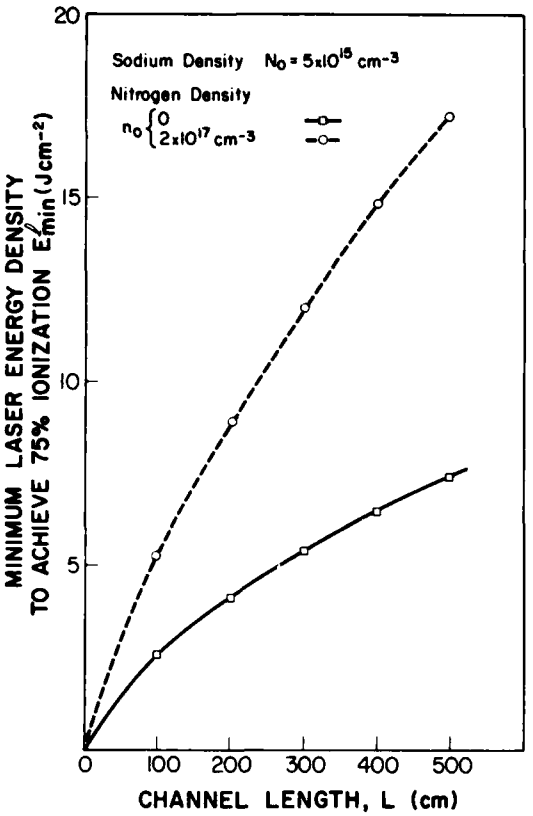

FIG. 12. Dependence of the minimum laser energy density E'_{min} (J cm^{-2}) necessary to achieve 75% ionization burnout at the end of channel—upon the channel length, assuming sodium/nitrogen atmospheres of (5×10^{15} cm^{-3}/zero) and (5×10^{15} cm^{-3}/2×10^{17} cm^{-3}).

while the latter case gives $E'_{min} = 17.2$ J cm^{-2}, $\tau' = 80$ nsec and $I'_0 = 2.15\times10^8$ W cm^{-2}.

We see that although the presence of 13 Torr of nitrogen increases the minimum laser energy density required for creating a 5-m plasma channel from 7.4 to 17.2 J cm^{-2}, this is not excessive. Furthermore, the actual laser energy required to create such a channel is still less than 2 J if a 0.1 cm^2 channel cross sectional area is acceptable and consistent with laser beam divergence and beam shaping optics. It should also be noted that the increase in the laser pulse duration (35–80 nsec) is also reasonable as it would lead to an ionization time that is well within the time required to avoid turbulent breakup of the channel (> 1 μsec).

In Fig. 12 we have evaluated the variation in the *minimum laser energy density* with length required to achieve at least 75% *ionization* in pure sodium vapor at about 300 m Torr ($N_0 = 5\times10^{15}$ cm^{-3}) and in the presence of about 13 Torr ($n_0 = 2\times10^{17}$ cm^{-3}) of nitrogen.

III. CONCLUSIONS

An inertial confinement fusion reactor based upon light ion beam drivers will require an efficient means of transporting the ion beams across the reactor to the fuel pellet. It appears that multiple plasma discharge channels could accomplish this task. One of the most attractive methods of ensuring that these discharge channels are straight, well defined and brought to a common focus is to create a system of well-ionized plasma channels prior to striking the discharges. *Laser ionization based on resonance saturation* of an alkali vapor has been proposed as ideal for the task of forming such highly ionized plasma channels very rapidly with a relatively low energy laser.

The purpose of the present study was to evaluate whether the presence of an appreciable background of molecular nitrogen was likely to effectively degrade this means of creating the discharge guide channels, or increase the laser energy requirement to the point where it might become impractical. In an attempt to compensate for the many poorly known cross sections used in our analysis we have been conservative wherever possible. Thus, although the accuracy of our analysis may not be better than a factor of two we feel that our conclusions will be reliable.

Our conclusions are:

(i) The primary effects of the nitrogen background gas upon LIBORS are to cool the free electrons, thereby increasing the ionization time, and to increase the laser energy requirement;

(ii) Near to fully ($> 80\%$) ionized channels can be rapidly created within a sodium (or lithium) seeded nitrogen atmosphere providing the alkali is present at a concentration of greater than 0.5%;

(iii) If the nitrogen density within a reactor is expected to be about 2×10^{17} cm^{-3}, then an electron density of close to 5×10^{15} cm^{-3} can be created over a 5 m path with a sodium density of 5×10^{15} cm^{-3}, provided the laser energy density is at least 17.2 J cm^{-2} and the pulse duration is about 80 nsec;

(iv) If the electron density required to create a discharge guide path is only 10^{13} cm^{-3}, then both the alkali seeding and the laser energy requirements could be considerably relaxed.

(v) The presence of nitrogen not only cools the free electrons but, in quenching the laser pumped species, is itself directly heated. This could further improve the channel capabilities of LIBORS through the creation of a low density core to the channel.

In light of our encouraging theoretical results we would recommend that an extensive experimental program be undertaken to test our conclusions and to see if plasma channels created through laser resonance saturation offer any advantages over other approaches towards the formation of discharge guide channels. In particular, it would be worth comparing LIBORS with direct photoionization (either single or two-photon) techniques. The latter only provides energy to the free electrons upon their creation while in LIBORS the laser continues to provide energy through superelastic energy conversion. This could be important when an electron cooling background gas, such as nitrogen, is present. Another important difference expected between direct photoionization and LIBORS is the predicted gas heating associated with the latter. This leads to the formation of a hot, low density core to the channel.

It is expected that the choice between the competing laser techniques for creating the discharge guide channel will probably be made on the basis of which technique can create a channel that is of high enough quality to ensure

efficient transport for the ion beams at a laser energy that is small enough to avoid appreciable pellet preheat. We feel that LIBORS will prove to be the most suitable technique when all factors are taken into consideration.

ACKNOWLEDGMENTS

Work supported by the U.S. Sandia National Laboratory under Contract No. 49-2859A and a Grant from the Natural Science and Engineering Research Council of Canada.

[1]J. N. Olsen, D. J. Johnson, and R. J. Leeper, Appl. Phys. Lett. **36**, 808 (1980).
[2]S. L. Sandel, S. C. Young, S. J. Stephanakis, F. W. Oliphant, G. Cooperstein, S. Goldstein, and D. Mosher, Bull. Am. Phys. Soc. **24**, 1031 (1979).
[3]R. J. Freeman, L. Baker, P. A. Miller, L. P. Mix, J. N. Olsen, J. W. Poukey, and T. P. Wright, " Electron and Ion Beam Transport to Fusion Targets," Sand. 79-0734C, Sandia Laboratories, 1979.
[4]J. N. Olsen and L. Baker, Bull. Am. Phys. Soc. **25**, 899 (1980).
[5]J. N. Olsen and R. J. Leeper, "Propagation of Ion Beams in Laser-Initiated Discharge Channels," Paper 2C1, presented at the 1981 IEEE International Conference on Plasma Science, Sante Fe, N. M., 18–20 May 1981.
[6]R. M. Measures, N. Drewell, and P. Cardinal, J. Appl. Phys. **50**, 2662 (1979).
[7]D. J. Ehrlich and R. M. Osgood, Jr., Appl. Phys. Lett. **34**, 655 (1979).
[8]R. M. Measures and P. G. Cardinal, Phys. Rev. A **23**, 804 (1981).
[9]R. M. Measures, P. G. Cardinal, and G. W. Schinn, J. Appl. Phys. **52**, 1269 (1981).
[10]G. A. Moses and R. R. Peterson, Nucl. Fusion **20**, 849 (1980).
[11]R. R. Peterson, G. W. Cooper, and G. A. Moses, "Cavity Gas Analysis for Light Ion Beam Fusion Reactors," University of Wisconsin Report No. 371, 1980.
[12]J. N. Olsen (private communication).
[13]A. V. Eremin, A. A. Kulikovskii, and I. M. Naboko, Opt. Spectrosc. (USSR) **49**, 9 (1980).
[14]J. C. Y. Chen, J. Chem. Phys. **40**, 3513 (1964) (see also Ref. 23).
[15]S. C. Brown, *Electron-Molecule Scattering* (Wiley, New York, 1980).
[16]A. Herzenberg, J. Phys. B **1**, 548 (1968).
[17]D. T. Birtwistle and Z. Herzenberg, J. Phys. B **4**, 53 (1971).
[18]H. Petschek and S. Byron, Ann. Phys. **1**, 270 (1957).
[19]J. F. Clarke and M. McChesney, *Dynamics of Relaxing Gases* (Butterworth, Boston, 1976).
[20]N. Chandra and A. Tomkins, NASA TND-8347, (1976).
[21]R. M. Measures, J. Appl. Phys. **39**, 5232 (1968).
[22]E. Bauer, E. R. Fisher, and F. R. Gilmore, J. Chem. Phys. **51**, 4173 (1969).
[23]H. F. Krause, J. Fricke, and W. L. Fite, J. Chem. Phys. **56**, 4593 (1972).
[24]A. N. Nesmeianov, *Vapour Pressure of the Elements*, translated by J. I. Carasso (Academic, New York, 1963), p. 443.
[25]J. Weiner and P. Polak-Dingels, J. Chem. Phys. **74**, 508 (1981).

SECURITY CLASSIFICATION OF THIS PAGE (When Data Entered)

REPORT DOCUMENTATION PAGE		READ INSTRUCTIONS BEFORE COMPLETING FORM
1. REPORT NUMBER AFOSR-TR- 83-0134	2. GOVT ACCESSION NO. AD-A126	3. RECIPIENT'S CATALOG NUMBER 366
4. TITLE (and Subtitle) THE APPLICATION OF LASER RESONANCE SATURATION TO THE DEVELOPMENT OF EFFICIENT SHORT WAVELENGTH LASERS		5. TYPE OF REPORT & PERIOD COVERED Annual, period ending Sept. 30, 1982 6. PERFORMING ORG. REPORT NUMBER
7. AUTHOR(s) Dr. R. M. Measures		8. CONTRACT OR GRANT NUMBER(s) AFOSR 80-0057
9. PERFORMING ORGANIZATION NAME AND ADDRESS University of Toronto, Institute for Aerospace Studies, 4925 Dufferin Street, Downsview, Ontario, Canada, M3H 5T6		10. PROGRAM ELEMENT, PROJECT, TASK AREA & WORK UNIT NUMBERS 61102F 2301/A8
11. CONTROLLING OFFICE NAME AND ADDRESS Air Force Office of Scientific Research/NA Bldg. 410, Bolling Air Force Base, D.C. 20332		12. REPORT DATE Sep 82 13. NUMBER OF PAGES 76
14. MONITORING AGENCY NAME & ADDRESS(if different from Controlling Office)		15. SECURITY CLASS. (of this report) UNCLASSIFIED 15a. DECLASSIFICATION/DOWNGRADING SCHEDULE

16. DISTRIBUTION STATEMENT (of this Report)

Approved for public release; distribution unlimited.

17. DISTRIBUTION STATEMENT (of the abstract entered in Block 20, if different from Report)

18. SUPPLEMENTARY NOTES

19. KEY WORDS (Continue on reverse side if necessary and identify by block number)

1. X-ray lasers, 2. Sodium plasma, 3. Laser resonance saturation, 4. Laser ionization, 5. Exploding foils, 6. Near resonance absorption photography, 7. Stark broadening, 8. Electron density measurements, 9. Spectral hole burning, 10. Atom density measurements, 11. Charge exchange collisions, 12. Ground level inversion, 13. Laser diagnostics, 14. Alkali oven.

20. ABSTRACT (Continue on reverse side if necessary and identify by block number)

Laser resonance saturation represents an extremely rapid and efficient new method of coupling laser energy into either a gas or plasma. We have continued to study this process both theoretically and experimentally and have shown that this interaction can lead to a very high degree of ground level burnout for the laser pumped species. During the past year we have undertaken the first time resolved Stark width measurements of the free electron density within a sodium plasma created by laser resonance saturation. Currently we are exploring

DD FORM 1 JAN 73 1473 EDITION OF 1 NOV 65 IS OBSOLETE UNCLASSIFIED

SECURITY CLASSIFICATION OF THIS PAGE (When Data Entered)

the feasibility of using this ground level burnout feature as the basis of a new approach towards the development of an efficient short wavelength laser. In a preliminary experiment we have been able to show that sudden joule heating of a thin foil looks promising as a technique for creating the steep gradient of neutral atoms necessary for charge exchange formation of a ground level population inversion within the species having suffered a ground level burnout through laser resonance saturation.

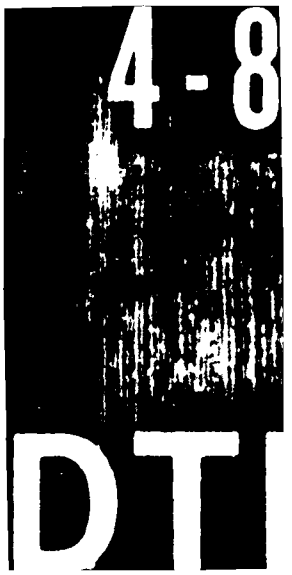
4-8
DT